



HAL
open science

Signatures of early microbial life from the Archean (4 to 2.5 Ga) eon

Kevin Lepot

► **To cite this version:**

Kevin Lepot. Signatures of early microbial life from the Archean (4 to 2.5 Ga) eon. Earth-Science Reviews, 2020, 209, pp.103296. 10.1016/j.earscirev.2020.103296 . insu-03190941

HAL Id: insu-03190941

<https://insu.hal.science/insu-03190941>

Submitted on 6 Apr 2021

HAL is a multi-disciplinary open access archive for the deposit and dissemination of scientific research documents, whether they are published or not. The documents may come from teaching and research institutions in France or abroad, or from public or private research centers.

L'archive ouverte pluridisciplinaire **HAL**, est destinée au dépôt et à la diffusion de documents scientifiques de niveau recherche, publiés ou non, émanant des établissements d'enseignement et de recherche français ou étrangers, des laboratoires publics ou privés.



Distributed under a Creative Commons Attribution - NoDerivatives 4.0 International License



Signatures of early microbial life from the Archean (4 to 2.5 Ga) eon

Kevin Lepot

Univ. Lille, CNRS, Univ. Littoral Côte d'Opale, UMR 8187 - LOG - Laboratoire d'Océanologie et de Géosciences, F-59000 Lille, France



ARTICLE INFO

Keywords:

Early life
Archean
Microfossils
Stromatolites
Isotopes
Biosignatures

ABSTRACT

The Archean era (4 to 2.5 billion years ago, Ga) yielded rocks that include the oldest conclusive traces of life as well as many controversial occurrences. Carbonaceous matter is found in rocks as old as 3.95 Ga, but the oldest (graphitic) forms may be abiogenic. Due to the metamorphism that altered the molecular composition of all Archean organic matter, non-biological carbonaceous compounds such as those that could have formed in seafloor hydrothermal systems are difficult to rule out. Benthic microbial mats as old as 3.47 Ga are supported by the record of organic laminae in stromatolitic (layered) carbonates, in some stromatolitic siliceous sinters, and in some siliciclastic sediments. In these deposits, organic matter rarely preserved fossil cellular structures (e.g., cell walls) or ultrastructures (e.g., external sheaths) and its simple textures are difficult to attribute to either microfossils or coatings of cell-mimicking mineral templates. This distinction will require future nanoscale studies. Filamentous-sheath microfossils occur in 2.52 Ga rocks, and may have altered counterparts as old as 3.47 Ga. Surprisingly large spheres and complex organic lenses occur in rocks as old as 3.22 Ga and ~ 3.4 Ga, respectively, and represent the best candidates for the oldest microfossils. Titaniferous microtubes in volcanic or volcanoclastic rocks inferred as microbial trace fossils have been reevaluated as metamorphic or magmatic textures. Microbially-induced mineralization is supported by CaCO₃ nanostructures in 2.72 Ga stromatolites. Sulfides 3.48 Ga and younger bear S-isotope ratios indicative of microbial sulfate reduction. Ferruginous conditions may have fueled primary production via anoxygenic photosynthesis—as suggested by Fe-isotope ratios—possibly as early as 3.77 Ga. Microbial methanogenesis and (likely anaerobic) methane oxidation are indicated by C-isotope ratios as early as 3.0 Ga and ~ 2.72 Ga, respectively. Photosynthetic production of O₂ most likely started between 3.2 and 2.8 Ga, i.e. well before the Great Oxidation Event (2.45–2.31 Ga), as indicated by various inorganic tracers of oxidation reactions and consistent with morphology of benthic deposits and evidence for aerobic N metabolism in N-isotope ratios at ~ 2.7 Ga.

This picture of a wide diversification of the microbial biosphere during the Archean has largely been derived of bulk-rock geochemistry and petrography, supported by a recent increase in studied sample numbers and in constraints on their environments of deposition. Use of high-resolution microscopy and micro- to nanoscale analyses opens avenues to (re)assess and decipher the most ancient traces of life.

1. Introduction – Co-evolution of life and environments during the Archean

The evolution of life is intimately linked to the modifications of environments, which were driven by a combination of biological and geodynamic processes (e.g., Lowe and Tice, 2007; Kump and Barley, 2007; Arndt and Nisbet, 2012). Continental, oceanic and atmospheric chemistries were largely controlled by magmatic activity through hydrothermal fluid and volcanic emissions and their transformation products, as well as the alteration of the early crust (or proto-crust) before and during the Archean (Huston and Logan, 2004; Kump and Barley, 2007; Arndt and Nisbet, 2012; Kasting, 2019; Catling and Zahnle, 2020). Major changes in geodynamics occurred during the Archean that

would have impacted the evolution of the surface chemistry and in turn, the evolution of life. Indeed, the Archean saw the growth of the juvenile continental crust with an increase in andesitic and felsic components in an ultramafic/mafic “protocrust” (Smit and Mezger, 2017; Hoffmann et al., 2019). It also likely saw the onset of plate tectonics (van Hunen and Moyen, 2012; Korenaga, 2013). Large subaerial igneous provinces appeared toward the end of the Archean whereas subaqueous lavas dominated this eon (Kump and Barley, 2007). Large asteroid impacts are indicated by spherule beds until the end of the Archean (Krull Davatzes et al., 2019). In spite of a fainter young sun, the Archean climate was mostly temperate to hot (Catling and Zahnle, 2020). The atmosphere, and also likely the surface, saw an intense ultraviolet flux as an ozone screen could not form from an anoxic

E-mail address: kevin.lepot@univ-lille.fr.

<https://doi.org/10.1016/j.earscirev.2020.103296>

Received 31 March 2020; Received in revised form 16 July 2020; Accepted 17 July 2020

Available online 22 July 2020

0012-8252/ © 2020 The Author. Published by Elsevier B.V. This is an open access article under the CC BY-NC-ND license (<http://creativecommons.org/licenses/by-nc-nd/4.0/>).

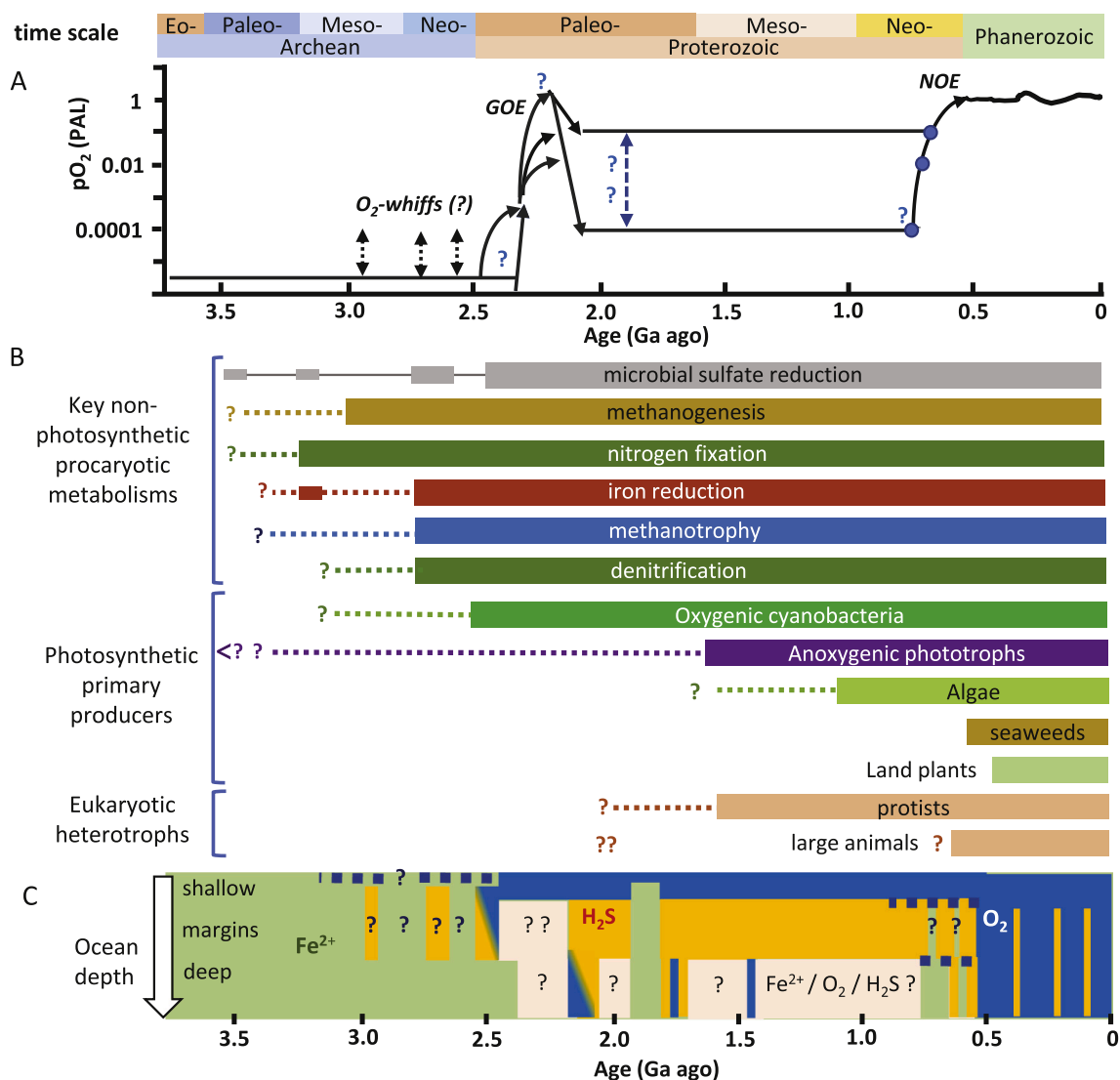


Fig. 1. Co-evolution of life and environments. **(A)** Evolution of atmospheric O_2 partial pressure (pO_2) relative to present atmospheric level (PAL), redrawn and adapted after [Lyons et al. \(2014\)](#). This model includes putative short-lived “whiffs” of O_2 release into the atmosphere, the Great Oxidation Event (GOE), uncertainties (question marks and multiple arrows) regarding the magnitude of the oxygen level increase, of the subsequent oxygen level decrease, and on the timing. A range consistent with geochemical proxies is given for Proterozoic atmospheric oxygen levels. Also indicated is the Neoproterozoic Oxygenation Event (NOE). **(B)** Model of early evolution of life, drawn and adapted from the present review and reviews in [Johnston et al. \(2009\)](#) and [Javaux and Lepot \(2018\)](#). Dashed lines: uncertainties. **(C)** Tentative reconstruction of seawater chemistry (constructed from review figures and data in: [Canfield et al., 2008](#); [Lyons and Gill, 2010](#); [Rasmussen et al., 2012](#); [Canfield et al., 2013](#); [Lyons et al., 2014](#); [Sperling et al., 2014](#); [Ostrander et al., 2019](#)). Current models imply a ferruginous (that is anoxic with Fe^{2+} , green in C) ocean during almost all the Archean. Surface waters progressively oxygenated during O_2 “whiffs” (blue dashes in C) and during and after the GOE. Euxinic (i.e., anoxic-sulfidic, orange in C) conditions formed at ocean margins from bacterial reduction of sulfate formed by oxidative weathering of sulfide minerals. The deep ocean remained ferruginous or euxinic for most of the Proterozoic until the Neoproterozoic Oxygenation Event (NOE), although local and/or temporary deep-water oxygenation may already have existed during this Eon. Highly uncertain water chemistries in various intervals are represented by question marks and pink boxes. (For interpretation of the references to colour in this figure legend, the reader is referred to the web version of this article.)

atmosphere; although this would not have prevented the emergence of life ([Cockell and Raven, 2007](#)), it could have favored photochemical reactions ([Kasting, 2019](#)). In this context, the atmosphere would have displayed concentrations in CO_2 , CH_4 and H_2 much higher than those of today (possibly by multiple orders of magnitude), and may have allowed high-altitude abiotic formation of trace O_2 ([Kasting, 2019](#); [Catling and Zahnle, 2020](#)). The Archean was dominated by mildly reducing, anoxic conditions ([Fig. 1](#); [Lyons et al., 2014](#), and references therein) as indicated by the mass-independent fractionations of sulfur isotopes imparted by photochemical reactions ([Farquhar and Wing, 2003](#)) and the preservation of oxidation-sensitive minerals in river-transported sands ([Rasmussen and Buick, 1999](#)). Oxygen was likely produced by photosynthesis as early as the Mesoarchean, but did not

rise in the atmosphere until the end of the Archean ([Fig. 1](#); see [Section 2.4](#)). This distinct Archean atmospheric composition, combined with evolving rock and sediment compositions ([Hazen et al., 2008](#); [Hoffmann et al., 2019](#)) and UV photochemistry, would likely have led to a chemistry of soils and water bodies that would have been drastically distinct from that of the Phanerozoic, and strongly evolving during the Archean. This, in turn, could have paved the way for the evolution and diversification of microbial metabolisms, as discussed below. Moreover, in this geodynamic and geochemical context, the basic building blocks of life—that is pre-biotic organic molecules acting as precursor to biological systems, could have been brought to the surface of early Earth by meteorites ([Sephton, 2002](#)), by comets ([Fray et al., 2016](#)), and could have formed by abiotic reactions occurring in

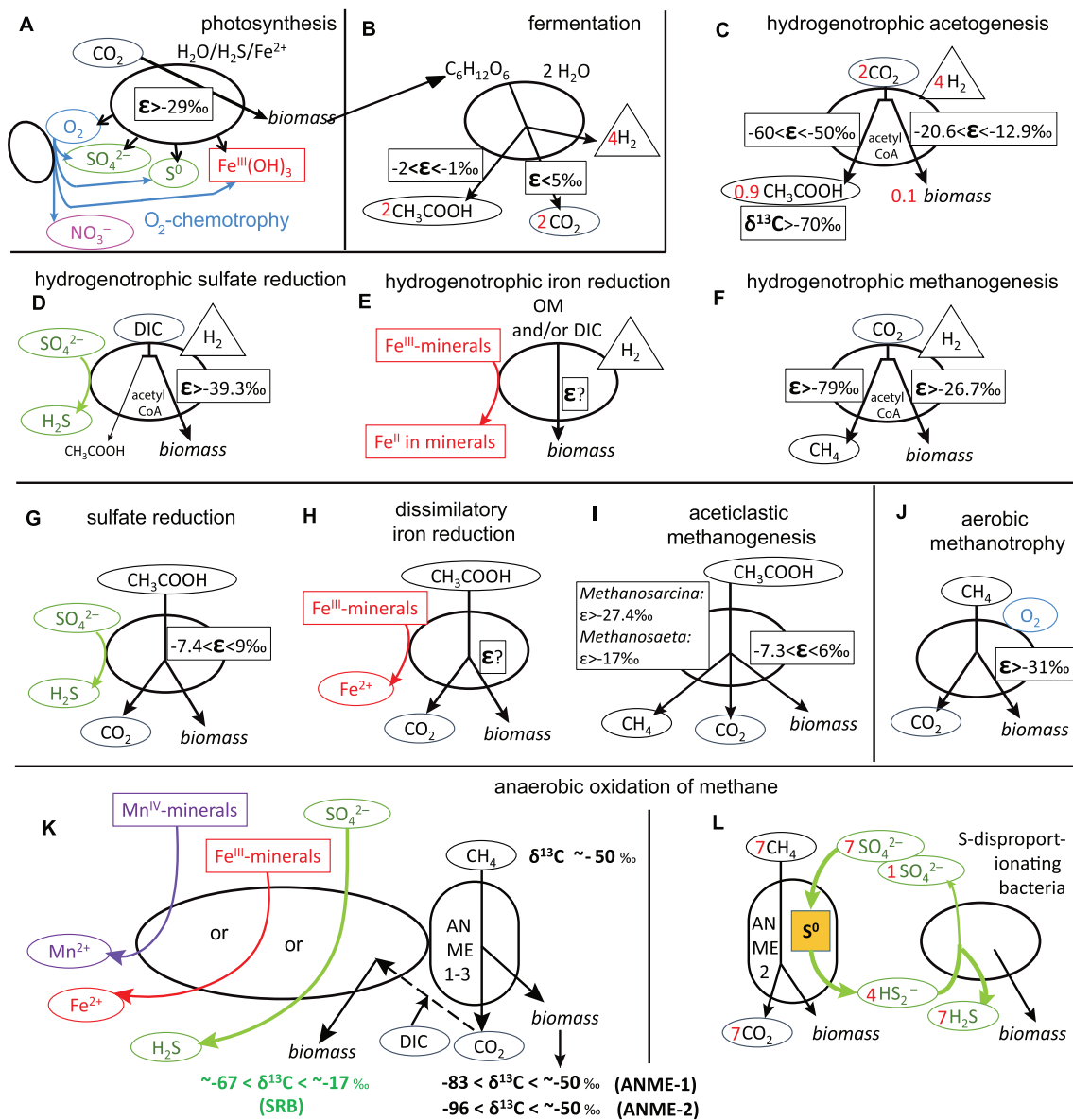


Fig. 2. Metabolisms discussed within this review. Microorganisms are schematized by spheres/ellipses. Products and substrates are shown in the lower and upper half of each schematic, respectively. Carbon-involving reactions are indicated with black lines through the cells and associated with fractionation values for C isotopes (ϵ notation: deviation relative to consumed substrate, δ notation: deviation relative to VPDB reference material). DIC: dissolved inorganic carbon. OM: organic matter. Other metabolic reactions using inorganic species are indicated with various colors. (A) Oxygenic photosynthesis and anoxygenic photosynthesis using iron or sulfur. Chemotrophic microbial metabolisms using photosynthetic O_2 are also shown in the lower left (blue arrows). Values of ϵ from Pearson (2010). (B) Example of a fermentation reaction (Penning and Conrad, 2006; Pearson, 2010; Conrad et al., 2014). (C–F) Hydrogenotrophic chemolithoautotrophic metabolisms (Gelwick et al., 1989; Preuß et al., 1989; Botz et al., 1996; House et al., 2003; Zegeye et al., 2005; Roh et al., 2006; Londry et al., 2008; Liu et al., 2011; Blaser et al., 2013; Etique et al., 2016; Freude and Blaser, 2016). (G–I) Heterotrophic metabolisms: (G–H) anaerobic respirations of sulfate and Fe^{3+} , respectively (Lovley, 1991; Londry and Des Marais, 2003; Govert and Conrad, 2008). (I) Aceticlastic methanogenesis (Valentine et al., 2004; Penning et al., 2006; Londry et al., 2008; Govert and Conrad, 2009). (J) Aerobic methanotrophy (Summons et al., 1994; Templeton et al., 2006). (K–L) Anaerobic methanotrophy pathways. In (K), anaerobic methane-oxidizing archaea (ANME) operate in consortia with bacteria that reduce sulfate, iron, or manganese (Orphan et al., 2002; Treude et al., 2007; Beal et al., 2009; Knittel and Boetius, 2009). In (L), ANME archaea reduce sulfate themselves and are associated with sulfur-disproportionating bacteria (Milucka et al., 2012). Adapted from *Geochimica et Cosmochimica Acta*, 244, Kevin Lepot, Kenneth H. Williford, Pascal Philippot, Christophe Thomazo, Takayuki Ushikubo, Kouki Kitajima, Smail Mostefaoui, and John W. Valley, Extreme ^{13}C -depletions and organic sulfur content argue for S-fueled anaerobic methane oxidation in 2.72 Ga old stromatolites, pages 522–547, Copyright (2019), with permission from Elsevier. (For interpretation of the references to colour in this figure legend, the reader is referred to the web version of this article.)

hydrothermal systems (Sherwood Lollar et al., 2002; McCollom and Seewald, 2006; Ménez et al., 2018) or by spark-discharge reactions in gas phase (Miller-Urey experiment, see McCollom, 2013).

2. Geochemical biosignatures recorded in minerals

2.1. Geochemical evidence for anoxygenic photosynthesis during the Paleoproterozoic

Anoxygenic photosynthesis could have been an important pathway for the primary production of organic matter. It could have been

performed through oxidation of iron and/or sulfur (Fig. 2A, Kappler et al., 2005). In particular, Fe^{2+} was fed into seawater by hydrothermal vents and basaltic eruptions, and probably more so than H_2S (Fioriel et al., 2004; Kump and Seyfried, 2005), so that ferruginous water likely dominated the Archean (Fig. 1C). Irrespective of the oxidation mechanism, the oxidation to Fe^{3+} , which unlike Fe^{2+} is highly insoluble at $\text{pH} > 2$, could have allowed the deposition of sedimentary iron minerals. Anoxygenic photosynthesis using Fe^{2+} (photoferrotrophy) thus can explain the deposition of banded iron formations in anoxic environments (Kappler et al., 2005; Konhauser et al., 2017), in particular during the Paleoproterozoic. Iron isotope ratios recorded in the 3.2 Ga Mapepe Formation (South Africa; Busigny et al., 2017), in the 3.46 Ga Marble Bar Chert (Australia; Li et al., 2013) and in the 3.77 Ga Isua Supracrustal Belt (Greenland; Czaja et al., 2013) indeed show that this element deposited through oxidation into Fe^{3+} in an anoxic reservoir that remained vastly dominated by the soluble form Fe^{2+} . Iron photo-oxidation reactions may produce similar isotope fractionations as reported in some of these Paleoproterozoic banded iron formations (Nie et al., 2017). These photo-oxidation reactions have, however, been deemed difficult to reconcile with the chemistry of the Archean Ocean (Konhauser et al., 2007). Thus, Paleoproterozoic banded iron formations could have formed through biological oxidation, likely via anoxygenic photosynthesis, possibly as early as 3.77 Ga (Czaja et al., 2013).

2.2. Geochemical evidence for microbial sulfur metabolism during the Paleoproterozoic

The sulfur cycle of the Archean differed considerably from that of the later Precambrian and of the Phanerozoic. Indeed, in absence of atmospheric O_2 , the photolysis of magmatic SO_2 could produce elemental sulfur and sulfate aerosols (Farquhar and Wing, 2003; Johnston, 2011). Sulfate ions could be used by chemolithoautotrophic metabolisms such as hydrogenotrophic microbial sulfate reduction (Fig. 2D; Londry and Des Marais, 2003). Sulfate ions may also have been used to oxidize organic compounds through anaerobic respiration (Fig. 2G; Londry and Des Marais, 2003). Elemental sulfur could have been metabolized via microbial disproportionation into sulfate and sulfide ions (metabolism at the right of Fig. 2L; Böttcher et al., 2001). In addition, sulfate ions could have been used by consortia of methanotrophic Archaea and sulfate-reducing bacteria (Fig. 2K; Orphan et al., 2001) and/or consortia of methanotrophic and sulfate-reducing Archaea with S-disproportionating bacteria (Fig. 2L; Milucka et al., 2012). Both microbial sulfate reduction (Habicht et al., 2002; Shen and Buick, 2004) and abiotic SO_2 photolysis reactions (Philippot et al., 2012) may produce large fractionations in ^{34}S relative to ^{32}S . Hence, ratios of ^{34}S and ^{32}S isotopes alone cannot demonstrate sulfur metabolism during the Archean.

However, the isotope fractionation patterns recorded in the abundance of the four stable isotopes of sulfur in pyrites of the Dresser Formation (3.48 Ga) can only be explained by microbial sulfate reduction (Philippot et al., 2007; Ueno et al., 2008; Shen et al., 2009). Although the relationships between the fractionations of the four stable sulfur isotopes can be explained by mixing models in hydrothermal systems, the observation that they are associated with high depletions in ^{34}S requires microbial sulfate reduction metabolism (Roerdink et al., 2016). Microbial sulfate reduction best explains the four S isotope patterns recorded in the 3.48 Ga Dresser Formation, 3.52 Ga rocks of the Theespruit Formation (Roerdink et al., 2016), 3.2 Ga rocks of the Sargur Group (Muller et al., 2017), 3.26–3.23 Ga rocks of the Mapepe Formation (Roerdink et al., 2013), and 2.97 Ga stromatolites of the Nsuze group (Eickmann et al., 2018). These isotopic fractionations can be considered as the oldest geochemical record of life. Although thermochemical sulfate reduction reactions have been considered as an alternative pathway to produce mass-dependent and mass-independent S isotope fractionations (Watanabe et al., 2009; Johnston, 2011), they cannot explain the complete four isotope fractionation pattern recorded

in the Dresser Formation (Oduro et al., 2011). Other studies have shown significant depletion of ^{34}S in Paleoproterozoic rocks that strongly suggest microbial sulfur metabolism (Bontognali et al., 2012; McLoughlin et al., 2012; Nabhan et al., 2020). However, deconvolution of abiotic signals associated with atmospheric (Philippot et al., 2012; van Zuilen et al., 2014) and hydrothermal processes (Roerdink et al., 2016) using measurements of ^{36}S abundances are required to fully support S metabolism in these cases.

Paleoproterozoic microbial sulfate reduction could have been chemolithoautotrophic (Fig. 2D, K-L) or heterotrophic (Fig. 2G). Signatures of microbial sulfur cycling have generally been recorded on microscopic pyrites (e.g. Fig. 14E), but not in the bulk of Paleoproterozoic sulfides (Shen and Buick, 2004; Philippot et al., 2007; Ueno et al., 2008; Shen et al., 2009; Montinaro et al., 2015). Thicker sulfide deposits with layered structures that could represent stromatolites (see Fig. 14D with Section 9.5, and Philippot et al., 2007) and/or pyritized microbial mats (Wacey et al., 2015) did not display diagnostic signatures of microbial sulfate reduction. This suggests that microbial sulfate reduction likely took place locally, in an environment that was otherwise likely depleted in sulfate. Indeed, ^{34}S depletions are otherwise highly muted in bulk rocks until ca. 2.97 Ga (Eickmann et al., 2018) and more commonly, 2.7 Ga (Grassineau et al., 2001; Johnston, 2011; Thomazo et al., 2013; Marin-Carbonne et al., 2018). Thus, although microbial sulfate reduction was present between 3.5 and 2.7 Ga, it rarely left traces in bulk-rock S isotope compositions because microbes and/or abiotic reactions likely reduced the scarce sulfates—produced from weathering with O_2 or in anaerobic atmospheric reactions—in a quantitative fashion without isotopic discrimination (Habicht et al., 2002; Crowe et al., 2014). In addition, mixture of hydrothermal sulfides (e.g., Philippot et al., 2007), clastic sulfides (Nabhan et al., 2020), or atmospheric sulfur (Farquhar et al., 2013) with sulfides fractionated by microbial sulfate reduction may also explain the scarcity of bulk-rock S isotope signatures for this metabolism before 2.97 Ga.

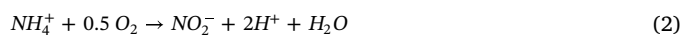
2.3. Geochemical evidence for biotic redox cycling of nitrogen

The metabolism driving the fixation of N_2 into NH_4^+ , which can in turn be assimilated into biomass (reaction 1) is indicated as early as 3.2 Ga by nitrogen isotope ratio values of $\sim 0\text{‰}$ ($\delta^{15}\text{N}$) measured on bulk rocks, including organic N and NH_4^+ stored in clays (Stüeken et al., 2015a).



Large depletions in ^{15}N have been measured in kerogens (insoluble organic matter) of Eoarchean to Mesoproterozoic cherts that could represent the use of NH_4^+ by chemolithotrophic microorganisms as well as the abiotic imprint of mantle-derived fluids or of metabasalt sources (Beaumont and Robert, 1999; Pinti and Hashizume, 2001; Pinti et al., 2009; van Zuilen et al., 2005).

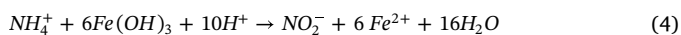
Aerobic N metabolisms (reactions 2 and 3) are indicated between ~ 2.7 and ~ 2.5 Ga by ^{15}N enrichments of bulk sediments (Garvin et al., 2009; Godfrey and Falkowski, 2009; Thomazo et al., 2011; Busigny et al., 2013).



The product nitrate could then have been fixed into organic N by aerobic microorganisms (Stüeken et al., 2016), provided O_2 was not completely used by reactions (2–3) and/or other aerobic metabolisms such as Fe-oxidation. Denitrification (reduction of nitrite and/or nitrate) can also proceed by anaerobic metabolisms (reviewed in Stüeken et al., 2016). Moreover, in Archean ferruginous environments, the reduction of nitrite/nitrate coupled to the oxidation of Fe^{2+} could have been an important process (Miot et al., 2009; Kluglein et al., 2014). Microbial denitrification is consistent with the N isotope ratios recorded

between ~ 2.7 and ~ 2.5 Ga (Garvin et al., 2009; Godfrey and Falkowski, 2009; Thomazo et al., 2011; Busigny et al., 2013). Relative enrichments in ^{15}N observed in terrestrial sandstones compared to nearby marine sediments of the 3.22 Ga Moodies Group have been used to infer denitrification on land, and to suggest an atmospheric source of nitrate (Fig. 8D; Homann et al., 2018).

In order to explain the record of N-isotope ratios in 2.5 Ga banded iron formations, the alternative anaerobic ammonium oxidation metabolism using Fe^{3+} -oxides (reaction 4, FeAmox, e.g. Huang and Jaffé, 2018) has been proposed (Busigny et al., 2013).



This could have been followed by the metabolism that coupled nitrite reduction to Fe-reduction, consistent with the N-isotope record (Busigny et al., 2013). However, FeAmox (4) operation during the Archean has been challenged on the basis of calculated thermodynamic infeasibility at pH 6–8 and the difficulty to reconcile this process with the global-scale N-isotope record (Stüeken et al., 2016). Nevertheless, recent studies have shown that FeAmox proceeded in sediments at pH of ~ 7.5 (Guan et al., 2018), raising again the possibility that this metabolism existed during the Archean.

2.4. Geochemical evidence for oxygenic photosynthesis

Oxygenic photosynthesis is inferred to have appeared in the Archean on the basis of changes in the geochemical behavior of a number of elements of sedimentary rocks. Oxygen production may have started as early as 3.8 Ga, as suggested by the record of Cr isotope ratios (Frei et al., 2009, 2016; Crowe et al., 2013; Wei et al., 2020). Uranium enrichments and positive $\delta^{53}\text{Cr}$ values in the 2.95 Ga Ijzermyn iron formation have been interpreted as the result of oxidative weathering with oxygen (Crowe et al., 2013), but Albut et al. (2018) have shown that these signatures resulted of modern oxidative weathering. Similarly, uranium enrichments and positive $\delta^{53}\text{Cr}$ in the ~ 3.77 Ga Isua Greenstone Belt have been used to argue for small amounts of reactive oxygen species (O_2 , H_2O_2) of either photosynthetic or atmospheric origin (Frei et al., 2016). Negative $\delta^{53}\text{Cr}$ values in the ~ 3.0 Ga Nsuze paleosol have been used to support oxidative weathering (Crowe et al., 2013), whereas non-redox processes have been proposed for such isotope fractionations (Albut et al., 2018). Coupled U abundances and Fe-isotope ratios have been used to suggest O_2 production during deposition of shallow-water banded iron formations 3.2 Ga ago (Satkoski et al., 2015). This inference is supported by the U-Th-Pb geochronology demonstrating the antiquity of the U proxy (Satkoski et al., 2015). In contrast, this geochronology method has been used to show the Phanerozoic oxidation of the ~ 3.4 Ga Apex Basalt (Li et al., 2012). Molybdenum isotope ratios indicate oxygen production as early as 2.95 Ga (Planavsky et al., 2014; Kendall et al., 2017). Negative Ce-abundance anomalies support O_2 production during formation of shallow-water limestones ~ 2.8 Ga ago (Riding et al., 2014), but late alteration is difficult to rule out for such anomalies (Planavsky et al., 2020). Changes in the amplitude and structure of the mass-independent fractionations of the four stable isotopes of sulfur have been interpreted as the result of the production of oxygen between 2.7 Ga (Zerkle et al., 2012; Kurzweil et al., 2013; Izon et al., 2015) and 2.5 Ga (Kaufman et al., 2007), or of increased SO_2 emission (Halevy et al., 2010, but see discussions in previous references). The concentrations of Molybdenum and Rhenium correlated with a Re–Os age of 2495 ± 14 Ma (Anbar et al., 2007; Kendall et al., 2015), also indicate production of oxygen at the very end of the Archean. Aerobic Nitrogen isotope cycling is indicated between 2.7 and 2.5 Ga (see Section 2.3). Selenium isotope ratios are also consistent with oxygen production at 2.5 Ga (Stüeken et al., 2015b).

However, it is widely accepted that oxygen levels remained extremely low in the atmosphere and the ocean until ca. 2.5 Ga (Anbar et al., 2007; Lyons et al., 2014; Catling and Zahnle, 2020). This could

have been caused by the buffering of O_2 through its reactions with volcanic gasses (Catling and Zahnle, 2020), with H_2 and/or CH_4 generated through serpentinization of ultramafic rocks (Smit and Mezger, 2017), with the abundant reduced metals such as Fe^{2+} and Mn^{2+} , as well as metabolisms using O_2 (e.g., Fig. 2A, J, reactions 2–3). Geochemical modelling suggests that under an O_2 -free atmosphere, oceanic oases with 1–10 μM O_2 could have persisted and allowed aerobic metabolisms during the Archean (Olson et al., 2013). In addition, non-photosynthetic biotic and abiotic pathways have been proposed to allow the formation of small amounts of oxygen during the Archean (review in Fischer et al., 2016). In this context, it has been proposed that oxygenic photosynthesis may not have evolved until the earliest stages of the Great Oxidation Event (Kopp et al., 2005; Fischer et al., 2016) that is, between 2.45 and 2.31 Ga ago (Guo et al., 2009; Luo et al., 2016; Philippot et al., 2018). Doubt has been raised by some authors on the validity of the redox proxies discussed above and the antiquity of the processes they indicate (review in Fischer et al., 2016). However, microbial mats in shallow-water siliciclastic deposits (see Section 8), stromatolites (Section 9) and associated C-isotope fractionations (Section 3.3.1), and some microfossils (Section 6.2) further support this widely accepted geochemical record of Archean oxygenic photosynthesis.

3. Archean kerogen and the carbon isotope record

3.1. Preservation of the C-isotope record

The record of C isotope ratios in organic matter and carbonates provide constraints on ancient metabolisms. Indeed, isotopic fractionations imparted by heterotrophic metabolisms are relatively small (Fig. 2B, G and associated references). Thus, recycling by heterotrophs is only expected to produce small shifts in the isotopic composition of the bulk organic matter relative to the primary biomass produced by various autotrophs (Pearson, 2010). Biosynthetic and heterotrophic processes are, however, fractionating C isotopes differently among various classes of organic molecules (Hayes, 2001; Galimov, 2006). Selective preservation of different classes of molecules may shift significantly the total organic carbon isotope record (e.g., Sinningh Damsté et al., 1998). Similarly, C isotope ratio heterogeneities occur within Proterozoic microfossils of the same species where different ultrastructures (i.e., likely of distinct initial molecular composition) are variably preserved (Williford et al., 2013). In addition, the bulk-rock record of C isotope ratios may be biased by the presence of pyrobitumen (possibly of exogenous origin) in Archean rocks (Rasmussen and Buick, 2000; Rasmussen et al., 2008; Williford et al., 2016; Lepot et al., 2019). Petrography coupled with secondary ion mass spectrometry (SIMS) can help distinguish bitumen from kerogen and suggested that the isotopic composition of bitumen has been modified by radiolytic alteration in some Neoproterozoic rocks (Williford et al., 2016; Lepot et al., 2019). Carbon isotope fractionation effects during catagenesis and metamorphism are also usually considered small when the kerogen is analyzed in bulk, imparting no more than $\sim 3\%$ shifts in greenschist- and lower-temperature facies; these shifts, moreover, appear to correlate with the decrease in H/C and can thus be estimated using measurements of the latter (Hayes et al., 1983; Des Marais, 2001). Larger shifts may, however, be associated with hydrothermal alteration through isotopic exchange between organic matter and CO_2 (van Zuilen et al., 2007). Partial re-equilibration of the isotopic compositions between kerogen and carbonate minerals starts at temperatures of ca. 300 °C and may reach completion at temperatures above 650 °C (Valley, 2001). To the best of my knowledge, these hydrothermal and metamorphic processes remain poorly constrained at the microscale where original molecular heterogeneities, fluid pathways and carbonate grain distributions may have variously affected the preservation of the C isotope compositions.

3.2. Biotic versus abiotic kerogen in hydrothermally-influenced Paleoproterozoic settings

In anaerobic environments of the Archean, several non-photosynthetic metabolisms could have been responsible for the primary production of organic matter. These include chemolithoautotrophic metabolisms that could, for example, use H_2 to reduce CO_2 to methane (Fig. 2C) or to acetate (Fig. 2F), or to reduce sulfate (Fig. 2D). The source of H_2 could be fermentation of organic matter (Fig. 2B), although in this case it would require another source of organic matter to ferment. Alternatively, H_2 could possibly be sourced in the atmosphere (Tian, 2005), although its abundance was probably highly limited due to high rates of hydrogen escape to space (Catling, 2006). The H_2 molecule can also be generated during hydrothermal reactions such as serpentinization of peridotites (Mével, 2003; Konn et al., 2015). Carbon isotope ratios recorded in CH_4 and CO_2 hosted in fluid inclusions of the 3.48 Ga Dresser Formation have been interpreted as possible signatures of microbial methanogenesis through either H_2 -oxidation (Fig. 2F) or acetate fermentation (Fig. 2I) (Ueno et al., 2006a; Ueno et al., 2006b). Indeed, the Paleoproterozoic hydrothermal dyke systems, which include these CH_4 - and CO_2 -bearing fluids, are associated with basalts and thus form an environment that could have been replete with hydrothermal H_2 . This hydrogen, however, could also have led to the abiotic reduction of CO_2 to CH_4 and organic molecules through Sabatier or Fischer-Tropsch-type (FTT) reactions (Konn et al., 2015). Condensed organic molecules have been produced during experimental serpentinization of olivine at 300 °C (Berndt et al., 1996) and during hydrothermal dissolution of siderite at 200 °C and 300 °C (Milesi et al., 2015). These abiotic hydrothermal carbonaceous condensates may represent precursors to kerogen/pyrobitumen (Marshall et al., 2007), as further discussed in Section 5. Thus, abiotic reactions could explain the isotopic compositions (Lollar and McCollom, 2006; McCollom and Seewald, 2006; McCollom, 2016) recorded in methane (Ueno et al., 2006a) as well as those recorded in the kerogens of the Dresser Formation (Ueno et al., 2004) and the ~ 3.4 Ga Strelley Pool Formation (Lindsay et al., 2005), both associated with hydrothermal systems in mafic/ultramafic settings. Recently, texture-correlated C-isotope ratio heterogeneities among various microfossils and disseminated kerogen structures of the ~ 3.4 Ga Strelley Pool Formation and ~ 3 Ga Farrel Quartzite (see Section 6.5; House et al., 2013; Lepot et al., 2013; Oehler et al., 2017) have been used to argue against abiogenic organic matter. Heterogeneities in organic C isotope compositions among various carbonaceous microstructures (clots, stylolites, laminae, veins) in the Dresser Formation have similarly been used to argue against an abiotic hydrothermal origin (Morag et al., 2016).

3.3. Kerogen C-isotope ratios in non-hydrothermal settings

In many Archean settings, however, serpentinization reactions leading to the formation of abiotic H_2 , CH_4 , and/or organics can be ruled out because the necessary peridotites (e.g., in seafloor basaltic systems, Mével, 2003) or komatiites (McCollom and Seewald, 2013) would have been absent. These include thick siliciclastic deposits (Homann et al., 2016) and widespread organic-rich shale deposits (Buick, 2008) as old as ~ 3.2 Ga. These also include organic-poor sequences of carbonates, shales, silts and sands deposited onto magmatic rocks of more intermediate composition, which are abundant after 2.8 Ga, such as the Tumbiana Formation (see Section 9.2). In these contexts, organic carbon isotope ratio can be considered robust signatures of life.

3.3.1. Primary photoautotrophic production

Organic carbon isotope ratios with $\delta^{13}C_{org}$ values higher than ca. -36‰, however, remain difficult to attribute to specific metabolisms (Fig. 2). The ratios of carbon isotopes in organic matter displaying $\delta^{13}C_{org}$ values ranging between ca. -10‰ and ca. -36‰ (Thomazo

et al., 2009a) are consistent with oxygenic photosynthesis using the Calvin cycle (Schidlowski, 2001; Kaufman and Xiao, 2003), although other autotrophic processes could form similar values (Fig. 2C-F). The lower $\delta^{13}C_{org}$ values down to ca. -36‰ could have been overprinted by biodegradation processes such as respiration and/or methanogenesis (Fig. 2F-I) or could have resulted more directly from photosynthesis in CO_2 -rich conditions (Kaufman and Xiao, 2003). Organic-C isotope ratios measured in various stromatolite facies of the 2.72 Ga Tumbiana Formation revealed that conical-laminated stromatolites displayed $\delta^{13}C_{org}$ values of ca. -16‰, hence combining morphological and isotope ratio signatures that are best explained by photosynthesis (Coffey et al., 2013). In the distribution of $\delta^{13}C_{org}$ values in the Tumbiana Formation, a peak at ca. -34‰ was interpreted as the signature of kerogens rich in photosynthesis-derived biomass (Thomazo et al., 2009a; Williford et al., 2016), whereas lower values are discussed below.

3.3.2. Methane production, methanotrophy and acetogenesis

In contrast, $\delta^{13}C_{org}$ values lower than -36‰ recorded in Neoproterozoic kerogens have been interpreted to reflect a contribution by hydrogenotrophic methanogenesis (Fig. 2F), heterotrophic methanogenesis (Fig. 2I), and/or acetogenesis (Fig. 2C) to the biomass (Stüeken and Buick, 2018). Methanotrophy can also drive $\delta^{13}C_{org}$ to values lower than -36‰ (Fig. 2J-L). Values of $\delta^{13}C_{org}$ lower than -50‰ have been considered to reflect aerobic (Hayes, 1994) or anaerobic (Hinrichs, 2002) methanotrophy (Fig. 2J-L), or hydrogenotrophic acetogenesis (Fig. 2C; Slotznick and Fischer, 2016). Interestingly, these $\delta^{13}C_{org}$ values lower than -50‰ are mostly restricted to the interval between 2.8 and 2.6 Ga (Thomazo et al., 2009a; Flannery et al., 2016), suggesting that concentrations of the chemical species that could be used to oxidize methane (O_2 , nitrate, sulfate, Fe^{3+} , Mn^{4+}) progressively increased in the environment (Stüeken and Buick, 2018). The wide range of S-isotope fractionations in pyrites of lacustrine stromatolites of the 2.72 Ga Tumbiana Formation is consistent with microbial reduction of sulfate (Marin-Carbonne et al., 2018). Microbial reduction of sulfate is expected to outcompete acetogenesis for H_2 (Hoehler et al., 1998; Madigan et al., 2009; see discussion in Lepot et al., 2019), hence limiting the potential for this latter metabolism. The source of sulfate could have been anoxygenic photosynthesis (Overmann, 2006) and/or sulfur aerosols (e.g., Zerkle et al., 2012). In addition, microanalyses revealing the association of organic sulfur enrichments and $\delta^{13}C_{org}$ values lower than -50‰ argue for sulfate-fueled (anaerobic) methanotrophy (Fig. 2K) in lacustrine stromatolites of the Tumbiana Formation (Lepot et al., 2019). The importance of methanogenesis in 3.0 to 2.8 Ga rocks is indicated by $\delta^{13}C_{org}$ values ranging between -30 and -38‰, a signature that is predominant in lacustrine compared to marine settings (Stüeken and Buick, 2018). As discussed above, methanogenesis may have operated as early as 3.48 Ga in hydrothermally-influenced settings (Ueno et al., 2004; Ueno et al., 2006a). Interestingly, methanogenesis may be carried by cyanobacteria in aerobic conditions (Bižić et al., 2020) in addition to anaerobic pathways (Fig. 2F, I). Furthermore, $\delta^{13}C_{org}$ values as low as -45‰ suggest that methanotrophy operated in marine stromatolites (Flannery et al., 2018) ~3.4 Ga ago, possibly also in conjunction with microbial sulfate reduction (Bontognali et al., 2012).

3.3.3. Microbial respiration

Anaerobic microbial respiration metabolism (Figs. 2G-H) is supported by the coupling of Fe- and S-isotope fractionations in 2.7 Ga rocks (Archer and Vance, 2006). The correlation of ^{13}C -depletion and ^{56}Fe -depletion in Fe-rich carbonates also argues for remineralization of organic matter by Fe-respiration during the Archean (Johnson et al., 2008), possibly as early as 3.77 Ga (Craddock and Dauphas, 2011). However, the $\delta^{13}C_{carb}$ of the 3.77 Ga carbonates (from Isua, Greenland) can also be interpreted as inherited from metamorphic fluids (van Zuilen et al., 2003), and the high metamorphic grade of these rocks has

been deemed to make the interpretation of the carbonate Fe-isotope composition problematic (Marin-Carbonne et al., 2020). Depletions in ^{56}Fe are found in pyrites as old as 3.4 Ga in the Barberton Greenstone Belt that could be the result of dissimilatory iron reduction metabolism (Yoshiya et al., 2015). However, abiotic precipitation of pyrite may form a wide range of Fe-isotope fractionations (Guilbaud et al., 2011; Mansor and Fantle, 2019), and only the most extreme ^{56}Fe -depletions ($\delta^{56}\text{Fe} < -3.1\%$) recorded at ca. 2.7 Ga may be considered diagnostic of microbial reduction metabolisms (Yoshiya et al., 2012). Interestingly, the association of large ^{13}C -depletions in organic matter with large ^{56}Fe -depletions in pyrites in ca. 2.6 to 2.72 Ga rocks has been proposed in support of the hypothesis that microbial reduction of Fe^{3+} could have been coupled to anaerobic methanotrophy (Fig. 2K) instead of organic-matter respiration (Czaja et al., 2010; Yoshiya et al., 2012). The intimate association of kerogen with $\delta^{13}\text{C}_{\text{org}}$ values lower than -50.6% with Fe-rich chlorite and its prevalence in pyrite-rich layer is also consistent with the operation of Fe^{3+} -mediated methanotrophy in the Tumbiana Formation stromatolites (Lepot et al., 2019). Depletions in ^{13}C recorded in Archean carbonates (Thomazo et al., 2009a) may thus record conversion of organic matter to CO_2 by respiration but also by methanogenesis followed by methanotrophy. Furthermore, a large range of Fe-isotope ratios displaying a bimodal distribution and intrapyrite zonations provided evidence for microbial iron reduction in ca. 3.27 Ga cherts of the Mendon Formation of the Barberton Greenstone Belt, South Africa (Marin-Carbonne et al., 2020). These Fe-isotopes signatures are associated with $\delta^{13}\text{C}_{\text{org}}$ values higher than -32.1% , which suggests that this Fe-metabolism was performed through respiration of organic matter (Fig. 2H, Marin-Carbonne et al., 2020) rather than anaerobic methanotrophy (Fig. 2K).

3.4. Eoarchean (and Hadean) graphite

Graphite occurs in rocks of the ca. 3.77 Ga Isua supracrustal belt (Schidlowski, 2001, and references therein), in > 3.83 Ga rocks of the Akilia Island in Greenland (Mojzsis et al., 1996), in > 3.75 Ga rocks of the Nuvvuagittuq supracrustal belt in Canada (Papineau et al., 2011), and in ca. 3.95 rocks of the Saglek block of Canada (Tashiro et al., 2017). Importantly, metamorphism and metasomatism rendered difficult the distinction of sedimentary against magmatic protoliths for many Eoarchean rocks (van Zuilen, 2019). Most Paleo- to Neoproterozoic formations discussed in Sections 3.1–3.3 were submitted to greenschist- to sub-greenschist facies metamorphism. In contrast, these mentioned Eoarchean rocks underwent amphibolite- to granulite-facies metamorphism (van Zuilen, 2019), which allows extensive re-equilibration of the isotopic compositions of carbonates and/or metamorphic fluids (i.e., CO_2) with those of graphite (Chacko et al., 2001). In addition, graphite can form through thermal decomposition of carbonate minerals in such metamorphic facies (van Zuilen et al., 2002, 2003; Galvez et al., 2013; Milesi et al., 2015). None of the $\delta^{13}\text{C} > -15\%$ values recorded in graphite from Isua allow the distinction of re-equilibrated biogenic graphite and graphite from carbonate decomposition (Ueno et al., 2002). Subsequent microscale C-isotope ratio analyses of Eoarchean graphite, however, revealed $\delta^{13}\text{C}$ values as low as ca. -37% that cannot be readily explained by carbonate decomposition reactions (Mojzsis et al., 1996; Rosing, 1999; Ueno et al., 2002; McKeegan et al., 2007; Papineau et al., 2010a; Tashiro et al., 2017).

Step-combustion experiments revealed that non-graphitic carbonaceous matter exists in Isua rocks that could explain the low $^{13}\text{C}_{\text{org}}$ compositions recorded in some bulk-rock analyses of graphite-poor samples (van Zuilen et al., 2002), consistent with microscopic observation of recent microbes in Isua rocks (Westall and Folk, 2003). However, $\delta^{13}\text{C}_{\text{org}}$ values lower than -20% have been found at the microscale in graphite inclusions as well as in bulk rocks of the Saglek block displaying values as high as 0.6 wt% organic carbon (compared to contaminant levels of less than 0.01% carbon measured in van Zuilen et al., 2002). Amorphous carbonaceous matter as well as relatively low-

crystallinity graphite have been observed in Akilia samples (McKeegan et al., 2007; Papineau et al., 2010b; Lepland et al., 2011) and poorly crystalline carbonaceous matter was also observed in a Nuvvuagittuq sample (Papineau et al., 2011). These findings have been used to suggest that a fraction of the carbonaceous matter could have been introduced after the earliest metamorphic event. Observation of fluid inclusions with CO_2 , H_2O , graphite and some CH_4 in a pillow basalt breccia in Isua (Heijlen et al., 2006) and in a gneiss of Akilia (Lepland et al., 2011) and graphite paragenesis in Akilia (Papineau et al., 2010b) indicate that graphite could have formed from CO_2 - and/or CH_4 -bearing metamorphic fluids. Nevertheless, the crystallinity of graphite (as studied with Raman spectroscopy) in the Saglek metapelites appears consistent with mineral indicators of the first peak metamorphism event, which has been used to support a sedimentary origin (Tashiro et al., 2017). Fluid-deposited and poorly-crystalline graphite could have formed relatively late in the history of these rocks from a biogenic organic source, from abiogenic carbon of magmatic origin, or from hydrothermal Fisher-Tropsch-Type (FTT) reaction products (see discussion in Papineau et al., 2010a). To my knowledge, microanalyses have not yet distinguished the isotopic compositions of fluid-deposited graphite and of poorly crystalline graphite against those of potentially sedimentary graphite (i.e., metamorphosed kerogen). Furthermore, a clastic geological context has been used to argue against FTT reactions as the origin of the Saglek graphite (Tashiro et al., 2017). However, abiotic insoluble carbonaceous matter may have formed/deposited in precursor rock(s) before their erosion and sedimentation in the Saglek block sediments.

Finally, graphite with $\delta^{13}\text{C}$ values of ca. $-24 \pm 5\%$ included in a ca. 4.1 Ga zircon has been considered as a potential trace of Hadean life (Bell et al., 2015). An alternative deep-carbon origin has been discussed by House (2015) who pointed out the occurrence of carbon in Martian basalts (Steele et al., 2012) and recent models involving deep Fe–C phases (Horita and Polyakov, 2015).

4. Archean organic biomarkers?

Hopanoic biomarker molecules indicative of cyanobacteria (Brocks et al., 1999) and/or anoxygenic photosynthetic bacteria (Rashby et al., 2007) and steranes diagnostic of eukaryotes have been extracted from the bitumen (soluble organic matter) of Neoproterozoic rocks (Brocks et al., 1999; Waldbauer et al., 2009). Hopanoic suggestive of methanotrophs (Eigenbrode et al., 2008) and/or other bacteria (Welander and Summons, 2012), as well as biomarkers suggestive of Archaea (Ventura et al., 2007) have been extracted in ca. 2.7 Ga old rocks. However, recent re-analysis of rocks of this age led to a consensus that these labile biomarkers represent contaminants. Indeed, the isotopic composition of the molecules in the extractable (bitumen) fraction is markedly distinct from that of the associated kerogen, hence they cannot be genetically related (Rasmussen et al., 2008; Close et al., 2011). Moreover, the increased concentration of hydrocarbons on the surface of previously sampled drill cores argues for anthropogenic contamination (Brocks, 2011). Most importantly, the same biomarkers were absent during analysis of recent cores drilled in contamination-limiting conditions (French et al., 2015). Hopanoic and steroid biomarkers have been detected after crush-leach of metaconglomerates that trapped oil-rich fluid inclusions between ca. 2.45 and 2.2 Ga (George et al., 2008) and of sandstones that trapped oily inclusions between ca. 2.1 and 1.98 Ga (Dutkiewicz et al., 2007). The oldest soluble biomarkers are thus most likely Paleoproterozoic in age.

5. Structure of Archean kerogen

5.1. Mass spectrometry

The insoluble fraction of the organic matter (the kerogen) is generally considered as syngenetic with the host rock. Biomarkers

molecules such as proteins and hopanoids can be physically encapsulated and/or covalently bound to kerogen (Abbott et al., 2001; Mongenet et al., 2001). Large saturated hydrocarbon molecules (i.e. with > 25 carbons, including diagnostic biomarkers), however, appeared absent from Neoproterozoic kerogen (Brocks et al., 2003) and from more mature ~ 3.4 Ga (Marshall et al., 2007) and 3.48 Ga (Derenne et al., 2008; Duda et al., 2018) kerogens. Gas-chromatographic mass-spectrometry (GC-MS) analyses, performed along catalytic hydro-pyrolysis of kerogen, have documented an essentially (poly)aromatic carbon structure in kerogens of the Neoproterozoic (Brocks et al., 2003) and of the ~ 3.4 Ga Strelley Pool Formation (Marshall et al., 2007). This abundance of aromatic structures has also been observed at the microscale using time-of-flight SIMS in the ~ 3.3 Ga Josefsdal chert (Westall et al., 2011) and in the Strelley Pool Formation (Fadel, 2018; Fadel et al., 2020). Aliphatic hydrocarbons have been detected by pyrolysis of Archean kerogens (Hayes et al., 1983). Pyrolysis (Derenne et al., 2008) and catalytic hydro-pyrolysis (Duda et al., 2018) of kerogens extracted from cherts of the 3.48 Ga Dresser Formation and catalytic hydro-pyrolysis of cherts of the ~ 3.4 Ga Strelley Pool Formation (Marshall et al., 2007) yielded alkanes with a strong decrease in abundances at carbon numbers > 18. This alkane size distribution is consistent with that observed in a Mesoproterozoic kerogen (Marshall et al., 2007) and in solvent-extracted cyanobacterial biomass (Duda et al., 2018), but is different from some abiotic alkane series generated using hydrothermal Fischer-Tropsch-Type (FTT) synthesis (Duda et al., 2018). However, it can be noted that higher relative abundances of alkanes with $n > 18$ were observed in other hydrothermal FTT syntheses (McCullom et al., 1999) and that alkane size distributions can be finely tuned using various catalysts in gas-phase (not hydrothermal) FTT syntheses (Subramanian et al., 2016). Moreover, hydrocarbons with an odd-over-even carbon number predominance, consistent with a biogenic origin, have been detected with pyrolysis GC-MS in a 3.48 Ga kerogen of the Dresser Formation (Derenne et al., 2008), but their origin has been questioned as their high abundance (inferred with Nuclear Magnetic Resonance) appeared at odds with the thermal maturity of the rock (Marshall et al., 2007). In addition, the predominance of certain isomers and the even-over-odd predominance that distinguish biotic lipids from FTT synthesis products have been shown to disappear during experimental maturation of biogenic kerogen (Mißbach et al., 2018), making such kind of predominance surprising in over-mature Paleoproterozoic kerogen.

5.2. Functional group signatures

Organic molecules commonly contain heteroatoms (that is, atoms other than C and H: mostly O, N, S, and P for biogenic molecules) that bond to C and H to form diverse functional groups. Various functional groups were detected in Archean organic matter with X-ray absorption spectroscopy. In the ~ 3.4 Ga Strelley Pool Formation and in the 3.45 Ga Apex Chert, organic oxygen occurs in the form of carboxyl and phenol/hydroxyl groups (De Gregorio et al., 2010; Alleon et al., 2018). Organic nitrogen occurs in the Strelley Pool Formation in the form of amide, nitrile and/or imine as well as aromatic N (Alleon et al., 2018). Organic S occurs as thiophene groups in kerogen of the 2.72 Ga Tumbiana Formation (Lepot et al., 2019), and is also likely common in various Archean kerogens as indicated by elemental analyses (Oehler et al., 2010; Bontognali et al., 2012; Sugitani et al., 2015a). The functional-group signature of the Strelley Pool Formation organic matter analyzed with X-ray absorption spectroscopy is similar to that of the 1.88 Ga Gunflint Iron Formation in spite of the higher apparent maturity, which is inferred from Raman spectroscopy (De Gregorio et al., 2010; Alleon et al., 2018). In particular, atomic N/C-ratios reach high values of up to 0.24 in microfossil-like structures (Alleon et al., 2018). In contrast, kerogen in veins of the Strelley Pool Formation analyzed with SIMS displayed extremely low N/C consistent with a distinct origin (Oehler et al., 2009). Similarly, kerogen in Strelley Pool Formation

veins displayed higher H/C ratios and higher $\delta^{13}\text{C}$ compared to other carbonaceous microstructures of the host chert (Lepot et al., 2013). Kerogen in cherts of the 3.47 Ga Mount Ada Basalt appeared highly aromatic, with only low abundance of H and O heteroatoms in spite of the apparent maturity (inferred with Raman spectroscopy) being close to that of Strelley Pool Formation kerogens (Alleon et al., 2019). Unlike the latter, organic matter in the Mount Ada Basalt deposit may derive from biomass that has been altered by hydrothermal fluids before encapsulation in silica; alternatively, it could represent abiotic pyrobitumen as suggested by the association with Fe-Cr-Ni alloys that could have catalyzed abiotic hydrocarbon formation (Alleon et al., 2019). Heteroatoms including H, N, P and S were also detected in graphite grains from Eoarchean rocks of Akilia using SIMS (Papineau et al., 2010b). Heteroatoms including C=O (carbonyl) groups and C≡N (nitrile) bonded to aromatic groups (but no C-H groups) have been detected in graphite from the > 3.7 Ga Isua supracrustal belt using infrared spectroscopy coupled to atomic force microscopy (AFR-IR, Hassenkam et al., 2017). The coupling of AFR-IR and Raman spectroscopy has been used to argue that these functional groups occurred on the outer surface of graphite grains, where they would have migrated during graphitization (Hassenkam et al., 2017). The presence of heteroatoms in Paleoproterozoic kerogen and Eoarchean graphite is consistent with formation after biogenic kerogen (e.g., Oehler et al., 2006; Lepot et al., 2009a; De Gregorio et al., 2010). Various heteroatoms are, however, also present in meteoritic organic matter (e.g., Garvie and Buseck, 2004; Le Guillou et al., 2014), on graphite and graphene surfaces produced during industrial processes (Hemraj-Benny et al., 2006; Girard-Lauriault et al., 2012), in abiotic macromolecular carbon found in Martian basalts (Steele et al., 2012), and in hydrothermal/FTT reaction products (Rushdi and Simoneit, 2004; McCullom and Seewald, 2006; De Gregorio et al., 2010). The mere presence of these heteroatoms is thus not diagnostic of life. Further analysis of their concentrations and associated molecular structures may help discriminate their origin. In addition, heterogeneities in heteroatom contents and molecular structures, combined with textures such as possible microfossils (Oehler et al., 2010; Lepot et al., 2013; Alleon et al., 2018) and isotopic compositions (House et al., 2013; Lepot et al., 2013) may provide important clues for the origin of Archean organic matter.

5.3. The elusive abiotic hydrothermal kerogen

Formation of solid carbonaceous matter can be favored thermodynamically during serpentinization of ultramafic rocks (Milesi et al., 2016). Serpentinization experiments have produced solids comprising aliphatic and aromatic molecules (Berndt et al., 1996), but it is not known if they were soluble or not. Thorough solvent extraction of some FTT synthesis products yielded solid residues, yet their pyrolysis only produced extremely small carbonaceous molecules; hence it is not yet known whether such residues could turn into kerogen during subsequent burial diagenesis and metamorphism (Mißbach et al., 2018). Although serpentinized ultramafic rocks displayed possibly abiotic asphaltene (soluble, Scirè et al., 2011), matured sub-seafloor biomass (Pasini et al., 2013), abiotic amino acids (Ménez et al., 2018), and poorly-ordered, likely-abiotic carbonaceous matter (Sforza et al., 2018), their association with insoluble abiotic organic matter has remained elusive. Poorly-crystalline to crystalline graphite forms at temperatures > 430 °C (e.g., Dufaud et al., 2009; Foustoukos, 2012; Galvez et al., 2013) that may compare with Eoarchean carbonaceous matter (Section 3.4). In contrast, abiotic formation of insoluble organic matter with functional groups including heteroatoms and alkanes, similar to those observed in biogenic kerogens and in the weakly-metamorphosed Archean kerogens as described above, has yet to be demonstrated in hydrothermal systems on Earth. In contrast, such complex insoluble organic matter is known from meteorites (Derenne and Robert, 2010) and from aerosols that may have formed in early Earth's atmosphere (Trainer et al., 2006; Maillard et al., 2018).

6. Archean microfossils?

Due to their simple shapes, and association with rocks that underwent complex alteration (during diagenesis, metamorphism, and sometimes metasomatism and/or weathering), many microstructures that have been considered as Archean microfossils have been re-evaluated as dubiofossils, pseudofossils, or contaminants (e.g., Schopf and Walter, 1983; Buick, 1990; Brasier et al., 2005). Thus, criteria have been developed to demonstrate the antiquity of microfossils, as summarized by Brasier et al. (2005), including: 1) their observation in thin sections where they are enclosed in primary minerals (such as quartz) that would be stable enough to withstand metamorphism, 2) the replicability of their finding, and 3) their association with specific sedimentary structures (e.g. laminae). More recently, Raman spectroscopy has allowed to correlate the maturity of carbonaceous matter and the metamorphic grade of host rocks (e.g., Tice et al., 2004; Lepot et al., 2008). Although this demonstrates pre-metamorphic ages for carbonaceous matter, this does not rule out oil migrations and hydrothermal emplacement during diagenesis. Moreover, criteria have been developed to assess the biogenicity of the morphology (e.g., cell wall or other anatomical parts) of carbonaceous microstructures or their mineral replacements/molds, also summarized in Brasier et al. (2005). These criteria, together with new micro-chemical analyses, are discussed below in a comparison between putative Archean fossils and plausible abiotic mimics.

6.1. Spherical and hemispherical microstructures

6.1.1. Microfossils versus cell-like mimics

Spherical, sub-spherical and hemispherical carbonaceous microstructures have been documented in several Archean cherts, e.g., Schopf et al. (2007) and citations below. However, spherical structures are so simple in shape that they can be mimicked by mineral growths such as abiotic amorphous silica (opal, Fig. 3A-B). Opal spheres can have a wide range of diameters with unimodal, bimodal (Fig. 3B) and multimodal size distributions (Jones and Renaut, 2007) that would be difficult to distinguish from cell populations (Schopf, 1975). Opal commonly forms coalescing hemispherical microstructures (Fig. 3A). Opal spheres commonly display concentric banding (Jones and Renaut, 2007). Similar populations of hemispherical quartz structures with concentric bands have been observed in Proterozoic (Fig. 3C, Javaux and Lepot, 2018) and in Archean (Buick, 1990; Ueno et al., 2006c; Fig. 3D) cherts; in these structures, organic matter particles coat concentric rings within hemispheres as well as the periphery of clusters of hemispheres. Such botryoid microstructures also form on a millimeter-to centimeter-scale and are thus undoubtedly abiotic. They have accreted carbonaceous matter (Buick, 1990) likely through migration enabled by hydrothermal fluids (Knoll et al., 2016). In a 3.0 Ga chert, Ueno et al., 2006c, reported a range of coccoid-like microstructures commonly forming single spheres or spheres doublets (Fig. 3E) that resemble microfossils of microorganisms such as cyanobacteria. However, they also found in the same assemblage sphere doublets and clusters of multiple hemispheres as part of botryoidal quartz (Fig. 3D) – accordingly, the microstructures of Fig. 3D were considered abiogenic and the associated cell-like structures of Fig. 3E remained putative microfossils (dubiofossils).

Experiments of copolymerization of amino-acids produced single and twinned microspheres (Fox and Yuyama, 2006) that resemble Archean microstructures such as those of Fig. 3E-H. Self-assembly of organic molecules with sulfur also formed microspheres (Cosmidis and Templeton, 2016). It remains unknown, however, whether such coprecipitates would remain (or become) insoluble during diagenesis and metamorphism (see Section 5.3).

Spherical to ovoid microfossil-mimicking structures can also form through aggregation of carbonaceous matter onto the walls of abiotic vesicles (gas bubbles) in volcanic ash grains (Wacey et al., 2018a;

Wacey et al., 2018b, Fig. 3F). This observation has led to the re-evaluation of some microstructures previously inferred as microfossils. In my view, it also warrants careful re-investigation of aggregates of putative coccoid microfossils recently reported in ~ 3.4 Ga volcanoclastic-rich deposits, which have been interpreted as cyanobacteria (Kremer and Kaźmierczak, 2017).

Because these various spherical mimics exist, additional biogenicity criteria beyond the simple spherical morphology (as listed in Brasier et al., 2005) are required for the small spherical microstructures described for example in Figs. 3G-H and 6B, in Pflug (1967), Engel et al. (1968), Knoll and Barghoorn (1977), Schopf et al. (2010), in Sugitani et al. (2010), and in Lepot et al. (2013).

6.1.2. Preservation of cell walls?

An important feature that has been proposed to distinguish abiotic spherical structures and cellular microfossils is the distribution of organic matter at the nanoscale. Some clearly abiotic, coalescing hemispherical microstructures are characterized by discontinuous halos of nanometric organic particles (e.g., Fig. 3C-D), whereas well-preserved microfossils display continuous carbonaceous walls (Javaux et al., 2004; Wacey et al., 2012; Fadel et al., 2017; Lekele Baghekema et al., 2017; Lepot et al., 2017). Nevertheless, a discontinuous carbonaceous wall structure may not rule out a microfossil origin, as discontinuities can form during alteration of cell walls or sheaths/capsules (Lekele Baghekema et al., 2017; Guo et al., 2018). The preservation of a continuous carbonaceous wall in flattened spherical vesicles (Fig. 3I; Javaux et al., 2010) or in spheres (Grey and Sugitani, 2009) during acid maceration of the host quartz has similarly been interpreted as a criterion for microfossil identification. Indeed, the discontinuous nanoparticles observed along microfossil-mimicking microstructures would likely disperse upon acid maceration. In the ~ 3.0 Ga Farrel Quartzite (Grey and Sugitani, 2009) and the ~ 3.4 Ga Strelley Pool Formation (Delarue et al., 2020), the preservation of simple carbonaceous spheres < 60 μm in diameter in macerates is in line with a cellular origin of some of the similarly-sized spheres observed in thin sections (e.g., Fig. 3G-H). As stressed above, this does not mean that all of the diverse spherical structures observed in macerates and thin sections are cellular. For instance, small spheres (1–15 μm) in diameter extracted by maceration of cherts of the 3.48 Ga Dresser Formation (Dunlop et al., 1978) have been reinterpreted as pyrobitumen droplets based on their dense carbonaceous structures observed under the optical microscope (Buick, 1990). Hence, cellularity inferences requires further ultrastructural investigations down to the nanoscale.

6.1.3. Large spherical microfossils

Large spheres, commonly up to ca. 300 μm in diameter have been observed in the macerates of the 3.22 Ga Moodies Group (Fig. 3I, Javaux et al., 2010) and in thin sections of the 2.52 Ga Gamohaan Formation (Czaja et al., 2016); these studies demonstrated thin-walled vesicular structures by transmission electron microscopy (TEM) and 3D laser-confocal imaging, respectively. The folding of these spheres, in particular, is not known in abiotic mimics (Buick, 2010; Javaux et al., 2010; Czaja et al., 2016). Modern cyanobacteria only reach up to 60 μm in diameter, and only few other bacteria can reach this size range including giant bacteria that oxidize sulfur using O₂ or nitrate (Javaux et al., 2010; Czaja et al., 2016). These sulfur-oxidizing and other giant bacteria are, however, « not known to form recalcitrant biopolymers » (Javaux et al., 2010), hence experimental taphonomy is required to address the preferred hypothesis of Czaja et al. (2016). Thus, giant bacteria, eukaryotes and/or unknown/extinct prokaryotes cannot be discriminated among these giant spherical microfossils (Javaux et al., 2010). In contrast with these large microfossils where ultrastructures can be investigated on macerated specimens, ultrastructural data (e.g., TEM) is lacking to supplement the optical documentation of smaller (1 to ~ 60 μm) spherical microfossils. Such nanoscale investigation performed on numerous microfossils in ultrathin rock sections could help

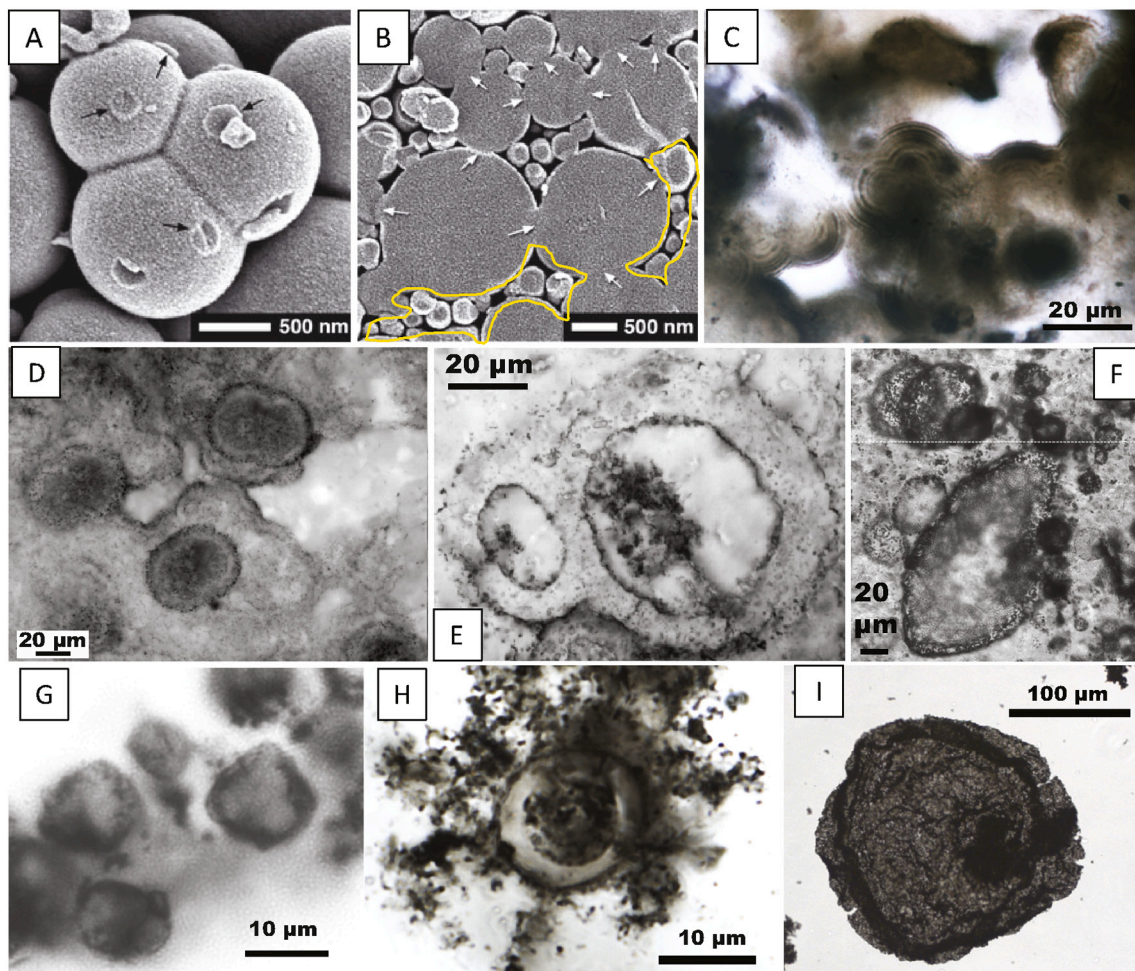


Fig. 3. Spherical microstructures. (A–B) Coalescing hemispherical opal-A microstructures from recent siliceous sinters of Iceland, from Jones and Renaut (2007), reproduction permission below. (A) Aggregates of opal spheres with variable diameters; arrows indicate connection of now-detached spheres. (B) Cross-section of aggregate of spheres with bi-modal size distribution. Arrows indicate coalescence of spheres. Places where segmented (and branching) filamentous structures may form are outlined in yellow (discussed in Section 6.3). (C) Microscopic botryoids, that is coalescing hemispherical microstructures, in cherts of the 1.88 Ga Gunflint Iron Formation. Organic matter was deposited on the concentric layering forming these structures. (D–E) Spheroids from the 3.0 Ga Clearville Formation, from Ueno et al., 2006c, reproduction permission below. (D) Botryoids similar to those in (C). (E) Coalescing cell-like microstructures. (F) Lenticular and ovoid vesicles in a volcanoclastic fragment of the ~ 3.4 Ga Strelley Pool Formation, from Wacey et al. (2018b), reproduction permission below, photomicrograph courtesy of David Wacey, University of Western Australia. (G) Sub-spherical microstructures in the ~ 3.0 Ga Farrel Quartzsite (sample GHTE-11). (H) Concentric spherical structures in the ~ 3.4 Ga Strelley Pool Formation (sample WF4). (I) Spherical microstructure commonly accepted as Archean microfossil in acid-macerated sample of the 3.22 Ga Moodies Group. Photomicrograph courtesy of Emmanuelle J. Javaux (Université de Liège). Panels (A–B) Reproduced from Jones and Renaut (2007), Copyright (2007) Wiley. Used with permission from (Brian Jones & Robin W. Renaut, Microstructural changes accompanying the opal-A to opal-CT transition: new evidence from the siliceous sinters of Geysir, Haukadalur, Iceland, *Sedimentology*, 54, 921–948, Wiley). Panels (D–E) reproduced from Coccoid-Like Microstructures in a 3.0 Ga Chert from Western Australia, Yuichiro Ueno, Yukio Isozaki, and Kenneth J. McNamara, *International Geology Review*, Vol. 48, p. 78–88, 2006, Taylor & Francis, reprinted by permission of the publisher (Taylor & Francis Ltd, <http://www.tandfonline.com>). Panel (F) reprinted from *Earth and Planetary Science Letters*, 487, David Wacey, Martin Saunders, Charlie Kong, Remarkably preserved tephra from the 3430 Ma Strelley Pool Formation, Western Australia: Implications for the interpretation of Precambrian microfossils, 33–43, © 2018, with permission from Elsevier. (For interpretation of the references to colour in this figure legend, the reader is referred to the web version of this article.)

constrain the taxonomy and biogenicity of the smaller spherical structures similar to what has been achieved on Paleoproterozoic microfossils (e.g., Lepot et al., 2017). Targets for nanoscale investigations are the internal structures and multiple layers—which may represent ultrastructures such as cell walls and/or capsules—observed in ~ 3.0 Ga spheroids (e.g., Fig. 3E, G–H; Sugitani et al., 2009), as well as combined colony-like association and capsule-like structures observed in spheroids of the ~ 3.4 Ga Strelley Pool Formation (Schopf, 2006).

6.1.4. Demonstration of antiquity required

Multi-layered hollow carbonaceous structures have been found in macerates of a carbonaceous chert vein of the ~ 3.45 Ga Hoogenoeg Formation of South Africa (Gliksun et al., 2008). Their association of an

outer layer with increased electron density, and thick, possibly concentrically layered inner layers is similar to microfossils observed in sub-recent Antarctic stromatolites (fig. 7D in Lepot et al., 2014). However, it remains difficult to confirm that these structures are indigenous to the studied metamorphic rocks as they have only been reported in ultrathin sections made for TEM, and evidence for mature graphitizing structures—which can be obtained by observation of dark colour and high reflectance under the optical microscope, by high-resolution TEM or by Raman spectromicroscopy—are still lacking. Such a demonstration of the indigenous nature of candidate microfossils is particularly necessary in surface-exposed rocks, as demonstrated by the observation of endolithic microbial contamination in Eoarchean rocks (Westall and Folk, 2003).

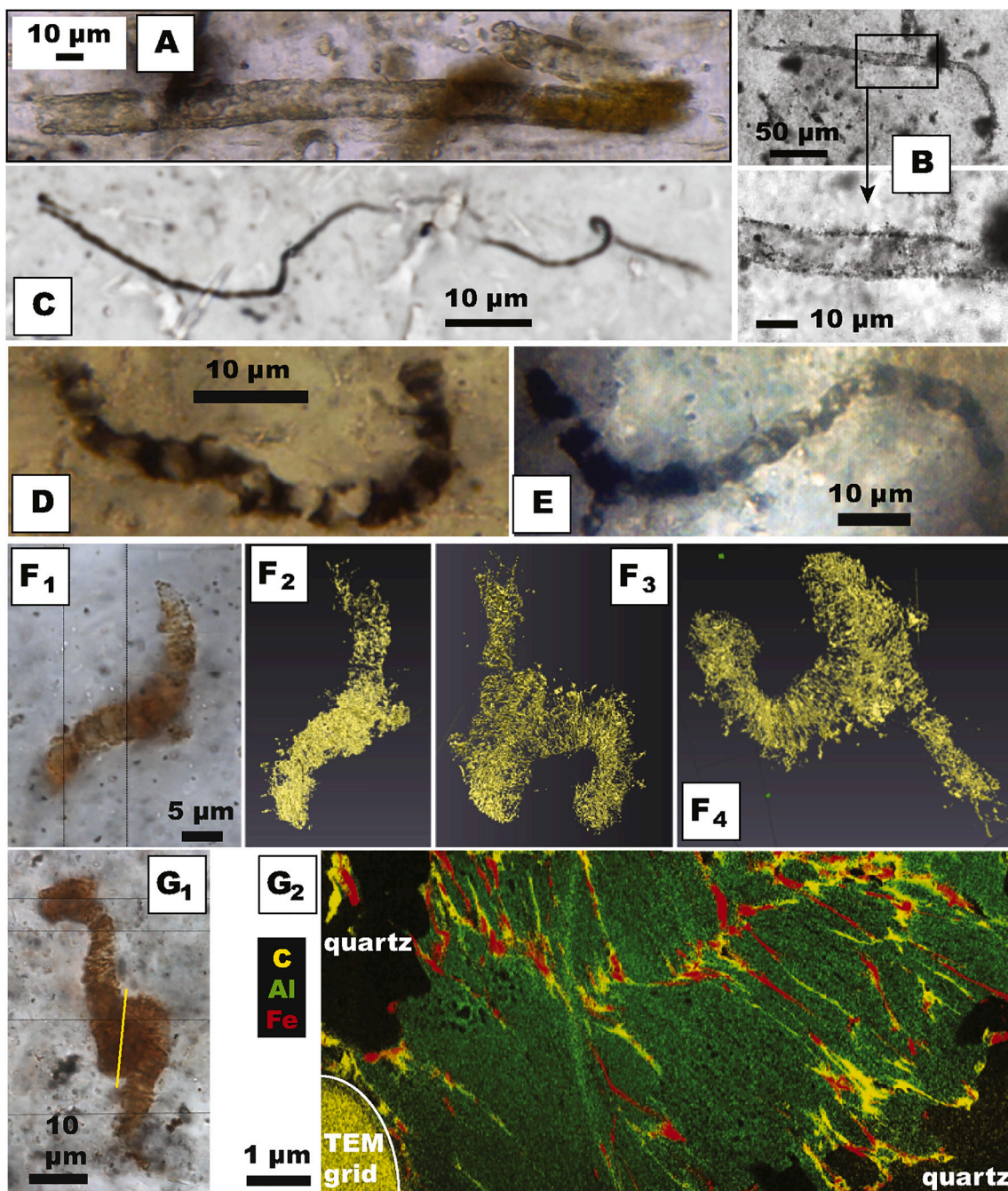


Fig. 4. Examples of Archean filamentous microfossils and/or dubiofossils. (A) Filamentous sheaths (*Siphonopycus transvaalensis*) of the 2.52 Ga Gamohaam Formation, South Africa. Photomicrograph courtesy of J.W. Schopf, UCLA (reproduction permission below). (B) Tubular filaments from the ~ 3.4 Ga Strelley Pool Formation, photomicrographs courtesy of K. Sugitani, Nagoya University (reproduction permission below). (C) Dense carbonaceous thread within botryoidal chert of the ~ 3.4 Ga Strelley Pool Formation (multiplane image obtained by combination of photomicrographs recorded at multiple focal depths using the Extended-Depth-of-Focus of Nikon NIS software, sample WF4). Note twisted morphology. (D-E) Dense, discontinuous carbonaceous filaments of the 3.465 Ga Apex Chert of Australia. Photomicrographs courtesy of J.W. Schopf, UCLA, reproduction permissions below. (F₁₋₄, G₁₋₂) Other filamentous structure of the 3.465 Ga Apex Chert, from Wacey et al. (2016b). Images courtesy of D. Wacey, University of Western Australia (reproduction permissions below). F₁, optical image; F₂-F₄, 3D reconstructions of Scanning Electron Microscope images recorded after sequential etching of the area with Focused Ion Beam (FIB) and displayed under various angles. (G₁) The yellow line on the photomicrograph shows the position of the Focused Ion Beam section. (G₂) Overlap of elemental maps recorded in a TEM for Carbon, Iron and Aluminum in the FIB section made in (G₁). Aluminosilicates fill the filament and are randomly interspersed with carbonaceous matter and iron minerals at the grain boundaries. **Panels 4A and 4E** reprinted from Precambrian Research, 158, J. William Schopf, Anatoliy B. Kudryavtsev, Andrew D. Czaja, Abhishek B. Tripathi, Evidence of Archean life: Stromatolites and microfossils, 141–155, Copyright (2007), with permission from Elsevier. **Panel 4B** reprinted from Precambrian Research, 226, Kenichiro Sugitani, Koichi Mimura, Tsutomu Nagaoka, Kevin Lepot, Makoto Takeuchi, Microfossil assemblage from the 3400 Ma Strelley Pool Formation in the Pilbara Craton, Western Australia: Results form a new locality, 59–74, Copyright (2013), with permission from Elsevier. **Panel 4D** reprinted from Gondwana Research, 22, J. William Schopf, Anatoliy B. Kudryavtsev, Biogenicity of Earth's earliest fossils: A resolution of the controversy, 761–771, Copyright (2012), with permission from Elsevier. **Panels F1–4 and G1–2** reprinted from Gondwana Research, 36, David Wacey, Martin Saunders, Charlie Kong, Alexander Brasier, Martin Brasier, 3.46 Ga Apex chert 'microfossils' reinterpreted as mineral artefacts produced during phyllosilicate exfoliation, 296–313, Copyright (2016), with permission from the International Association for Gondwana Research, Elsevier. (For interpretation of the references to colour in this figure legend, the reader is referred to the web version of this article.)

6.2. Tubular filaments (sheaths?)

6.2.1. Neoproterozoic sheath microfossils

Filamentous sheaths have been found in the 2.52 Ga Gamoha Formation in South Africa (Fig. 4A; Klein et al., 1987; Schopf et al., 2007). Although these filaments did not preserve their internal chains of cells, their large diameter and apparent thickness are consistent with a cyanobacterial affinity (Klein et al., 1987), and their orientation in fossil microbial mats suggests phototactism (Butterfield, 2015). Other bacteria may display similarly large sheaths (Knoll et al., 1988), but are usually far thinner. The high apparent sheath thickness, as observed under the optical microscopes, may have increased due to organic matter migration (Knoll et al., 1988). Nanoscale analysis invalidated this taphonomic hypothesis for Paleoproterozoic sheaths of similar metamorphic grade (Lekele Baghekema et al., 2017).

6.2.2. Ambient inclusions trails

A group of tubular microstructures named Ambient Inclusions Trails (AITs) can mimic some features of filamentous microfossils. AITs are commonly found in Archean cherts (Knoll and Barghoorn, 1974; Buick, 1990; Wacey et al., 2008a). These tubes have been inferred to form through displacement of a crystal, enhancing tubular dissolution of its mineral matrix (e.g., quartz) aided by the pressure of ambient fluids generated through biotic and/or thermal decomposition of organic matter (Knoll and Barghoorn, 1974; Wacey et al., 2008a; Luo et al., 2018) and possibly aided by reactions involving clays (Wacey et al., 2016a). Ambient inclusions trails may also form through migration of carbonaceous particles, as observed at the tip of garnet microtubes in amygdules of Neoproterozoic volcanic rocks (Lepot et al., 2009b). Indeed, AITs are commonly found in sedimentary rocks in association with organic matter and display a size and tubular shape that is consistent with those of microfossils. For this reason, they have been mistaken for microfossils before the abiotic AIT model of Tyler and Barghoorn (1963). In particular, their association with organic carbon, including late internal coating by organic matter, may enhance their similarity to microfossils (Wacey et al., 2008b). Some tubular microstructures remain difficult to interpret (Grey, 1986), perhaps because we still lack a full comprehension of the mechanism(s) that can form AITs and the diversity of associated abiotic microstructures. The formation of AITs in Archean volcanoclastic grains is discussed in Section 7.3.

6.2.3. Meso- to Paleoproterozoic carbonaceous tubes

Tubular carbonaceous microstructures, although rare, have been found in Meso- and Paleoproterozoic cherts (Awramik et al., 1983; Kiyokawa et al., 2006; Wacey et al., 2011; Sugitani et al., 2013), as shown in Fig. 4B. The oldest examples occur in cherts of the 3.47 Ga Mount Ada Basalt (Awramik et al., 1983; Sugitani, 2019), for which a possible abiotic origin of carbonaceous clots has been proposed (Section 5, Alleon et al., 2019). However, simple tubular microstructures can be generated by quartz crystallization (Kleitz et al., 2001) and also commonly occur in volcanoclastic material (see Section 7.3). Coating of these structures with minute amounts of migrated carbonaceous matter could form the granular carbonaceous textures observed in those tubes. In vitro self-assembly of organic molecules onto elemental sulfur could form tubules with extremely thin organic walls (Cosmidis and Templeton, 2016) that may decompose into such granular carbonaceous filaments. Thus, with the exception of mat-forming, thick and folded sheath microfossils as shown in Fig. 4A, the abiotic origins of carbonaceous microtubes remains so far difficult to distinguish from true Archean microfossils. Nanoscale characterization of highly degraded Paleoproterozoic microfossils demonstrated that granular textures and filamentous microstructures are not (in those cases) directly related with quartz growth structures (Fadel et al., 2017; Lekele Baghekema et al., 2017). Similar nanoscale investigations of Paleoproterozoic tubes may help distinguish biotic from abiotic microstructures. Interestingly, one such tubular filament of the Strelley Pool

Formation displays a spherical microstructure that could correspond to a cell remnant (fig. 6f in Sugitani et al., 2013).

Tubular carbonaceous filaments, also with a highly granular appearance, have been described within cobweb-like carbonaceous textures in cherts of the ~ 3.4 Ga Strelley Pool Formation (Sugitani et al., 2010; Schopf et al., 2017). A highly similar “cobweb macrostructure” is formed by some Paleoproterozoic microfossil assemblages (Schopf et al., 2015; Fadel et al., 2017; Barlow and van Kranendonk, 2018). Granularization of kerogen was documented in filamentous sheaths of these Paleoproterozoic cobwebs (Fadel et al., 2017). The cobweb-forming Paleoproterozoic microfossil assemblages have been interpreted as deepwater communities of bacteria that metabolized sulfur (Schopf et al., 2015; Barlow and van Kranendonk, 2018) or iron (Fadel et al., 2017).

6.2.4. Eoarchean hematitic tubes

Tubular Fe₂O₃ microstructures in a 3.77–4.28 Ga quartzite have recently been proposed as the oldest possible microfossils (Dodd et al., 2017); in this case, the absence of carbonaceous matter in the tubes makes a biogenic origin even more tenuous. Their Fe-mineralization and filamentous morphology has been compared with Fe-oxidizing bacteria occurring in modern hydrothermal vents (Dodd et al., 2017). However, similarly large and branching Fe-oxide filaments form abiotically in such environments (Johannessen et al., 2020).

6.3. Segmented filaments

6.3.1. Regularly segmented filaments

Chains of highly degraded (granular) barrel-shaped microstructures have been documented in cherts associated with stromatolitic carbonates of the 2.72 Ga Tumbiana Formation (Schopf and Walter, 1983). Their microstructure is consistent with those of cyanobacteria, although other bacteria such as some sulfur-oxidizers can form similar microfossils (e.g., Knoll et al., 1988). These microfossils, together with other evidence, are consistent with photosynthesis during the deposition of the Tumbiana Formation (Buick, 1992; Thomazo et al., 2009b; Flannery and Walter, 2012; Sim et al., 2012; Coffey et al., 2013; Williford et al., 2016). Filament molds with regular segmentation very similar to (cyano)bacteria were described in silicified cavities of the 3.22 Ga Moodies Group (Homann et al., 2016). However, they apparently did not preserve kerogen and their antiquity remains to be demonstrated as they occurred on (freshly-made) fracture surfaces in possibly poorly-crystalline minerals.

6.3.2. Discontinuous threads

Discontinuous solid threads of carbonaceous matter, commonly less than one to a few micrometers in diameter and up to several hundred micrometer long (Fig. 4C) are commonly found in Paleoproterozoic cherts (Awramik et al., 1983; Buick, 1984; Walsh, 1992; Ueno et al., 2001a; Sugitani et al., 2013). Similar solid threads of carbonaceous matter are also observed in Paleoproterozoic microfossil assemblages (Knoll et al., 1988; Schopf et al., 2015; Lekele Baghekema et al., 2017; Barlow and van Kranendonk, 2018). In ~2.1 Ga cherts, carbonaceous matter that appeared as thick threads under the optical microscope displayed a filamentous sheath structure in TEM (Lekele Baghekema et al., 2017). However, the narrow population of these Paleoproterozoic threads so far has not shown any diagnostic ultrastructures such as cell wall or sheath that would help demonstrate that they are true microfossils (Buick, 1990). They might represent filamentous microfossils that have been compressed between aligned quartz crystals (Knoll et al., 1988). Alternatively, some of the Paleoproterozoic carbonaceous threads may represent migrated carbonaceous matter (Buick, 1990). Indeed, they radiate in places from carbonaceous clots (Buick, 1984, 1990). Their common occurrence in botryoidal quartz zones but absence in non-botryoidal chert of the same rock [that instead hosts other forms such as spheres and lenses: Figs. 3H, 5A, and 6; Sugitani et al., 2013] makes it

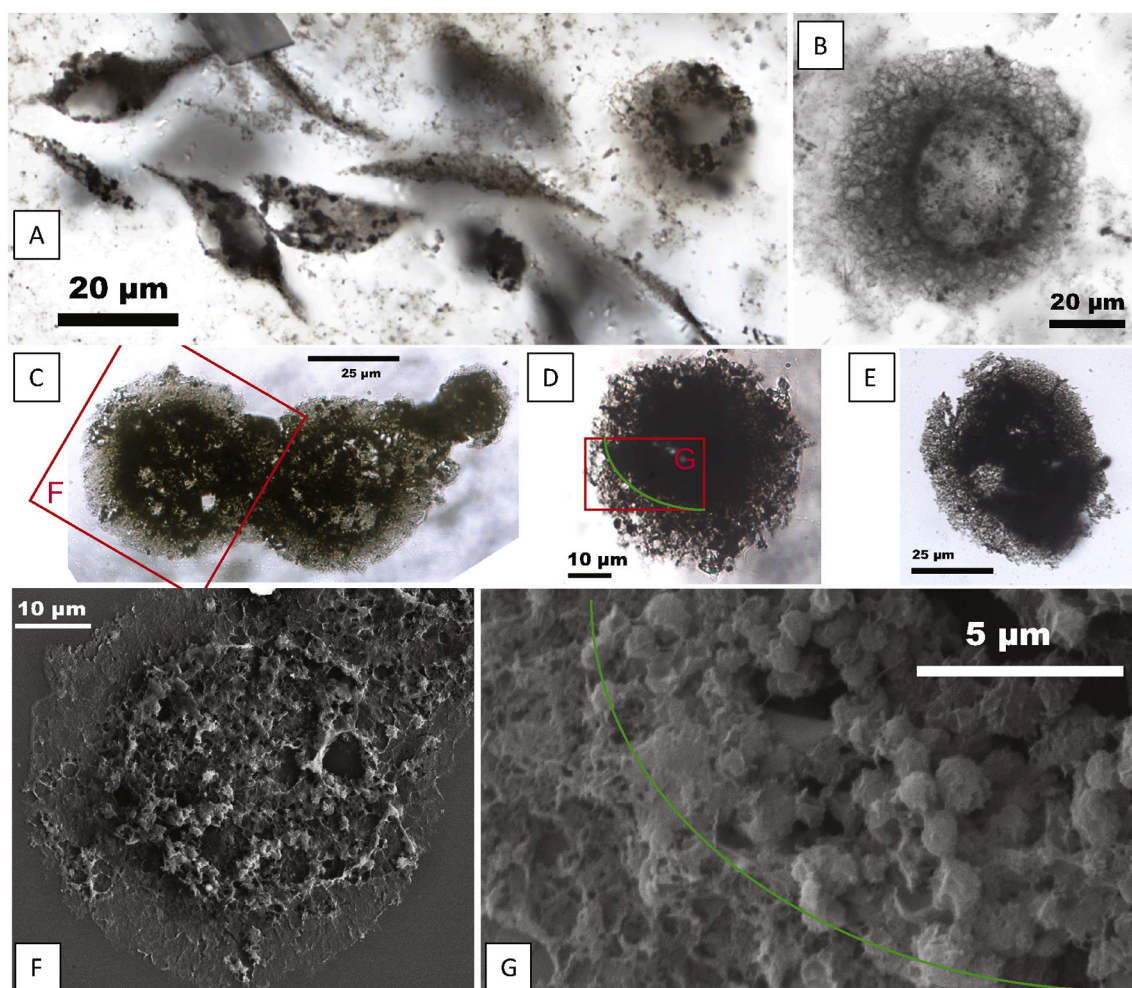


Fig. 5. Lenticular carbonaceous microstructures from the ~ 3.4 Ga Strelley Pool Formation. **(A)** Assemblage of lenticular microstructures displaying equatorial flanges disposed in various positions (sub-horizontal: top-right, oblique: all other). Note internal vesicles filled with clear white chert and dark carbonaceous globules. **(B)** Multiplane image (assemblage of four focal-plane photomicrographs combined by the CombineZP software by Alan Hadley). Source photomicrographs courtesy of K. Sugitani, Nagoya University. The internal vesicle is outlined by a darker wall and the equatorial flange is reticulated by fine-grained quartz. **(C-G)** Lenticular microstructures recovered by acid maceration residue as detailed in Sugitani et al. (2015a). **(C-E)** Optical images. **(F-G)** Backscattered electron images of the regions boxed in **(C)** and **(D)**, respectively. The lens in **(F)** displays a relatively smooth flange surrounding a reticular central body. In **(D, G)**, the green lines denote the transition between the central body (upper right) rich in carbonaceous globules, and the flange (lower left) with reticulate texture. **Panels C-D and F** are Copyright (2015) Wiley. Used with permission from K. Sugitani, K. Mimura, M. Takeuchi, K. Lepot, S. Ito, and E. J. Javaux, Early evolution of large micro-organisms with cytological complexity revealed by microanalyses of 3.4 Ga organic-walled microfossils, *Geobiology*, John Wiley and Sons Ltd. (For interpretation of the references to colour in this figure legend, the reader is referred to the web version of this article.)

difficult to count these structures among microfossils.

Pyritic filaments found in a 3.2 Ga volcanogenic massive sulfide deposit have been interpreted as pyritized fossils of microorganisms that could have inhabited a sub-seafloor environment (Rasmussen, 2000). Recent study of these pyritic filaments at the nanoscale found their structure consistent with pyritized Paleoproterozoic *Gunflintia* microfossils, but possible abiogenic origins were also discussed (Wacey et al., 2014b).

6.3.3. Paleoarchean filaments with cell-like structures?

Some segmented carbonaceous threads with a larger (< 20 µm) diameter have been found in the 3.465 Ga Apex Chert (Fig. 4D-G) and have been considered as the oldest microfossils (Schopf, 1993; Schopf et al., 2007; Schopf and Kudryavtsev, 2012). Similar microstructures have been found in cherts of the 3.48 Ga Dresser Formation (Ueno et al., 2001b) and of the 3.47 Ga Mount Ada basalt (Awramik et al., 1983; Sugitani, 2019). The segmentation of carbonaceous matter in these structures is reminiscent of chains of barrel-shaped cells commonly found in cyanobacteria (Schopf et al., 2007). Several problems

have been raised in subsequent studies questioning the microfossil nature of these structures: first, the Apex Chert microstructures have been shown to occur in a hydrothermal black chert vein rather than in a stratiform seafloor-precipitated chert (Brasier et al., 2002, 2005). In these veins, the carbonaceous threads are relatively scarce and the carbonaceous matter texture is dominantly clotted (Brasier et al., 2005). Second, the observed microstructures have been interpreted as formed through displacement of carbonaceous matter during recrystallization of amorphous silica to spherulitic quartz by Brasier et al. (2005). Alternatively, the same microstructure could have formed earlier, after initial precipitation of silica in the vein: in Fig. 3B is shown a spherulite of opal, the porosity of which could be filled by migrated hydrocarbons, to form segmented microstructures reminiscent of chains of cells. Third, abiotic precipitation of silica and barium carbonate has been shown to form various microstructures that partly resemble (in size and shape) the Apex Chert candidate microfossils (García-Ruiz et al., 2003, 2017; Rouillard et al., 2018). Importantly, these abiotic models allow for the formation of branching filaments as shown in Fig. 4F, which is more difficult to reconcile with the ultrastructure of

living microorganisms (Wacey et al., 2016b). However, in my view, fusion of adjacent filamentous microfossils during advanced post-mortem alteration might also form similar branching, in particular in such rocks affected by metamorphism and metasomatism. In line with this idea, it has been proposed that the Apex Chert microstructures could have formed through advanced thermal maturation of colonies of coccoid microorganisms as observed in Silurian rocks (Każmierczak and Kremer, 2009). Fourth, recent nanoscale studies of filaments in the Apex Chert have shown that they are commonly filled by aluminosilicates (Fig. 4F-G) and used this criterion to infer an abiogenic morphology (Brasier et al., 2015; Wacey et al., 2016b, 2019). Nevertheless, some Proterozoic microfossils are fossilized internally with aluminosilicates (Wacey et al., 2014c); hence small-scale migration of kerogen during recrystallization of these aluminosilicates might produce similar structures starting with a filamentous microfossil.

Recently, microanalyses have shown heterogeneities in organic carbon isotope ratios among various filamentous structures of the Apex Chert (Schopf et al., 2018). Similar heterogeneities occur among candidate microfossils of the Strelley Pool Formation (see Section 6.5). These heterogeneities argue that not all carbonaceous textures originated from a single migrated source and are consistent with a biotic origin for the observed organic matter. However, the Apex Chert has a complex hydrothermal alteration history that is reflected in its Raman spectra (Sforna et al., 2014), which remains to be addressed in conjunction with the C-isotope signatures. Altogether, the Apex Chert segmented microstructures and their counterparts in the Dresser Formation are best considered as dubiofossils.

6.4. Lenticular microstructures

Lenticular (also called “spindle-shaped”) microstructures found in Archean cherts have been considered as microfossils. Such lenticular microstructures have first been found in ca. 3.3 Ga rocks (Pflug, 1967), now assigned to the upper Onverwacht Group by Schopf (1975), then in the ~ 3.4 Ga Kromberg Formation of the upper Onverwacht Group (Walsh, 1992). Other similar structures (Fig. 5) have been found in Australian cherts of the ~ 3.4 Ga Strelley Pool Formation (Sugitani et al., 2010; Sugitani et al., 2013) and the ~ 3.0 Ga Farrel Quartzite (Sugitani et al., 2007). These “spindles” are characterized by a “flange”, which is a disk surrounding the main lenticular structure in equatorial position (Fig. 5). Flange-free lenses with a more regular outline occurring in sandstones of the Strelley Pool Formation (Fig. 3F) have initially been interpreted as microfossils (Wacey et al., 2011). However, it has been recently shown that carbonaceous and titaniferous coating of volcanic vesicles formed such structures in Archean sandstones (Wacey et al., 2018a; Köhler and Heubeck, 2019).

Acid maceration of cherts of the Strelley Pool Formation revealed important ultrastructural features of the flanged lenticular microstructures. The flanged lenses are 20 to ~ 100 µm large individuals formed of acid-resistant organic matter that does not disperse upon removal of the mineral matrix (Sugitani et al., 2015a), which has been used to infer the microfossil nature of spherical microstructures (Section 6.1). The lenses can form chains of up to seven individuals that are connected by the central body and/or the flange (e.g., Fig. 5C), a structure that to my knowledge cannot be related to known microorganisms, and which has been suggested to represent a division pattern (Sugitani et al., 2015a). Moreover, the central body is commonly populated by vesicles and carbonaceous globules (Fig. 5). These internal structures could represent relicts of reproductive cells (Sugitani, 2019) such as baecocytes of pleurocapsalean cyanobacteria (Waterbury and Stanier, 1978), which is not compatible with the hypothesis that overarching chains of lenses are related by division. Alternatively, the internal globules could represent storage granules or taphonomic accumulations of molecules (such as lipids) into kerogen (Lepot et al., 2013; Williford et al., 2013), or microfossils of heterotrophic cells (e.g., Glikson et al., 2008; Grey and Willman, 2009).

The lens-forming structures and their flanges comprise a reticulated network of carbonaceous matter. Together with granules, this reticulated network is commonly filling part of the central body (Figs. 5A, C-G, and 6A). The central body is, however, sometimes almost free of organic matter and surrounded by a reticulate wall (Fig. 5B-C). When observed after acid maceration, the overall flanged structure of the Strelley Pool Formation lenses appear strikingly similar to Proterozoic microfossils such as *Simia simica*, *Simia annulare*, or *PterospERMOSIMORPHA* (Schopf, 1992; Tang et al., 2013; Miao et al., 2019). This together with the empty central body of some lenses is consistent with a cellular nature. Alternatively, the alveolar structure observed in many lenticular structures has led to the proposition that these represent microscopic colonies rather than single cells (Javaux, 2019). In this scenario, the abundant globules in lenses may represent remains of colony-forming microorganisms.

6.5. Heterogenous C-isotope signatures in Archean microfossils

Microanalyses of organic carbon isotope ratios in cherts of the Strelley Pool Formation using SIMS show that the main textural types of kerogen all have isotopic compositions distinct from that of the late cross-cutting carbonaceous veins ($\delta^{13}\text{C}$ values of ca. -26 to -30‰ ; Fig. 6; Lepot et al., 2013), hence implying a distinct origin. Spherical structures displayed distinct $\delta^{13}\text{C}$ values clustering at ca. -35 to -36‰ (Fig. 6B; Lepot et al., 2013), whereas lenses displayed a wider range of $\delta^{13}\text{C}$ values from ca. -29 to -44‰ (Fig. 6A; Lepot et al., 2013; Oehler et al., 2017). Detailed SIMS investigation of lenses in a sample (Fig. 6A) revealed that the reticulate network of organic matter that shape the lenses has a distribution of $\delta^{13}\text{C}$ values that peaks sharply between -30 and -32‰ whereas lower values down to -40‰ could be attributed to globule-rich parts. Kerogen clots display a bimodal distribution of isotope ratios, with the more ^{13}C -depleted mode clustering close to the values of the globule-poor lenses, whereas lens-independent clusters of globules display low $\delta^{13}\text{C}$ values similar to those observed in the in-lens globules (Figs. 6A and C-D; Lepot et al., 2013). The much lower $\delta^{13}\text{C}$ values recorded in the globules within the lenses cannot be readily explained as the heterotrophic biomass feeding on lenticular microfossils, as the globules would be expected to have a similar isotopic composition (Fig. 2G-I; Pearson, 2010) to that of the reticulate lens-forming organic matter. Methanogens or other chemoautotrophs could have generated such low $\delta^{13}\text{C}$ values (Fig. 2C-F and J-L), and hydrothermal alteration of methanogenic archaea could have formed similar globules (Glikson et al., 2008). Alternatively, selective preservation of lipid aggregates in the globules and of structural (i.e., wall-forming) polysaccharides in the reticulate network could explain the isotope ratio heterogeneity recorded in the lenses (Lepot et al., 2013; Williford et al., 2013).

In the ~ 3 Ga Farrel Quartzite, spheres and lenses displayed $\delta^{13}\text{C}$ values averaging at ca. -37‰ (House et al., 2013; Oehler et al., 2017). Although the globular and globule-free lenses were not distinguished in these studies, my inspection of the figures in House et al. (2013) and of Farrel Quartzite thin sections suggests that the analyzed lenses were globule-rich, which would make the isotope ratio of both spheres and globule-rich lenses in the Farrel Quartzite similar to their counterparts of the Strelley Pool Formation. House et al. (2013) and Oehler et al. (2017) observed that the background carbonaceous matter in the Farrel Quartzite displayed higher $\delta^{13}\text{C}$ values than associated lenses. Finally, $\delta^{13}\text{C}$ values of ca. -35 to -39‰ were measured in lenses (likely globular based on my interpretation of the published microscopy) of the Kromberg Formation of South Africa, although these could not be clearly distinguished from the background carbonaceous matter (Oehler et al., 2017).

Altogether, these texture-coupled C isotope heterogeneities (and the associated H/C heterogeneities) argue that the different carbonaceous microstructures were generated from biotic organic matter rather than from hydrothermally-generated abiotic hydrocarbons (Lepot et al.,

2013). These data also further support the hypothesis that the spheres and the lenses represent microfossils, and suggest that the parent microorganisms could have performed distinct metabolisms (House et al., 2013; Lepot et al., 2013; Oehler et al., 2017). The consistency of C isotope ratios in spheres and lenses from three different formations on different cratons spanning about 400 Ma strongly supports this view. However, the metabolisms of these microfossils remain difficult to constrain. The $\delta^{13}\text{C}_{\text{org}}$ values of about -36‰ recorded in spherical and lenticular microstructures studied by House et al. (2013), Lepot et al. (2013) and Oehler et al. (2017) are consistent with heterotrophic biomass (such as that of sulfate-reducers or methanogens, Fig. 2G, I) or hydrogenotrophic acetogens / sulfate reducers (Fig. 2C-D), possibly influenced by methanotrophic (Fig. 2K-L) biomass. However, the Strelley Pool Formation lenses display a reticulate wall structures with higher $\delta^{13}\text{C}$ that is interspersed with low $\delta^{13}\text{C}$ granules of possible taphonomic origin (lipid granules, heterotrophs; Lepot et al., 2013) suggesting that photoautotrophy ($\delta^{13}\text{C}_{\text{org}} > -36\text{‰}$, Section 3.3.1) and other autotrophic metabolisms are also possible. Photosynthesis is consistent with the proposition that these lenses represent planktonic forms (House et al., 2013) whereas most microorganisms using other autotrophic pathways may not form such large and complex cells today.

7. Archean trace fossils?

7.1. Titanite microtubes in Archean rocks

Titanite (CaTiSiO_5) microtubes have been found in several occurrences of metamorphosed basaltic pillow-lava rims and basaltic hyaloclastite breccias spanning ~ 3.5 to ~ 2.5 Ga (Furnes et al., 2004; Banerjee et al., 2006, 2007; Bridge et al., 2010; McLoughlin et al., 2010) as well as in Silurian metabasalts (Fliegel et al., 2011). They also occur in 2.72 Ga metamorphosed volcanoclastic rocks (Philippot et al., 2009; Lepot et al., 2011, Fig. 7).

7.2. Possible modern counterparts: biotic or abiotic?

The titanite microtubes display some morphological similarities with microtubes occurring in unmetamorphosed, only partly altered basaltic glass. It has been proposed that such microtubes as well as granular textures occurring at the margins of basaltic glass formed through microbially-induced dissolution (Fisk et al., 1998; Furnes et al., 2007 and references therein), consistent with experiments demonstrating that microbes can corrode volcanic glass (Staudigel et al., 1995, 1998; Thorseth et al., 1995a). However, granular textures have been generated in abiotic alteration experiment (Fisk et al., 2013; McCollom and Donaldson, 2019). Tubular alteration textures have never been reproduced experimentally in biotic or abiotic experiments. Microbes have only—to my knowledge—been directly imaged at the interface between glass and secondary alteration phases (Thorseth et al., 2001; Fisk et al., 2003) and in thick alteration phases occurring in contact with fresh glass or in fractures (Thorseth et al., 2003; Ivarsson et al., 2008; Templeton et al., 2009; Cockell et al., 2010; McLoughlin et al., 2011), but not in the granular or tubular textures directly. Filamentous and sub-spherical structures occurring at the root of microtubes in glass have been proposed as microbial remains (Banerjee and Muehlenbachs, 2003), but their carbonaceous nature was not demonstrated and the filamentous structure displayed a range of diameters including nanostructures that are difficult to reconcile with cells. Organic compounds have been detected in the microtubular and the granular textures using electron microscopy, fluorescent dye staining, and spectromicroscopy (Thorseth et al., 1995b; Torsvik et al., 1998; Furnes et al., 2001; Banerjee and Muehlenbachs, 2003; Walton and Schiffman, 2003; Benzerara et al., 2007; Fliegel et al., 2012; Wacey et al., 2014a; Wacey et al., 2017). It is, however, conceivable that the organic matter located in these textures may have migrated, from biomass living outside of the glass or from overlying deep-sea sediments. Extracellular DNA is, for

instance, abundant in deep-sea sediments where it largely dominates biomass-associated DNA (Dell'Anno and Danovaro, 2005). The clay minerals that fill the microtubes (Benzerara et al., 2007; Wacey et al., 2014a) may thus act as sites of retention and preservation of migrated molecules such as nucleic acids (Cai et al., 2006). In addition, common fluorescent dyes can bind to clays and/or clays loaded with labile organic compounds (Fisk et al., 2003; Klauth et al., 2004). Location of organic matter in petrographic sections of porous materials (Wacey et al., 2014a) also remains difficult without assessment of plausible contamination by slide-mounting glue (e.g., Torsvik et al., 1998; Fadel et al., 2020). Furthermore, abiotic organic matter may form in basalts (Steele et al., 2012). Hydrothermal alteration in presence of smectite—which is a common basaltic glass alteration product within microtubes (Crovisier et al., 2003; Benzerara et al., 2007; Wacey et al., 2017)—may also load these clays with abiotic organic molecules (Ménez et al., 2018). This absence of direct and conclusive observation of cells of endolithic glass-boring microorganisms in tubular and granular alteration texture, and the observation that pores in granular alteration zones are often too small to host bacteria (Alt and Mata, 2000) suggest that these alteration textures could be formed by remote microbes (Fliegel et al., 2012; Fisk et al., 2019). In contrast, dendritic microtubes in basaltic glass that display an irregular cross-section have been considered as likely abiotic (Pedersen et al., 2015). Weaknesses in the glass induced by stress and/or variations in chemical compositions, as well as similarities with dendritic structures observed in glass and in steel have been used to argue for a possible abiotic origin to such and other microtubes (Pedersen et al., 2015). Microtubes have also been found in olivine grains of terrestrial and Martian basalts, and the terrestrial examples also bound fluorescent dyes (Fisk et al., 2006; White et al., 2014). The sub-parallel nature of these generally-straight and locally-curved microtubes suggests that they could represent decorated dislocation networks as observed in olivine (e.g., Zeuch and Green, 1977). A similar preferential alteration may provide an alternative abiotic explanation to the directionality of bundles of microtubes observed in some volcanic glass samples (Walton, 2008 versus Pedersen et al., 2015). Altogether, it remains so far difficult to show that microtubular and granular alteration textures arise from biocorrosion in recent volcanic glass, hence limiting the use of their putative metamorphosed equivalent as biosignatures.

7.3. Origin of the titanite microtubes

7.3.1. Carbonaceous matter?

In support of the biogenicity of the Archean titanite microtubes, carbonaceous matter has been detected in some of the Archean tubes by X-ray mappings (Furnes et al., 2004; Banerjee et al., 2006, 2007), but the antiquity of this carbon has not been addressed by techniques such as Raman spectroscopy or high-resolution TEM, and contamination by late hydrocarbons and/or slide-mounting glue remains plausible. Extensive, high-sensitivity (NanoSIMS) investigations failed to detect carbonaceous matter in the oldest titanite microtubes (McLoughlin et al., 2012), consistent with my hypothesis that the earlier reports of organic compounds (Furnes et al., 2004; Banerjee et al., 2006) may represent topography-related artefacts of electron microprobe mapping.

7.3.2. The Tumbiana Formation microtubes

The Mingah member of the 2.72 Ga Tumbiana Formation displays what represents to date the most diverse assemblage of microtubular structures occurring in chloritized volcanoclastic material (Fig. 7; Lepot et al., 2011). Abundant pre-metamorphic carbonaceous matter occurs at the edge of grains and as nanoparticles at the tip of and/or within microtubes (Fig. 7D and L). Among the various microtube types are those terminated by sulfide crystals and carbonaceous matter and filled by quartz, titanite, \pm chlorite \pm TiO_2 (Fig. 7G and J-L). Evidence of striation on the edge of some tubes (Lepot et al., 2011) and spallation of the terminal particles (Fig. 7J-L, arrows) support the origin of these

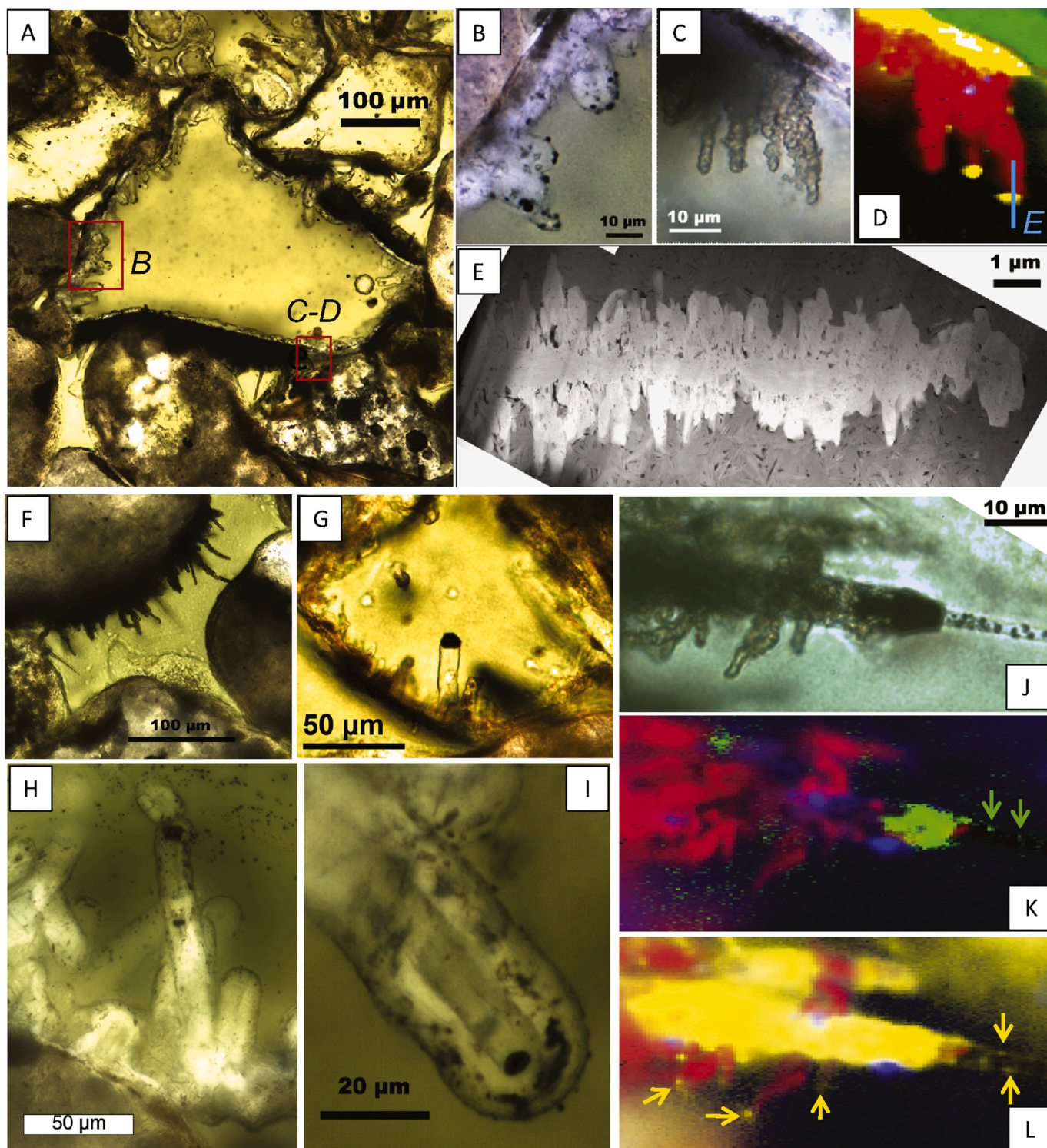


Fig. 7. Microtubes in volcanoclastic rocks of the Tumbiana Formation. (A) Angular and sub-rounded volcanoclastic material. Chlorite appears in green. (B) Calcite (white) microtubes associated with chalcopyrite (black) in chlorite at the edge of the ash grain in the left box in (A). (C) Titanite (brown) microtubes radiating from the ash grain into chloritized cement at the right box in (A). (D) Raman map of the zone in (C) showing titanite (red) in the microtubes, the calcite rim (green) of the grain in (A), and the abundant carbonaceous matter (yellow) at the root of the microtubes but also at their tip. (E) Scanning TEM image of the FIB section cut along the blue line in (D) showing the dendritic structure of the titanite (white) microtube in chlorite (grey). (F) Titanite microtubes in the chlorite zone between sub-rounded volcanoclastic grains. (G) Pyrite-terminated and quartz-filled ambient inclusion trail occurring in a chloritized ash grain. (H–I) Calcite (white) microtubes with terminal sulfide (pyrite and/or chalcopyrite) inclusions and central chlorite (green) core. (J) Pyrite-terminated AIT overgrown by titanite microtubes. (K–L) Raman maps of (J) showing pyrite inclusions (green, green arrows), carbonaceous matter (yellow, yellow arrows), titanite (red) and TiO_2 (blue). (A–L) Reprinted from Earth and Planetary Science Letters, 312, Kevin Lepot, Karim Benzerara, Pascal Philippot, Biogenic versus metamorphic origins of diverse microtubes in 2.7 Gyr old volcanic ashes: Multi-scale investigations, 37–47, Copyright (2011), with permission from Elsevier. (For interpretation of the references to colour in this figure legend, the reader is referred to the web version of this article.)

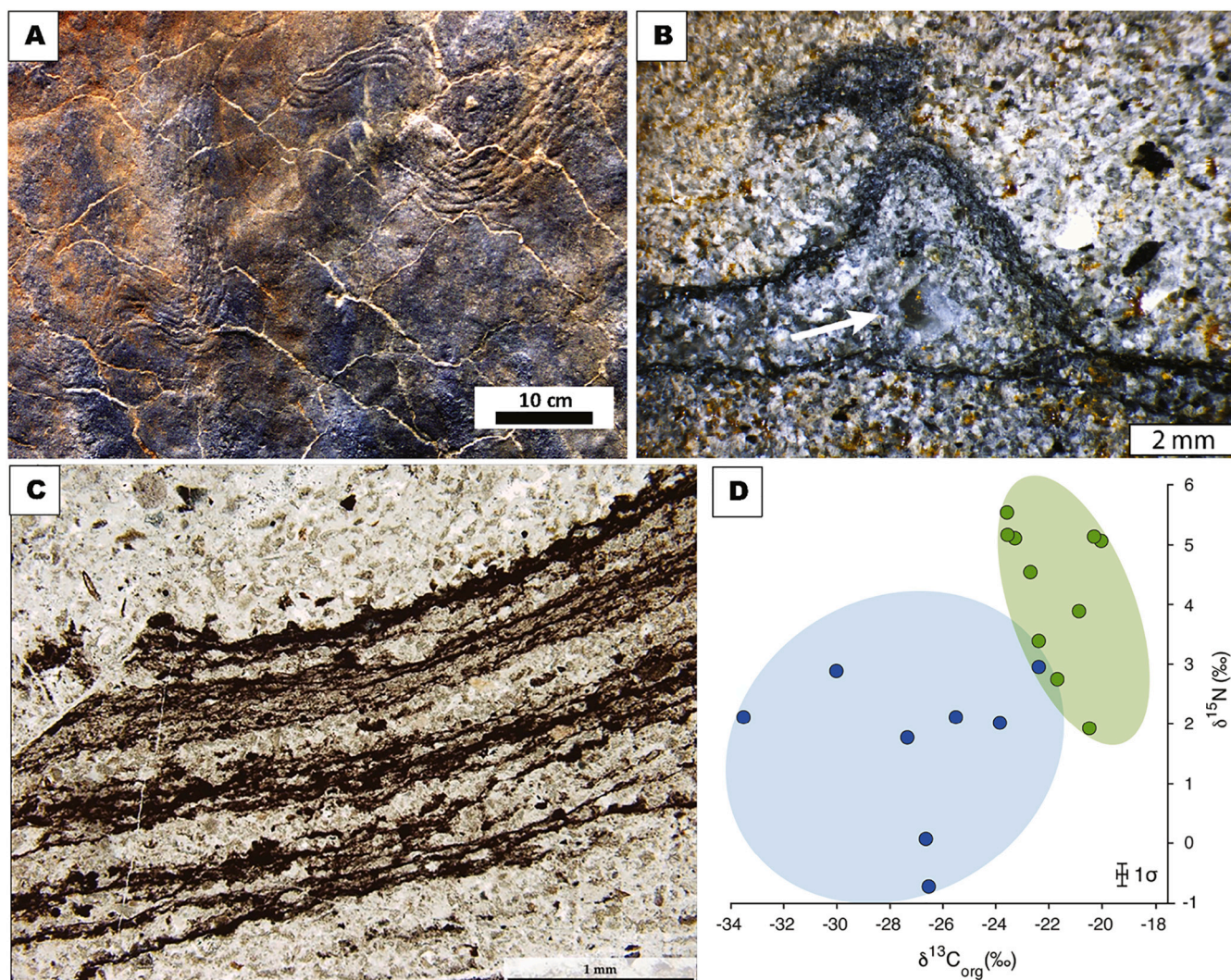


Fig. 8. Microbially-induced sedimentary structures (MISS). **(A)** Wrinkle structures and dewatering cracks on fine grained sandstone of the 3.22 Ga Moodies Group, South Africa. Photograph courtesy of Nora Noffke, Old Dominion University (reproduction permission below). **(B)** Tufted structure in another sandstone of the Moodies Group, Photograph courtesy of Martin Homann, University College London (reproduction permission below). The chert-filled void (arrow) has been interpreted as the result of a gas bubble trapped under the tufted microbial mat by Homann et al. (2015). **(C)** Crinkly-laminated carbonaceous matter in silicified volcanic ash of the ~ 3.47 Ga Middle Marker, South Africa, from Hickman-Lewis et al. (2018), reproduction permission below. **(D)** Ratios of C and N isotopes recorded in marine (blue) and terrestrial (green) siliciclastic facies of the Moodies Group. Diagram courtesy of Martin Homann, University College London (reproduction permission below). **Panel (A)** used with permission of the Geological Society of America, from A new window into Early Archean life: Microbial mats in Earth's oldest siliciclastic tidal deposits (3.2 Ga Moodies Group, South Africa), Nora Noffke, Kenneth A. Eriksson, Robert M. Hazen, Edward L. Simpson, *Geology*, 34, 2006; permission conveyed through Copyright Clearance Center, Inc. **Panel (B)** reprinted from Precambrian Research, 266, Martin Homann, Christoph Heubeck, Alessandro Airo, Michael M. Tice, Morphological adaptations of 3.22 Ga-old tufted microbial mats to Archean coastal habitats (Moodies Group, Barberton Greenstone Belt, South Africa), 47–64, Copyright (2015), with permission from Elsevier. **Panel (C)** reprinted from Precambrian Research, 312, Keyron Hickman-Lewis, Barbara Cavalazzi, Frédéric Foucher, Frances Westall, Most ancient evidence for life in the Barberton greenstone belt: Microbial mats and biofabrics of the ~3.47 Ga Middle Marker horizon, Copyright (2018), with permission from Elsevier. **Panel (D)** reprinted by permission from Springer Nature Customer Service Centre GmbH: Springer Nature, *Nature Geoscience*, Microbial life and biogeochemical cycling on land 3220 million years ago, Martin Homann, Pierre Sansjofre, Mark Van Zuilen, Christoph Heubeck, Jian Gong, Bryan Killingsworth, Ian S. Foster, Alessandro Airo, Martin J. van Kranendonk, Magali Ader, Stefan V. Lalonde, Copyright Springer Nature (2018). (For interpretation of the references to colour in this figure legend, the reader is referred to the web version of this article.)

tubes as ambient inclusion trails (AITs, Section 6.2).

Several features argue that the various types of titanite microtubes, including those terminated by carbonaceous matter and/or sulfides, could have a metamorphic origin similar to the AITs: first, they sometimes appear to overgrow some AITs (Fig. 7J-L). Moreover, they are made of dendritic monocrystals (Fig. 7E). In addition, the titanite microtubes cut across the chloritized cements between chloritized volcanoclastic grains (Fig. 7A and F), suggesting that they may not have formed after glass microboring. Such dendritic microstructures could have formed as quenching microlites, or during metamorphism,

consistent with the displacement of carbonaceous matter at the tip of some microtubes (Fig. 7D, Lepot et al., 2011). Some broader, straight calcitic microtubes are systematically rooted in the margins of the chloritized ash shards and not found in the cement (Fig. 7A-B and H-I). This localization, together with the fact that they are much broader than putative biocorrosion textures (Fisk and McLoughlin, 2013; Grosch and McLoughlin, 2014), linear in shape, and terminated by magmatic/hydrothermal sulfides such as chalcocopyrite (Fig. 7B) suggest that this latter type of microtubes could have formed after glass-quenching microstructures.

7.3.3. *In situ* dating of titanites

Although initially dated at ca. 3.34 Ga (Fliegel et al., 2010), the titanite microtubes in the pillow lavas of the ca. 3.47–3.43 Ga Hoogenoeg Formation have recently been re-dated at ca. 2.8–2.9 Ga (Grosch and McLoughlin, 2014). This rules out the initial hypothesis that the titanite formed during seafloor hydrothermal alteration soon after biocorrosion (Furnes et al., 2004; Fliegel et al., 2010), because the regional metamorphism (that would have re-crystallized any remaining glass) is dated at 3.23 Ga, and rather supports the hypothesis that titanite formed in association with later contact metamorphism (Grosch and McLoughlin, 2014). Similarly, other Archean titanite microtubes display *in situ* U–Pb dates that correlate with regional metamorphism (Banerjee et al., 2007; McLoughlin et al., 2010).

7.3.4. Other titanite microtubes

The Hoogenoeg Formation microtubes displayed an average diameter of 12 μm that is much larger than that of the tubes occurring in volcanic glass, which are few micrometer across (Grosch and McLoughlin, 2014). This size and the occurrence at the center of metamorphosed glass and not only at its edges has been used to argue for a purely metamorphic origin (porphyroblasts) to the Hoogenoeg microtubes (Grosch and McLoughlin, 2014). Nevertheless, narrower microtubes occurred in the Hoogenoeg Formation, but their host matrix, although poorly described, is likely quartz and/or calcite rather than chloritized glass (Banerjee et al., 2006). Narrow microtubes also occur in chloritized zones of the ca. 3.35 Ga Euro Basalt (Pilbara, Western Australia; Banerjee et al., 2007), for which a metamorphic origin was also proposed (McLoughlin et al., 2020). The microcrystalline nature of the titanite observed by transmission electron microscopy in the Hoogenoeg Formation (Fliegel et al., 2010) also remains to be reconciled with metamorphic growth as porphyroblasts (Grosch and McLoughlin, 2014) or metamorphic dendrites / ambient inclusion trails (Lepot et al., 2011). Altogether, this suggests that the formation of the various Archean titanite microstructures may not be related to a single metamorphic process or was templated by a pre-metamorphic microstructure that is replaced by titanite. This template could have been biogenic/abiogenic corrosion, and/or abiogenic structures such as structural/chemical heterogeneities in glass (Vogel, 1971), and/or quenching microphenocrysts (Ross, 1962). Interestingly, pyroxene and feldspar can form elongated crystals with twisted, coiled, segmented and/or radiating structures in volcanic glass (Ross, 1962). Additional high-resolution petrography is thus required to fully understand the origin of tubular microstructures in pristine to metamorphosed volcanic glass.

8. Archean microbial mats in siliciclastic deposits

A variety of small (centimetric to sub-centimetric) structures can form on the surface of recent siliciclastic sediments in presence of microbial mats, including various types of sedimentary figures stabilized by mats (e.g. ridges) and mat structures such as cracks, wrinkles, bulges, tufts, roll-up structures or reticulate patterns (Gerdes, 2007). Similar structures found on rock outcrop bedding planes (Fig. 8A–C) suggest structuration of sediments by microbial mats and, when a biogenic origin can be demonstrated, they can be named Microbially Induced Sedimentary Structures (MISS; Porada and Bouougri, 2007; Noffke, 2009; Davies et al., 2016). In general, support for biogenicity of MISS is provided by the combined observation of carbonaceous laminae draping sand grains (e.g., Tice, 2009; Homann et al., 2018), the textures of MISS (including tufts and wrinkles), oriented quartz grains (e.g., Heubeck, 2009; Noffke, 2009), the association with MISS of sedimentary structures formed after detachment of cohesive mat fragments such as flakes and roll-up structures, and structures interpreted as (bio)gas-trapping domes (Noffke et al., 2006, 2008, 2013; Gerdes, 2007; Porada and Bouougri, 2007; Tice, 2009; Homann et al., 2015). Small pitted and ridged sedimentary wrinkles may also form by transport of clastic

material by microbial mat fragments or by sticky aggregates of microbes, which may provide an alternative to benthic mats that can form MISS (Mariotti et al., 2014). Sediment surfaces textures alone such as wrinkles (including “Kinneyia”-type), bubbles and multiple-directed ripple marks may form abiotically (Davies et al., 2016), hence implying the need for multiple lines of evidence to demonstrate fossil microbial mats in clastic environments. Unfortunately, cellular microfossils are generally not distinguished in MISS, and the microbial communities that led to their formation remain enigmatic, although photosynthesis has usually been considered predominant in the shallow-water benthic environments associated with Archean MISS (Tice and Lowe, 2004; Noffke et al., 2006; Homann et al., 2015).

Wrinkles and tufted structures of the 3.22 Ga Moodies Group of South Africa (Fig. 8A–B) represent some of the oldest MISS that have been described both on the macroscopic and microscopic scales (Noffke et al., 2006; Heubeck, 2009, 2019; Homann et al., 2015). The wavy-crinkly, tufted and domed aspect of the carbonaceous mats, the occurrence of mat chips, and the correlation of morphologies with shallow-water tidal settings has been used to infer microbial mats that are physically supple and resistant to shear-stress (Homann et al., 2015, 2018). Sediment biostabilization is further supported by sub-parallel mat layers wrapping around oriented sand grains (Noffke et al., 2006; Heubeck, 2009). The tufted morphology and the domes (Fig. 8B) have been interpreted as growth patterns of mats of oxygenic phototrophs and associated production of gas (O_2) domes (Homann et al., 2015). Recent analyses of organic C and N isotope ratios in coeval siliciclastic sediments of the Moodies Group (Fig. 8D) show marked difference in the metabolisms carried by the associated microbial communities (Homann et al., 2018). In the terrestrial environment, the ^{13}C -rich values are consistent with oxygenic/anoxygenic photosynthesis using the Calvin cycle (Fig. 2A), possibly coupled to fixation of nitrate, which could have been oxidized by lightning (Homann et al., 2018). In the marine environment, the more ^{13}C -depleted values could record higher contributions of microbial sulfate-reduction, methanogenesis, and/or acetogenesis (Figs. 2C–F; Homann et al., 2018).

Delicate carbonaceous layers draping clasts in the 3.42 Ga Buck Reef Chert of South Africa may be among the oldest preserved fossil microbial mats (Tice and Lowe, 2006; Tice, 2009); in this case, however, no macroscopic-scale MISS (e.g., Fig. 8A–B) have been reported (to my knowledge). Silicified volcanoclastic sediments of the ca. 3.47 Ga Middle Marker of the Hoogenoeg Formation, South Africa, also display sets of carbonaceous laminae interpreted as microbial mats (Fig. 8C, Hickman-Lewis et al., 2018). Their crinkly (i.e., microscopically-tufted) and tufted textures have been interpreted as the result of photosynthetic communities (Hickman-Lewis et al., 2018). However, the co-existence of crinkly textures and pseudo-tufts formed by syndimentary deformation within the Middle Marker volcanoclastic deposits raised doubts on the photosynthetic origin of the former structures (Homann, 2019). Stratiform granular cherts deposited in the \sim 3.46 Ga Apex Basalt include grains with carbonaceous laminations that can be wrinkly or undulating and form putative roll-up structures, which have been interpreted as fragments of MISS (Hickman-Lewis et al., 2016). However, the peculiarly laminated texture of these grains could also be explained as the result of exfoliation of biotite crystals during weathering (Bisdom et al., 1982; McMahon et al., 2017) and inter-foliar growth of pyrites in biotite (Claeys and Mount, 1991). Subsequent silicification of biotite and pyrite and migration of carbonaceous matter into these structures is consistent with the local-scale carbonaceous migration, massive carbonaceous feeder dykes, and pervasive silicification documented at this site (Hickman-Lewis et al., 2016). Other possible MISS occur in the 3.48 Ga Dresser Formation (Noffke et al., 2013).

9. Archean stromatolites

9.1. Stromatolite definition

Stromatolites are laminated sedimentary rocks showing domed, conical, columnar (branching/unbranched), or tabular external shapes. Microorganisms, in particular cyanobacterial mats, are usually considered as responsible for their formation (Walter, 1976a). However, sedimentary accretion models suggest a possible abiotic origin, at least for some types of stromatolitic morphologies (Grotzinger and Rothman, 1996; Grotzinger and Knoll, 1999; Jettestuen et al., 2006; Cuerno et al., 2012). It has been proposed by Semikhatov et al. (1979) that “*Stromatolites are laminated, lithified, sedimentary growth structures that accrete away from a point or limited surface of attachment. They are commonly, but not necessarily, of microbial origin and calcareous composition.*” Biogenicity is, on the other hand, implied in the definition of *microbialites* by Burne and Moore (1987), that is “*organosedimentary deposits that have accreted as a result of a benthic microbial community trapping and binding detrital sediment and/or forming the locus of mineral precipitation.*” Following this definition, biogenic stromatolites would thus represent internally laminated microbialites. Trapping of sediment particles can be caused by sticky films of extracellular polysaccharides (EPS) and/or bundles/colonies of (cyano)bacteria (Monty, 1976; Reid et al., 2000). Precipitation of carbonates in microbial mats can be induced biologically, by autotrophic metabolism such as oxygenic and/or anoxygenic photosynthesis, by heterotrophic metabolism such as bacterial sulfate reduction, and/or by the presence of reactive cell surfaces, EPS, or decaying organic matter (see Dupraz et al., 2009 for a review).

Stromatolites are abundant in Archean strata, but they only contain scarce fossil microorganisms that do not help demonstrate their biogenic accretion (Hofmann, 2000; Schopf et al., 2007). In contrast, some Proterozoic stromatolites display luxuriant microfossil communities whose compositions correlate with stromatolite structures (Awramik, 1976; Sharma and Sergeev, 2004; Knoll et al., 2013). Indirect morphological and geochemical arguments are thus sought to demonstrate the biogenicity of Archean (and younger) stromatolites in cases microfossil assemblages failed to do so.

9.2. Neoproterozoic to Mesoproterozoic carbonate stromatolites

9.2.1. Stromatolite fabrics

One of the most iconic stromatolite deposits of the Archean is the Tumbiana Formation, which formed in a giant lake 2.72 Ga ago (Buick, 1992; Awramik and Buchheim, 2009; Coffey et al., 2013). It includes a diversity of columnar, domical (e.g., Fig. 9A), stratiform and conical stromatolite morphologies that compares with those of Proterozoic stromatolites (Buick, 1992; Bosak et al., 2013; Martindale et al., 2015). Within stromatolitic laminae, palisade fabrics of vertically erect sinuous filaments, now filled with calcite (Buick, 1992) are strongly reminiscent of micrite-encrusted bundles of cyanobacterial filaments observed in modern stromatolites (Monty, 1976). Tufted stromatolite structures also strongly support an origin linked to microbial mats, likely cyanobacterial (Buick, 1992; Flannery and Walter, 2012).

9.2.2. Microbially-induced calcification

Although the calcium carbonate of the Tumbiana stromatolites is essentially preserved as microcrystalline calcite, some nanoglobular structures composed of aragonite nanocrystals could be found (Figs. 9B-D; Lepot et al., 2008). These nano-aragonite structures associated with organic matter are interpreted as relics of the primary carbonate mineral that precipitated in presence of microorganisms. Indeed, these carbonate nanostructures are similar to those that comprise the main building blocks of microbially-induced carbonate mineralization in modern stromatolites (Castanier et al., 1999; Sprachta et al., 2001; Kaźmierczak and Kempe, 2003; Reid et al., 2003; Dupraz et al., 2004; Benzerara et al., 2006; Bontognali et al., 2008; Spadafora et al., 2010;

Perri et al., 2012; Dupraz et al., 2013; Lepot et al., 2014) and in vitro experiments with microorganisms (Aloisi et al., 2006; Pedley et al., 2009) or with organic molecules (Kirkland et al., 1999).

9.2.3. Metabolic signatures

Three types of organic matter have been identified in the Tumbiana stromatolites. Type A is essentially aromatic and mainly found at the grain boundaries of quartz and chlorite (Figs. 9E-F), in siliceous clusters in carbonate laminae or in the dark siliceous laminae forming the stromatolites (Fig. 9A). This distribution of (Fe,Mg)-chlorite and quartz suggests that this silicate could be early diagenetic rather than clastic similar to the poorly crystalline Mg-silicates forming layers in modern stromatolites (Arp et al., 2003; Burne et al., 2014; Zeyen et al., 2015; Pace et al., 2016; Wacey et al., 2018c). The strong ^{13}C depletions recorded in Type-A organic matter, together with the association with Fe-minerals, suggest anaerobic methane oxidation coupled to microbial Fe^{3+} -reduction (Section 3.3). Type-B organic globules are only found within carbonate laminae, are enriched in organic sulfur and preserve other functional groups (Fig. 9E-F). They could correspond to remains of microorganisms that have been preserved owing to diagenetic sulfuration (Lepot et al., 2008, 2009a). Their sulfuration and the most extreme ^{13}C -depletions they record support a coupling of microbial sulfate-reduction with anaerobic methane oxidation (Fig. 2K; Lepot et al., 2019). The fact that sulfurized globules are only found in calcite suggests that microbial sulfate reduction could have been an important driver of the calcification of the stromatolite laminae, a situation similar to modern stromatolites (Visscher et al., 2000; Vasconcelos et al., 2006). Finally, Type C comprises pyrobitumen nodules displaying higher $\delta^{13}\text{C}$ values (Lepot et al., 2019) consistent with distinct metabolisms such as photo- and/or chemo-autotrophy (Thomazo et al., 2009b). However, this bitumen could have been introduced in some stromatolites after migration from other sediment types.

9.2.4. Fenestrae

The Tumbiana stromatolites contain abundant fenestrae (Buick, 1992; Flannery and Walter, 2012), which could represent relics of former gas bubbles of photosynthetic oxygen or heterotrophic degradation products trapped by microbial mats (Monty, 1976; Bosak et al., 2013), structures formed after desiccation/wetting cycles, voids left after degradation of clusters of unlithified microbial colonies, or microbial dissolution structures (Monty, 1976). Fenestrae within 2.7 Ga stromatolites of the Ventersdorp Supergroup, South Africa, display a morphology comparable to those observed in modern siliceous stromatolites of the Yellowstone Park (Wilmeth et al., 2019). Filament-like textures appear to wrap these fenestrae, a situation similar to the distribution of filamentous microorganisms in the Yellowstone stromatolites (Wilmeth et al., 2019). However, the low-magnification microscopy provided in Wilmeth et al. (2019) does not allow to resolve filamentous microfossils from abiotic filament-like structures (see Sections 6.2 and 6.3) and reticulated networks of kerogen. Microscopic textures interpreted as fenestrae found in 2.98 Ga stromatolites of the Pongola Supergroup, South Africa, together with conical morphology, have been proposed to result from the trapping of bubbles of photosynthetic oxygen by the microbial mats (Bosak et al., 2013). Enigmatic fenestrate microbialite textures have been reported in three 2.5 to ~ 3 Ga carbonate deposits, which display a relatively thick vertical “support” structure associated with thin net-like to cusped sub-horizontal laminae (Sumner, 1997, 2000; Schröder et al., 2009). Detailed petrographic and geochemical characterization of these fenestrate-bearing microbialites may provide important clues on the mat communities and the associated stromatolite-building processes.

9.3. Dolomitic stromatolites of the Strelley Pool Formation (~ 3.4 Ga)

The ~ 3.4 Ga Strelley Pool Formation of Australia hosts stromatolitic structures of partly silicified, coarse crystalline dolomite (Allwood

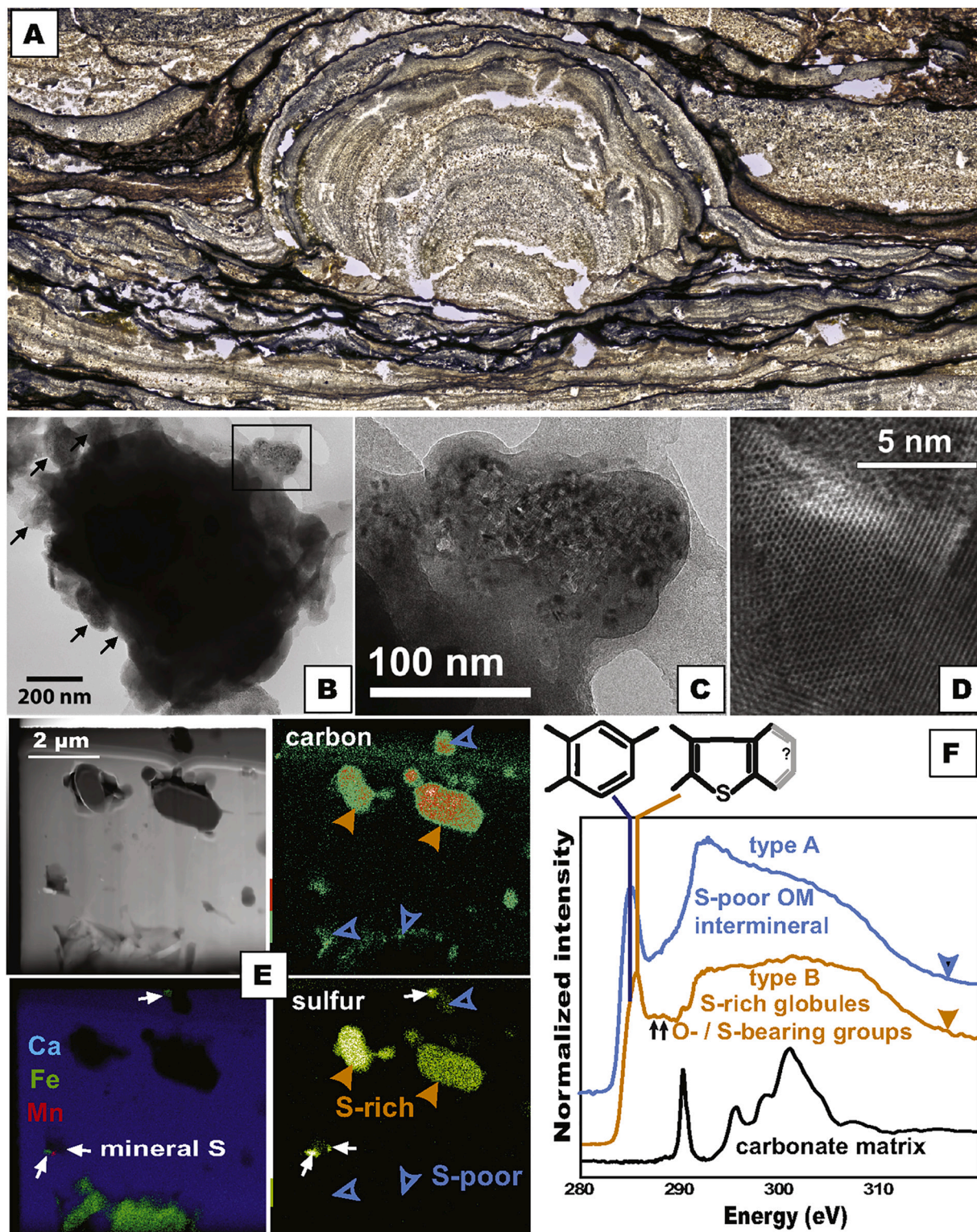


Fig. 9. Stomatolites of the Tumbiana Formation. (A) Mosaic of photomicrographs; height ~ 1 cm. (B–D) Transmission Electron Microscopy (TEM) of powdered stromatolite. (B) Organic globule (in black) associated with nanograins of CaCO_3 (arrows and box). (C) The carbonate grain boxed in (B) is nanoglobular and made of nanocrystallites. (D) High-resolution TEM image of aragonite lattice planes showing a nanocrystallite ca. 5 nm large. (E) Scanning TEM image and X-ray elemental maps showing that globules included in carbonates (orange arrows) are rich in organic S, whereas organic matter spread at the grain boundaries of chlorite is S-poor (blue arrowheads). (F) X-ray absorption spectroscopy at the carbon K-edge. Type A organic matter (blue) is essentially aromatic, whereas Type B organic matter (orange) is rich in O- and S-bearing functional groups. **Panels (B–D)** reprinted by permission from Springer Nature Customer Service Centre GmbH: Springer Nature, Nature Geoscience, Microbially influenced formation of 2724-million-year-old stromatolites, Kevin Lepot, Karim Benzerara, Gordon E. Brown Jr. and Pascal Philippot, Copyright Springer Nature (2008). **Panels (E–F)** reprinted from *Geochimica et Cosmochimica Acta*, 73, Kevin Lepot, Karim Benzerara, Nicolas Rividi, Marine Cotte, Gordon E. Brown, Pascal Philippot, 6579–6599, Copyright (2009), with permission from Elsevier. (For interpretation of the references to colour in this figure legend, the reader is referred to the web version of this article.)

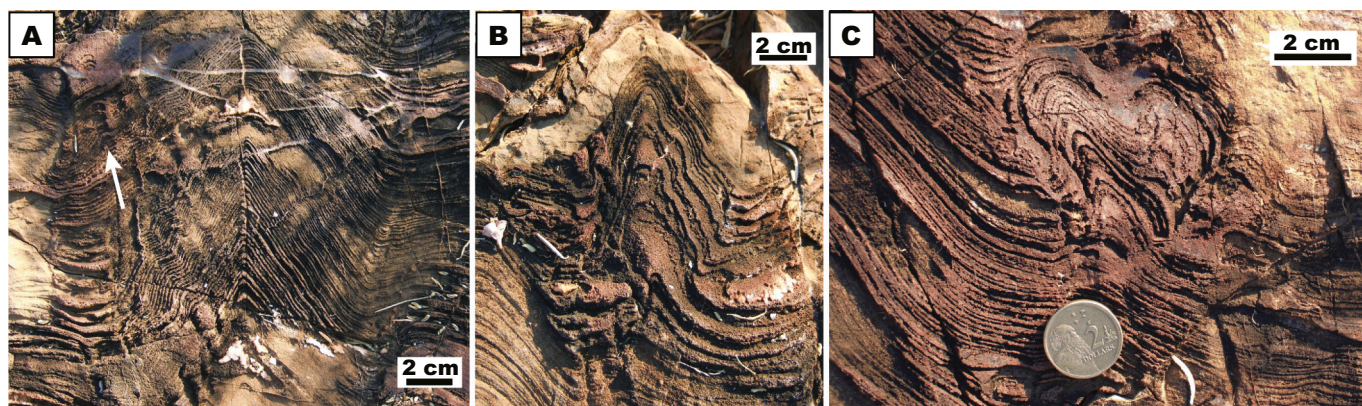


Fig. 10. Stromatolites of the Strelley Pool Formation at the Trendall (type) locality. (A) Large conical structures with wrinkly laminae on the left forming subordinate columnar structures above the white arrow. (B) Conical structure with steep flanks. (C) Small, branching columns overgrowing the flanks of a large conical structure (to the left).

et al., 2009). Observation of conical shapes (Fig. 10A-B) and possible fenestrae structures initially supported a biogenic origin (Lowe, 1980), although it has later been suggested that these could have formed abiotically through evaporation (Lowe, 1994). Detailed study of laminae structures, of their relationships with surrounding sediments, and finding of steep-sided cones and branching pseudocolumns on the flanks of larger cones (Fig. 10) argued for a biogenic accretion (Hofmann et al., 1999; Allwood et al., 2006a; Allwood et al., 2007; van Kranendonk, 2007). Seven stromatolite morphotypes have later been elucidated and their distributions shown to correlate with specific environments of deposition (Allwood et al., 2006a, 2007). Dark layers interpreted as remnants of microbial mats have been observed in some of the best-preserved stromatolites (Allwood et al., 2009). Organic matter in these stromatolites is enriched in organic sulfur, for which isotope microanalyses are consistent with microbial sulfur metabolism (Bontognali et al., 2012). However, recent experiments have shown that organic sulfur isotopes may also—depending on the solid source of sulfate used—fractionate during thermochemical sulfate reduction (Meshoulam et al., 2016). Altogether, these studies strongly argue that the Strelley Pool Formation stromatolites represent the oldest known carbonates of microbial origin.

9.4. Cavity-dwelling biofilms

Siliceous laminated structures with convex-downward growth orientation have been observed in sediments deposited in fluvio-lacustrine setting in the 2.75 Ga Hardey Formation, Australia (Rasmussen et al., 2009). They have been compared to microbialites that form in basaltic caves (Léveillé et al., 2007) and hence interpreted as the imprint of synsedimentary cavity-dwelling terrestrial microorganisms (Rasmussen et al., 2009). Similar structures occur in sparitic zones within sediments of the Tumbiana Formation and are illustrated in Fig. 11. The oldest evidence for such cavity-dwelling biofilms occurs in chert-filled elongate “blisters”, which probably represent former gas/air bubbles, in tidal sandstones of the 3.22 Ga Moodies Group (Homann et al., 2016) where benthic microbial mats have also been documented (e.g., Fig. 8B and Homann et al., 2015).

9.5. Paleoproterozoic siliceous stromatolites

In contrast with carbonate microbialites, where metabolic activity can induce calcification (Section 9.2.2.), silicification in hot springs is generally considered as an abiotically-driven reaction (Benning et al., 2005). During the Archean, before the evolution of silica biomineralization, the ocean was supersaturated with respect to silica and allowed seafloor and/or water column precipitation (Maliva et al., 2005;

Stefurak et al., 2014). Extracellular polymers (Handley et al., 2008) and bacterial sheaths (Benning et al., 2005) can enhance the aggregation of silica. Microorganisms and microbial mats are thus readily silicified, which is observed even in high-temperature (> 73 °C) “geyserite” sinters (Cady and Farmer, 1996). The morphogenesis of various siliceous sinters or siliceous stromatolites is thus controlled by a combination of the spatially/temporally heterogeneous distribution of microorganisms and abiotic processes such as cycles of wetting, evaporation, and drying (Braunstein and Lowe, 2001; Konhauser et al., 2001; Guidry and Chafetz, 2003; Cangemi et al., 2010; Orange et al., 2013; Campbell et al., 2015). In this context, the observation of diagnostic carbonaceous lamina shapes and/or abundant remains of microorganisms is required in addition to macroscopic shapes to infer former biological activity in siliceous stromatolites.

9.5.1. Josefsdal Chert (~ 3.3 Ga)

Wavy, sometimes torn, carbonaceous layers occur in the ~ 3.3 Ga Josefsdal Chert of South Africa (Fig. 12A-C), an informal stratigraphic unit within the Barberton Greenstone Belt (Westall et al., 2006, 2015). They have been interpreted as fossil microbial mats that have been preserved by hydrothermal silicification (Westall et al., 2006, 2015). As such, they fall in the category of “siliceous sinters” (Walter et al., 1976). A spectacular feature of these carbonaceous layers is their thick kerogenous structures containing fibrillar to filamentous shapes, which were proposed to represent microfossils (Westall et al., 2006).

Organic carbon isotope ratios and sedimentary environment have been used to argue that the Josefsdal microbial mats performed photosynthesis (Westall et al., 2015). Interestingly, these mats are interspersed with dense, fluffy carbonaceous clots (upper-right corner of Fig. 12B), which are generally a dominant carbonaceous fabric in Paleoproterozoic cherts/veins associated with hydrothermal deposits/activity (e.g. Fig. 6C; Ueno et al., 2004; Philippot et al., 2009; Lepot et al., 2013; Kiyokawa et al., 2014) or in Paleoproterozoic cherts not clearly connected to hydrothermal activity (Tice and Lowe, 2006). Textural and chemical evidence for hydrothermal fluid injection in the Josefsdal cherts and high clot abundance “at sites of greatest hydrothermal activity” led Westall et al. (2015) to suggest that these clots formed after chemotrophic microorganisms that sourced energy in hydrothermal fluids. Note that the presence of Fe-Cr-Ni alloys has been used to propose an abiotic hydrothermal origin for carbonaceous clots in a 3.47 Ga chert (Section 5, Alleon et al., 2019). Additional constraints on metabolic signatures and possible contributions from abiotic hydrothermal compounds could be obtained by a combination of thorough microscale measurements of isotope ratios of these diverse organic matter textures in the Josefsdal cherts as well as S and other elements in associated minerals (e.g. Fig. 6; c.f. discussion in Homann, 2019), in combination with

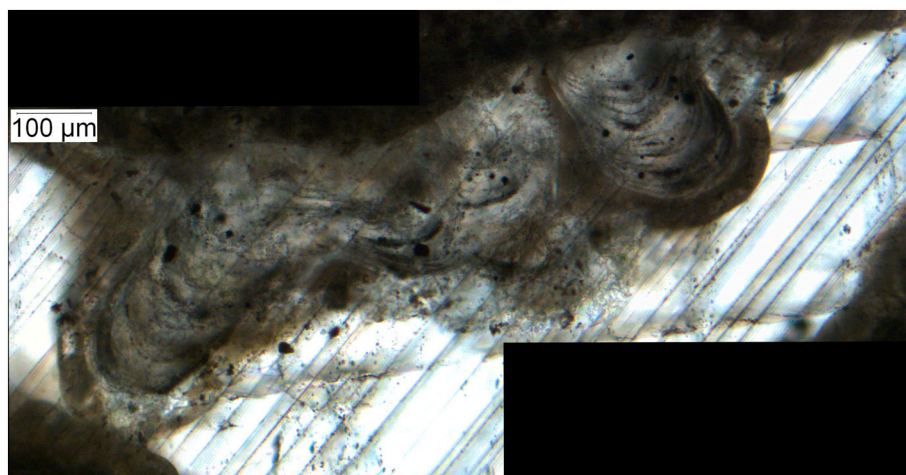


Fig. 11. Possible microbialites formed in cavities in the 2.72 Ga Tumbiana Formation. Photomicrograph of a thin section of the PDP1 drillcore (Philippot et al., 2009), 75.1 m depth.

spectromicroscopy (e.g. Fig. 9E-F) and microscale mass-spectrometry (Westall et al., 2011; Fadel et al., 2020).

9.5.2. Mendon Formation (~ 3.3 Ga)

Domed to pseudo-columnar siliceous sinters (Fig. 12D), initially assigned to the ~ 3.4 Ga Kromberg Formation (Byerly et al., 1986; Byerly and Palmer, 1991), are now assigned to the ~ 3.3 Ga Mendon Formation (Hickman-Lewis et al., 2019 and references therein). These have been initially interpreted as stromatolites based on the similarity with the Paleoproterozoic examples of the Gunflint Iron Formation (Byerly et al., 1986; Byerly and Palmer, 1991). The dark laminae shown

in Fig. 12D were initially inferred as carbonaceous, although Lowe (1994) indicated that the lamination was mostly defined by dark-colored tourmaline crystals. The structures were thus redefined as abiotic siliceous sinters, consistent with the early view that such laminated siliceous structures could form abiotically in hydrothermal systems (Walter, 1976b). However, later studies showed that such siliceous sinters rather formed in the presence (and likely with the participation) of microorganisms (Cady and Farmer, 1996; Konhauser et al., 2001; Barbieri et al., 2014). Thus far, a clear identification of carbonaceous remnants (e.g., as shown in Fig. 12B-C) in these sinters, in support of a possible biological origin, is thus lacking.

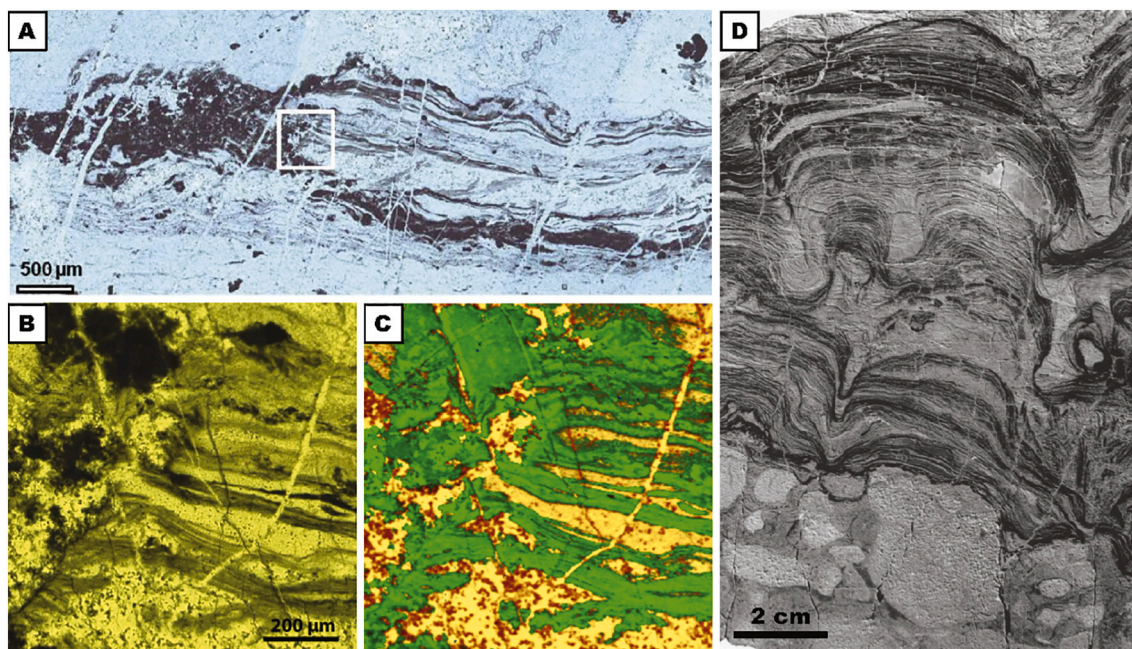


Fig. 12. Laminated Paleoproterozoic siliceous sinters from South Africa. (A-C) Laminated carbonaceous microstructures of the ~ 3.3 Ga Josefsdal Chert, images courtesy of Frances Westall, CNRS Orléans (reproduction permission below). (A) Optical microscopy of wavy carbonaceous layers in chert. (B) Zoom on the boxed zone in (A) showing torn laminae. (C) Raman spectromicroscopy map of the carbonaceous matter (green) and quartz (yellow-orange) in (B). (D) Siliceous sinter from the ~ 3.3 Ga Mendon Formation, polished and etched rock surface picture, from Byerly and Palmer (1991), reproduction permission below. (A-C) Reprinted from “Archean (3.33 Ga) microbe-sediment systems were diverse and flourished in a hydrothermal context” by Frances Westall, Kathleen A. Campbell, Jean Gabriel Bréhéret, Frédéric Foucher, Pascale Gautret, Axelle Hubert, Stéphanie Sorieul, Nathalie Grassineau, and Diego M. Guido © 2015 Geological Society of America, published under the terms of the CC-BY license. Doi:10.1130/G36646.1 (D) Reprinted by permission from Springer Nature Customer Service Centre GmbH: Springer Nature, Contributions to Mineralogy and Petrology, Tourmaline mineralization in the Barberton greenstone belt, South Africa: early Archean metasomatism by evaporite-derived boron, Gary R. Byerly and Martin R. Palmer, © Springer-Verlag (1991). (For interpretation of the references to colour in this figure legend, the reader is referred to the web version of this article.)

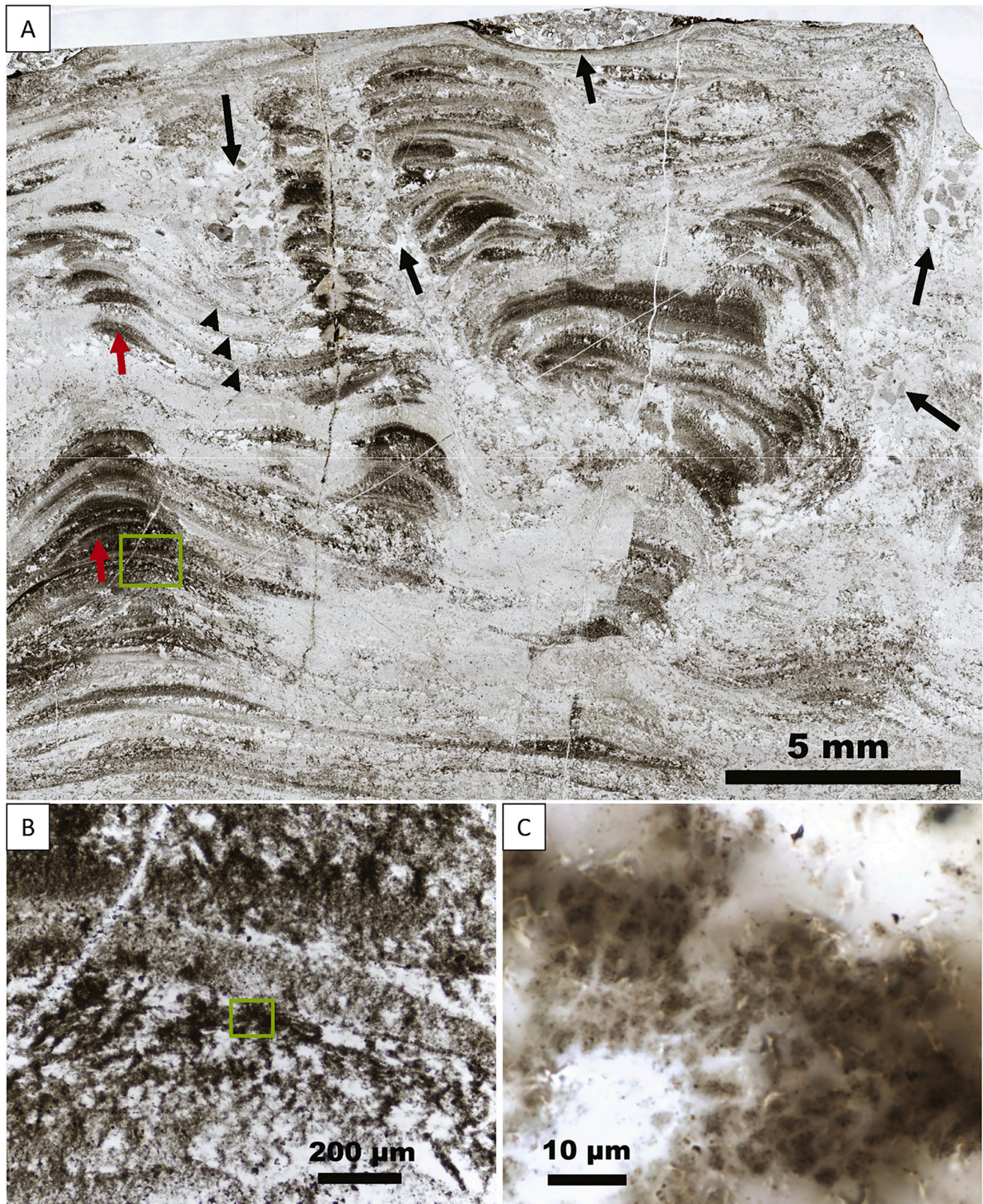


Fig. 13. Stromatolitic chert of the Strelley Pool Formation. Photomicrographs of sample WF8', which was provided by Kenichiro Sugitani (Nagoya University). (A) Mosaic of multiple images of the thin section showing branching pseudo-columnar structures. Black arrows indicate pockets of clastic materials. Red arrows indicate examples of convex lenticular zones in the columns. Arrowheads indicates thin laminae that connect the convex laminae forming the two columns to the right. (B) Zoom on the carbonaceous laminae in the green box in (A). (C) Zoom on the carbonaceous clusters in the green box in (B), showing globular aggregates of sub-micrometric carbonaceous particles. (For interpretation of the references to colour in this figure legend, the reader is referred to the web version of this article.)

9.5.3. Strelley Pool Formation (~ 3.4 Ga)

Conical and columnar siliceous stromatolites occur in the Strelley Pool Formation (Sugitani et al., 2010, 2015b; Lepot et al., 2013). Conical structures display “dark laminae, which are oriented at a high angle relative to the sidewall of the cones, and appear to be abruptly terminated by the outer thin crust of the cones” (Sugitani et al., 2015b). This contrasts with the convergence of laminae forming multi-layered walls at the edge of stromatolites (Preiss, 1976). Although these cones displayed putative lenticular microfossils, the laminae are mostly defined by pyrite and organic matter is scarce, which led Sugitani et al. (2015b) to propose that these cones represent abiogenic silica sinters rather than biogenic stromatolites.

In contrast, columnar siliceous stromatolites of the Strelley Pool Formation (Fig. 13; Lepot et al., 2013; Sugitani et al., 2015b) display a number of features similar to those of microfossil-rich stromatolites of the 1.88 Ga Gunflint Iron Formation (Awramik and Semikhatov, 1979; fig. 3A in Petrash et al., 2016; Lepot et al., 2017) and their modern counterparts of the Yellowstone National Park (Walter et al., 1976; Guidry and Chafetz, 2003). The Strelley Pool Formation siliceous stromatolites are branching (Fig. 13), with highly-convex structures in the branches that are reminiscent of the convex structures observed in the modern siliceous, biogenic stromatolites *Conophyton*, which grow at the Yellowstone hot springs (e.g., figs. 27–28 of Walter et al., 1976b). Similar to the Yellowstone and Gunflint stromatolites, pockets of clastic material are included between columns, indicating trapping of sediment during columnar growth.

Laminae have also been observed to “pinch out laterally” in other siliceous stromatolites of Yellowstone (fig. 8B in Guidry and Chafetz, 2003), with bundles of laminae forming convex-upward shapes similar to those shown in Fig. 13A. Thinner carbonaceous layers form bridges between the columns (arrowheads in Fig. 13A), similar to the Gunflint stromatolites (fig. 3A in Petrash et al., 2016). Organic laminae of the Gunflint stromatolites are defined by populations of microfossils (Awramik and Semikhatov, 1979; Strother and Tobin, 1987; Lepot et al., 2017). Similarly, microfossils are abundant in recent stromatolitic siliceous sinters (Walter et al., 1976; Cady and Farmer, 1996; Konhauser et al., 2001, 2004; Guidry and Chafetz, 2003). In the columnar stromatolites of the Strelley Pool Formation, organic matter in laminae is diffuse, clotted, or forming “three-dimensional networks of bundles of carbonaceous threads” (Sugitani et al., 2015b). Clotted structures are dominant in the convex laminae of the sample in Fig. 13. Some clots comprise clusters of globules that show a darker core of carbonaceous nanoparticles and a rounded translucent rim (Figs. 13B-C; Lepot et al., 2013). The general shape and distribution of these globules are reminiscent of those of populations of *Eoentophysalis belcherensis*, which form clusters and laminae in Proterozoic stromatolites (Hofmann, 1976; Sergeev et al., 1995; Sharma, 2006). However, their nanogranular nature and the apparent absence of cell-wall preservation thus far prevent clear identification as microfossils.

Interestingly, the globular clots of a stromatolite similar to that shown in Fig. 13 yielded distinct C isotope compositions compared to those of microfossils and clots in cherts with thick and flat laminae (Fig. 6A-D; Lepot et al., 2013; Sugitani et al., 2015b, Sugitani et al., 2010). Distinct microbial communities may have been fossilized in the two types of cherts. However, carbonaceous matter in the former stromatolites appeared more mature than in other cherts (Lepot et al., 2013), possibly due to more intense *syn*-sedimentary or post-depositional hydrothermal alteration (Allwood et al., 2006b; Marshall et al., 2012; Sforza et al., 2014; Reinhardt et al., 2019) that may also have modified their C isotope composition.

Siliceous stromatolites have also been reported in the Strelley Pool Formation at the locality of the carbonate stromatolites discussed in Section 9.3 (Duda et al., 2016). In these stromatolites, layered and clotted organic matter host microspheres of CaCO₃. These have been compared with microfossils (Duda et al., 2016), but no cellular structure (e.g. cell wall) appeared preserved organically or by carbonate

replacement. Calcification by heterotrophic degradation of the organic matrix has also been proposed (Duda et al., 2016). Sub-spherical carbonate micropeloids are indeed an important component of modern biogenic stromatolites (Dupraz et al., 2004; Lepot et al., 2014). However, carbonate microspheres may also form abiotically (Bosak et al., 2004) and during thermal mineralization of organic matter (Köhler et al., 2013). Investigation of their nanostructure (e.g., Lepot et al., 2014) may help assess the biogenicity of these Paleoarchean carbonate microspheres.

9.5.4. Dresser Formation (3.48 Ga)

Siliceous sinter deposits have been found in the 3.48 Ga Dresser Formation (Djokic et al., 2017). Two principal arguments have been put forward to argue that they once hosted microbial life: spherical structures in highly-weathered parts of the cherts have been inferred to represent bubbles that were trapped by extracellular polymeric substances. These are reminiscent of the siliceous granules observed in cobweb-forming assemblages of microfossils (Fadel et al., 2017; Barlow and van Kranendonk, 2018). However, they could also represent primary silica granules that precipitated in the water column (Stefurak et al., 2014). Secondly, palisade fabrics of quartz have been suggested to form in presence of vertically-erect microbial filaments (Djokic et al., 2017). However, such palisade of quartz may also represent replacement of anhydrite fibers (Chowns and Elkins, 1974). So far, no organic remnant has been reported in these structures that could argue for the presence of extracellular substances around putative bubbles or for vertical microfossils.

9.6. Pyritic stromatolites of the 3.48 Ga Dresser Formation

Banded structures with domical, conical, wrinkly and columnar structures occur in the Dresser Formation (e.g. Fig. 14A-D). “Upward-broadening and/or upward-branching” shapes of digitate structures have been inferred as biogenic (Baumgartner et al., 2019 and references therein). However, similar structures have produced abiotically (McLoughlin et al., 2008). On the outcrop, bands comprise Fe-oxides, silica and barite (Buick et al., 1981; van Kranendonk, 2006). Drillcores (van Kranendonk et al., 2006, 2008) provided fresh sections of these stromatolites (Fig. 14D), demonstrating that the Fe-oxides laminae derive from a sulfide (essentially pyrite with minor sphalerite) and ankerite/dolomite mineralogy. Based on the presence of carbonate, it has been proposed that these stromatolites formed after pyritization of primary carbonate stromatolite lithologies (van Kranendonk et al., 2008). However, similar sulfide-chert-barite laminated structures are also observed in recent hydrothermal vents that are interpreted to form as primary hydrothermal phases (Hannington and Scott, 1988), consistent with an earlier proposition that the Dresser sulfide-chert-barite laminae could represent “primary chemical precipitates” (Buick et al., 1981). Indeed, the disposition of the Dresser stromatolites with respect to hydrothermal veins argue for growth linked with hydrothermal fluid circulation (van Kranendonk, 2006).

Nanoparticulate and fibrous carbonaceous matter has been recently discovered in pyrite of the Dresser Formation stromatolites and interpreted as remnants of extracellular polysaccharide from once organic-matter-rich biofilms (Baumgartner et al., 2019). Extensive pyritization of such organic matter has been proposed to account for the pyritic nature of the Dresser stromatolites (Baumgartner et al., 2019). In agreement with this model, sulfur isotope ratios recorded in stromatolitic sulfides are consistent with a sulfidization through reduction of a mixture of photochemically-derived and of hydrothermal/magmatic-derived sulfate, possibly accompanied by reduction of photochemically-derived elemental sulfur (Baumgartner et al., 2020a). Nevertheless, to the best of my knowledge, the proposed extensive texture-replacing pyritization (rather than patchy framboidal growth) has yet to be characterized in recent stromatolites and/or hydrothermal vent precipitates.

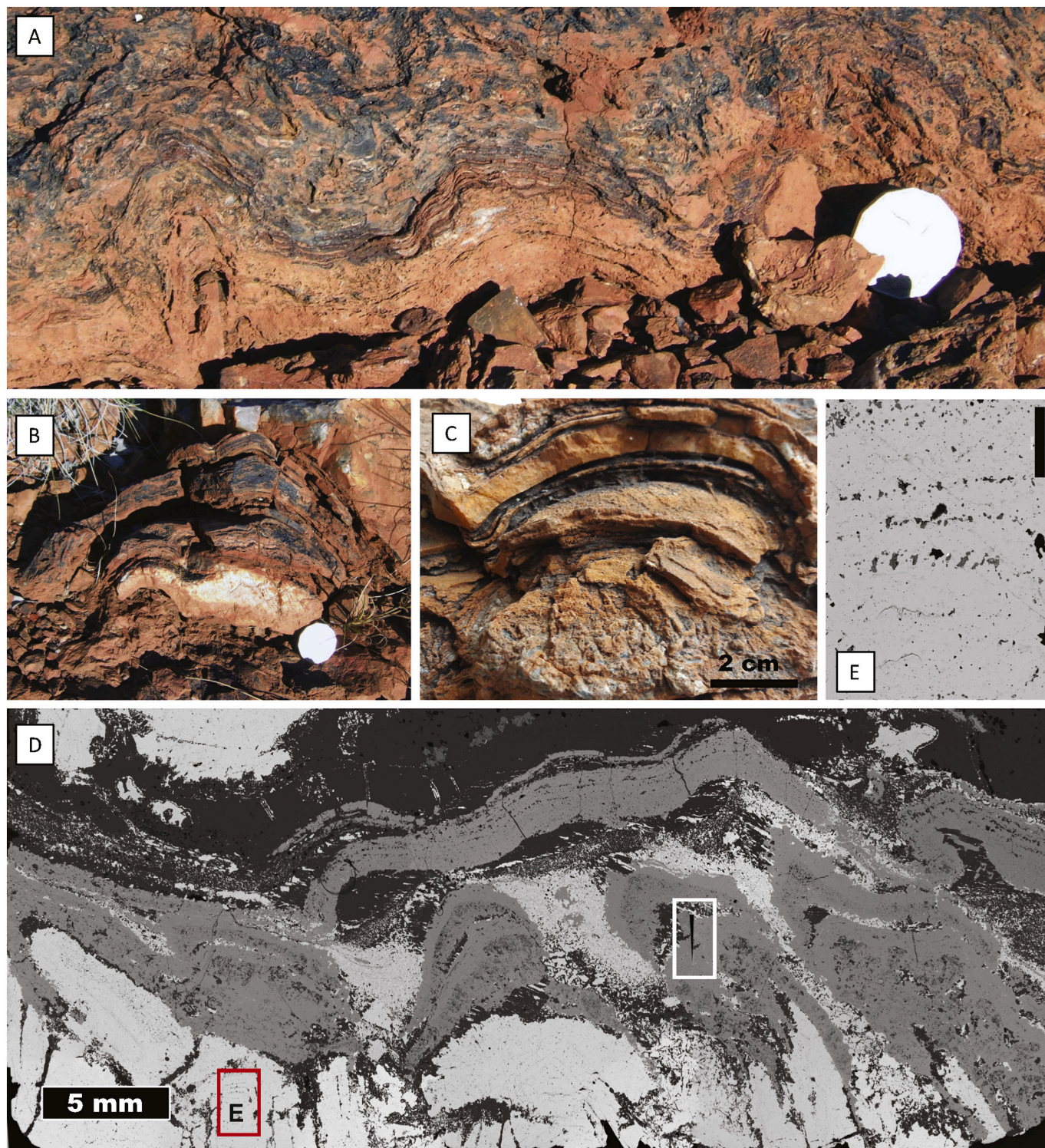


Fig. 14. Possibly biogenic stromatolites in the Dresser Formation. (A-B) Wrinkly (A) and overlying domical (B) stromatolites, Panorama locality (see also [van Kranendonk, 2006](#)). Diameter of 2 AUSS coin is 31.5 mm. (C) Putative stromatolites (at the PDP2 drilling locality, [van Kranendonk et al., 2008](#)) displaying domed structures of chert (white) and Fe-oxides (black, inferred as weathering products of sulfides) overgrowing clusters of millimetric barite blades (lower half). (D) Wrinkly barite-sulfide-chert structures in the PDP2c drillcore (sample F95.1b). Mosaic obtained by stitching of 33 backscattered electron images with Microsoft ICE; the white box marks a stitching artefact. Barite appears in white, pyrite in light grey, carbonates in medium grey (e.g., rhombs at top center), and quartz in dark grey. (E) Enlargement of the red box in (D) showing pyrite (dark grey) microcrystals and quartz (black) on the growth zones of coarse barite (white) crystals; scale bar = 300 μm . (For interpretation of the references to colour in this figure legend, the reader is referred to the web version of this article.)

Colloform sulfides that commonly occur in hydrothermal massive volcanogenic sulfide deposits can form reniform ([Revan et al., 2014](#)), upward-branching, and digitate structures ([Maslennikov et al., 2017](#)) with internal layering similar to those of Dresser Formation sulfides.

Abiogenic routes and processes involving microorganisms and/or organic matter have been proposed to form such colloidal sulfides ([Agangi et al., 2015](#); [Gao et al., 2016](#); [Li et al., 2019](#)). Interestingly, layered and pseudocolumnar sulfides associated with Mesoproterozoic

hydrothermal vents have been proposed to represent sulfide microbialites based on the presence of carbonaceous laminae (Li and Kusky, 2007). Although carbonaceous microstructures occurring in the vent pores suggest the presence of a vent biota at this time, it remains difficult to demonstrate that the sulfide laminae are themselves microbial in origin (Li and Kusky, 2007) solely based on the presence of carbonaceous matter. Carbonaceous matter could have migrated in the hydrothermal system, as shown in recent serpentinites (Pasini et al., 2013) and hydrothermally-influenced lacustrine cherts (Reinhardt et al., 2019). Although the Mesoproterozoic laminated sulfides studied by Li and Kusky (2007) lack diagnostic morphological evidence for microbial participation in their formation (as shown for example in Figs. 9, 12A-D, 13), they represent a counterpart of plausible biogenic origin for the Dresser Formation stromatolites. Furthermore, BaSO₄ microspherulites in the Dresser stromatolites may have formed due to microbial activity or to the presence of organic matter (Baumgartner et al., 2020b). Finally, high-resolution mapping of the Dresser stromatolites has shown heterogeneities in the distributions of minor and trace metalloids and transition metals that revealed or highlighted microdigitate and wrinkly textures in the pyrite (Baumgartner et al., 2020c). These texture-correlated heterogeneities have been proposed to result from the presence of organic matter (Baumgartner et al., 2020c). In conclusion, the biogenic interpretation of the Dresser stromatolites has been strengthened recently and could be further assessed by detailed investigations of hydrothermal systems targeting the distinction between biogenic and abiogenic sulfide mineralization and organic matter sources.

9.7. Stromatolites in Isua (~ 3.7 Ga)?

Coniform and domical structures ca. 1–4 cm in height have been reported in ~ 3.7 Ga metamorphic carbonate of the Isua supracrustal belt, Greenland (Fig. 15A-B) and interpreted as the oldest biogenic stromatolites (Nutman et al., 2016). Subsequent observation suggested that the structures may be ridges rather than cones and that they formed along a specific direction of the rock (not in three dimensions),

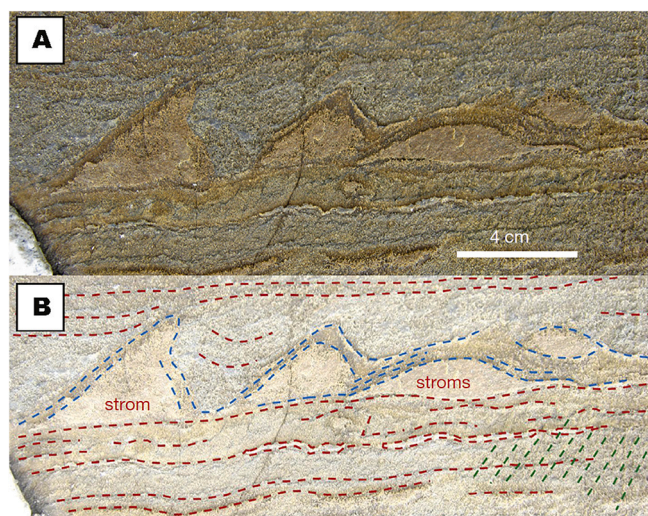


Fig. 15. ~3.7 Ga old stromatolites? (A-B) Possible stromatolites of the Isua supracrustal belt, from Nutman et al. (2016): outcrop picture in (A) and interpretative sketch in (B) showing irregular laminae (blue dashed) and flat laminae (red dashed). Panels (A-B) Reprinted by permission from Springer Nature Customer Service Centre GmbH: Springer Nature, Nature, Rapid emergence of life shown by discovery of 3700-million-year-old microbial structures, Allen P. Nutman, Vickie C. Bennett, Clark R. L. Friend, Martin J. van Kranendonk, Allan R. Chivas, © Springer Nature (2016). (For interpretation of the references to color in this figure legend, the reader is referred to the web version of this article.)

which led to a re-interpretation of the putative stromatolites as deformation structures (Allwood et al., 2018). The observation that cones/ridges grew downwards as well as upwards has been used against growth on the seafloor (Allwood et al., 2018). Downward growth may not rule out stromatolites completely as downward stromatolitic growth structures may occur in cavities (Section 9.4). Furthermore, it has been proposed that, unlike the upward cones/domes, the downward structures could have been formed by a cross-cutting secondary generation of carbonates (Nutman et al., 2019). Soft-sediment deformation has been discussed as a plausible mechanism that could have generated the observed structures (Nutman et al., 2019). An important observation that the domes/cones are “tall structures relative to the thickness of the source bed” (Nutman et al., 2019) may make an origin as soft-sediment fluid-escape structures less likely.

Moreover, Nutman et al. (2019) have recently argued that the local tectonic deformation allows for the 2-D preservation of stromatolitic textures in low-strain fold cores, although the third direction can be strongly elongated. The surface of a sample imaged in 3D by Nutman et al. (2019) displayed one conical and one domical section that have been deemed difficult to reconcile with deformation ridges. However, recent observation revealed ridge structures, possibly as long as 34 cm, that cannot be explained by deformation of cones that are only a few centimeter high (Zawaski et al., 2020). These ridges, oriented parallel to a principal deformation axis, could have formed by boudinage, a deformation process associated with the distinct rheological properties of discontinuous quartz layers (forming boudins) in calc-silicate schist (Zawaski et al., 2020). The possibility that differently-deformed structures were observed by Allwood et al. (2018) and Nutman et al., (2016, 2019) has been refuted on the basis of homogenous microscale deformation texture of quartz at different sampling sites (Zawaski et al., 2020).

Most problematic is the fact that lamination in the conical/domical structures cannot be fully distinguished from chemical zonation (Nutman et al., 2016; Allwood et al., 2018; van Zuilen, 2018; Zawaski et al., 2020), which make these structures difficult to relate to stromatolites *stricto sensu* (c.f. Section 9.1). Thus, a biogenic origin to these structures may not be claimed solely based on morphology (Zawaski et al., 2020).

10. Summary

Highly ¹³C-depleted graphites in Eoarchean rocks have been considered as the oldest geochemical traces of life, but due to the high metamorphic grade of these rocks, it remains difficult to rule out abiotic processes that may have deposited the carbonaceous matter. The oldest, generally accepted evidence of life currently is the sulfur isotope pattern recorded in pyrites indicative of microbial sulfate reduction in the 3.48 Ga Dresser Formation (Fig. 1B). Methanogenesis is indicated as early as 3.0 Ga by ¹³C-depletion in kerogen of sedimentary rocks, and possibly as early as 3.5 Ga as suggested by ¹³C-depletions of fluid inclusions and kerogens, although in the latter case abiotic hydrothermal reactions remain difficult to rule out. Banded iron formations display Fe-isotope signatures indicative of partial oxidation of a Fe²⁺-dominated reservoir, which could have been carried out by anoxygenic photosynthesis likely by 3.46 Ga and possibly as early as 3.77 Ga.

Biomarker molecules that would be diagnostic of specific classes of organisms and/or environments found in Archean rocks have been critically re-evaluated to be contaminants, consistent with the view that the metamorphic grade of these rocks would not allow the preservation of such molecules. Nevertheless, in situ spectroscopic and spectrometric analyses have shown that functional groups with abundant heteroatoms (N, S, O) can be detected in Archean kerogen. Heterogeneities in the distribution of these functional groups, if correlated with textural features (such as microfossils or veins) and C-isotopes compositions, may help distinguish biotic from abiotic carbonaceous matter.

Microtubular titanite textures found in metamorphosed volcanic

glass were initially proposed as the imprints of glass-etching microorganisms (i.e., trace fossils), but are now seen to be more likely metamorphic textures. Moreover, the biotic origin of their modern counterparts remains difficult to demonstrate. Further studies of metamorphic and glass-quenching textures are required to assess the use of microtubes as possible traces of life in ancient seafloors and in volcanoclastic sediments.

With the exception of the youngest Neoproterozoic microfossils associated with stromatolites, virtually all spherical, ovoid and filamentous structures found in Archean cherts have been debated as possible abiotic morphologies generated by accretion/displacement of kerogen along various mineral templates. Large and folded carbonaceous vesicles found in 3.22 Ga siliciclastic rocks and flanged lenticular structures found in ~3.0 to ~3.4 Ga bedded cherts are, however, difficult to reconcile with abiogenic morphogenesis. Once extracted by acid maceration, they display some stunning morphological similarities with some Proterozoic and younger microfossils, and a size and morphological complexity that is surprising for such an early life record. Lenticular forms have been suggested to represent planktonic autotrophs. Texture-specific C-isotope compositions further support a biogenic origin for the carbonaceous matter in these lenticular forms, but still fail to constrain their metabolism.

In the Neoproterozoic, some clearly biogenic carbonate stromatolites display metabolic signatures for methanotrophy, microbial sulfate reduction, and microbial iron reduction in addition to petrographic textures and C-isotope compositions consistent with accretion in presence of photosynthetic microorganisms. Carbonate and siliceous stromatolites displaying a correlation between mineral and organic matter textures demonstrating a role of microorganisms in their formation can be tracked as early as ~3.4 Ga. Other putative stromatolites occur in the Paleoproterozoic to Eoproterozoic rock record, but the absence of carbonaceous remnants and the possible growth by hydrothermal and/or deformation processes limit their use as biosignatures. Sulfidized stromatolites rich in carbonaceous matter formed in hydrothermally-associated environment are candidates for the oldest (3.48 Ga) microbial accretion structures. Along with the biogenic stromatolite record, carbonaceous laminae that display wavy or crinkly textures consistent with formation as microbial mats can be tracked in siliciclastic deposits as old as 3.47 Ga. Further evidence for microbial mats, consistent with participation of oxygenic photosynthesis, lie in the tufted and domed textures of the layered organic matter of 3.22 Ga siliciclastic deposits, and the associated, distinct C and N isotope ratios recorded in marine and terrestrial mats.

Evidence of oxygenic photosynthesis during the Archean is given by the geochemical signatures indicating redox cycling of various metallic elements sensitive to the presence of O₂. Mass-independent fractionation of sulfur isotopes indicates very low O₂ partial pressures throughout the Archean (Fig. 1 and associated references). However, a change in the structure of these mass-independent fractionations occurring at the end of the Mesoproterozoic (Kurzweil et al., 2013; Izon et al., 2017) is consistent with other features of the rock record that suggest photosynthetic production of oxygen at this time, although in environments where the atmosphere was still O₂-depleted (Fig. 1). These features include the textures recorded in Neoproterozoic stromatolites (tufts, palisades, fenestrae) and the associated relatively ¹³C-rich kerogens. However, unambiguous microfossils of oxygenic photosynthetic microorganisms (cyanobacteria) are only demonstrated in ~1.9 Ga (Butterfield, 2015; Lepot et al., 2017) and younger rocks. Autotrophic and/or heterotrophic methanogenesis (Fig. 2F and I, respectively) could have led to the production of organic aerosols in the atmosphere, forming Titan-like organic haze periodically during the Neoproterozoic (Izon et al., 2017 and references therein). Methanotrophs could, however, have interfered with this sun-shielding haze formation (Thomazo et al., 2009b). The latter could have used various oxidants, including the products of anoxygenic photosynthesis (sulfate, Fe³⁺), the direct (O₂) and indirect (nitrate, Fe³⁺, sulfur species) products of

oxygenic photosynthesis, or the sulfuric products of atmospheric photochemistry. The use of these various oxidants as energy sources for metabolisms is indicated in the N, Fe, and S isotope records of the Neoproterozoic, consistent with increasingly oxidizing conditions at the surface of the early Earth.

11. Perspectives

The variety of evidences of life and the diversity of metabolisms appear to increase during the Archean, coincident with the increase in amounts of continental crust. This, together with the associated increase in variety of rock types increased the spatial and chemical diversity of niches that could have been colonized by microorganisms. For example, the development of biological soil crusts and benthic microbial mats may have favored local oxidative weathering, releasing nitrate, sulfate and trace metals (Lalonde and Konhauser, 2015; Thomazo et al., 2018) for other metabolisms, and possibly acting as a local sink for in-situ-produced oxygen without eliminating atmospheric anoxia. Moreover, the evolution of minor and trace metal availability has been linked with the expansion of oxidative weathering and evolution of exposed magmatic rock compositions. Changes in the availabilities of specific metals (Large et al., 2014; Konhauser et al., 2015) may have allowed the rise to prominence, or the relative demise, of some key metabolisms. For example, methanogens may have suffered a nickel famine linked with a decrease in (ultra)mafic volcanism (Konhauser et al., 2015), and an increase in copper availability toward the end of the Archean (Chi Fru et al., 2016) may have favored aerobic metabolisms (Moore et al., 2017). The primary productivity driven by oxygenic photosynthesis (or other metabolisms) maybe have been limited during the Archean by the presence of a large mineral iron sink for phosphorus, and/or by a weak biological recycling of the latter element in anaerobic conditions (Kipp and Stüeken, 2017; Reinhard et al., 2017; Ossa Ossa et al., 2019). Phosphorus limitation may have been alleviated by an increase in the abundance of this element in magmatic rocks toward the end of the Archean (Cox et al., 2018). At the same time, other factors also linked with evolving geodynamics such as increases in the oxidation states of volcanic sulfur (Gaillard et al., 2011) and of magmatic iron (Andraut et al., 2017), and increase in organic matter burial (Eguchi et al., 2020), may have limited reductive sinks for O₂, thus altogether leading to the Great Oxidation Event (Fig. 1A).

The evolution of metabolisms during the Archean (Fig. 1B) has been largely envisioned on the global scale based on geochemical analysis of an increasing number of bulk-rock samples. Interestingly, metabolic signatures recorded with bulk-rock C and N isotope ratios have been contrasted between marine and lacustrine settings (Eigenbrode and Freeman, 2006; Flannery et al., 2016; Stüeken and Buick, 2018), or between lakes associated with drainage basins of felsic and mafic volcanics (Stüeken et al., 2017). These contrasts are suggestive of important environmental controls on the diversification and/or on the relative importance of various metabolisms during the Archean. High-spatial resolution analyses of isotope compositions, of microfossil populations, of mineral assemblages, and of major-to-trace element distributions (as highlighted in this review) have the potential to deconvolve the signals from various microbial communities, their associated mesoscale to microscopic environments, and to decipher the relative importance of their various components. However, preservation biases become particularly important when reaching these scales. Sources of preservation biases diversified in parallel with the development of different environmental “niches”. For example, cherts deposited in hydrothermally-influenced environments, such as many Paleoproterozoic occurrences (Hofmann and Bolhar, 2007), and early diagenetic cherts of the late Archean and Proterozoic (Maliva et al., 2005) may not have had the same preservation potential for microfossils, organic matter, and/or biosignatures in associated minerals. The study of younger and modern, less metamorphosed fossil microbial ecosystems and their experimental alteration products is thus crucial to decipher the most

ancient record of life.

Finally, the selection of reliable methods and criteria that we could use to distinguish biotic from abiotic signatures in Archean rocks is highly relevant to the search for extant or past life beyond Earth. Mars is a plausible and accessible target for the search of past extraterrestrial life as its surface displays abundant rocks older than 3 Ga, and shows evidence that the planet was habitable at this time (Solomon et al., 2005; McMahan et al., 2018).

Declaration of Competing Interest

The authors declare that they have no known competing financial interests or personal relationships that could have appeared to influence the work reported in this paper.

Acknowledgements

Kenichiro Sugitani (Nagoya University), Pascal Philippot (Université de Montpellier), Emmanuelle Javaux (Université de Liège) and Andrew Knoll (Harvard University) are highly thanked for providing most of the samples that I studied. Kenichiro Sugitani is also thanked for allowing me to observe his thin sections at the Nagoya University. Pascal Philippot (U. Montpellier) and Martin van Kranendonk (University of New South Wales) are thanked for taking me and colleagues to outcrops in the Pilbara and explaining them in detail. I thank many colleagues for discussions, for help with analytical techniques, as well as the PhD and Master students I supervised over the years. Nicolas Tribouvillard is thanked for his comments on an early version of this manuscript. I thank Prof. Dr. Karsten Pedersen (editor), Prof. Dr. Christoph Heubeck, and an anonymous reviewers for their constructive comments that helped improve this manuscript. Funding was provided by the Agence Nationale de la Recherche (ANR, France) M6fossils grant ANR-15-CE31-0003 to K.L.

References

- Abbott, G.D., Bashir, F.Z., Sugden, M.A., 2001. Kerogen-bound and free hopanoic acids in the messel oil shale kerogen. *Chirality* 13, 510–516. <https://doi.org/10.1002/chir.1069>.
- Agangi, A., Hofmann, A., Rollion-Bard, C., Marin-Carbonne, J., Cavalazzi, B., Large, R., Meffre, S., 2015. Gold accumulation in the Archaean Witwatersrand Basin, South Africa — Evidence from concentrically laminated pyrite. *Earth-Science Rev.* 140, 27–53. <https://doi.org/10.1016/j.earscirev.2014.10.009>.
- Albut, G., Babechuk, M.G., Kleinhans, I.C., Bengler, M., Beukes, N.J., Steinhilber, B., Smith, A.J.B., Kruger, S.J., Schoenberg, R., 2018. Modern rather than Mesoarchaean oxidative weathering responsible for the heavy stable Cr isotopic signatures of the 2.95 Ga old Ijzermijn iron formation (South Africa). *Geochim. Cosmochim. Acta* 228, 157–189. <https://doi.org/10.1016/j.gca.2018.02.034>.
- Alleon, J., Bernard, S., Le Guillou, C., Beyssac, O., Sugitani, K., Robert, F., 2018. Chemical nature of the 3.4 Ga Strelley pool microfossils. *Geochemical Perspect. Lett.* 7, 37–42. <https://doi.org/10.7185/geochemlet.1817>.
- Alleon, J., Flannery, D.T., Ferralis, N., Williford, K.H., Zhang, Y., Schuessler, J.A., Summons, R.E., 2019. Organo-mineral associations in chert of the 3.5 Ga Mount Ada Basalt raise questions about the origin of organic matter in Paleoproterozoic hydrothermally influenced sediments. *Sci. Rep.* 9, 16712. <https://doi.org/10.1038/s41598-019-53272-5>.
- Allwood, A.C., Walter, M.R., Kamber, B.S., Marshall, C.P., Burch, I.W., 2006a. Stromatolite reef from the early Archaean era of Australia. *Nature* 441, 714–718. <https://doi.org/10.1038/nature04764>.
- Allwood, A.C., Walter, M.R., Marshall, C.P., 2006b. Raman spectroscopy reveals thermal palaeoenvironments of c.3.5 billion-year-old organic matter. *Vib. Spectrosc.* 41, 190–197. <https://doi.org/10.1016/j.vibspec.2006.02.006>.
- Allwood, A.C., Walter, M.R., Burch, I.W., Kamber, B.S., 2007. 3.43 billion-year-old stromatolite reef from the Pilbara Craton of Western Australia: ecosystem-scale insights to early life on Earth. *Precambrian Res.* 158, 198–227. <https://doi.org/10.1016/j.precamres.2007.04.013>.
- Allwood, A.C., Grotzinger, J.P., Knoll, A.H., Burch, I.W., Anderson, M.S., Coleman, M.L., Kanik, I., 2009. Controls on development and diversity of early Archean stromatolites. *Proc. Natl. Acad. Sci. U. S. A.* 106, 9548–9555. <https://doi.org/10.1073/pnas.0903231106>.
- Allwood, A.C., Rosing, M.T., Flannery, D.T., Hurovitz, J.A., Heirwegh, C.M., 2018. Reassessing evidence of life in 3,700-million-year-old rocks of Greenland. *Nature* 563, 241–244. <https://doi.org/10.1038/s41586-018-0610-4>.
- Aloisi, G., Gloter, A., Krüger, M., Wallman, K., Guyot, F., Zuddas, P., 2006. Nucleation of calcium carbonate on bacterial nanoglobules. *Geology* 34, 1017–1020. <https://doi.org/10.1130/G22986A.1>.
- Alt, J.C., Mata, P., 2000. On the role of microbes in the alteration of submarine basaltic glass: a TEM study. *Earth Planet. Sci. Lett.* 181, 301–313. [https://doi.org/10.1016/S0012-821X\(00\)00204-1](https://doi.org/10.1016/S0012-821X(00)00204-1).
- Anbar, A.D., Duan, Y., Lyons, T.W., Arnold, G.L., Kendall, B., Creaser, R.A., Kaufman, A.J., Gordon, G.W., Scott, C., Garvin, J., Buick, R., 2007. A Whiff of Oxygen before the great oxidation event? *Science* 317, 1903–1906. <https://doi.org/10.1126/science.1140325>.
- Andraut, D., Muñoz, M., Pesce, G., Cerantola, V., Chumakov, A., Kantor, I., Pascarelli, S., Rüffer, R., Hennet, L., 2017. Large oxygen excess in the primitive mantle could be the source of the great oxygenation event. *Geochemical Perspect. Lett.* 6, 5–10. <https://doi.org/10.7185/geochemlet.1801>.
- Archer, C., Vance, D., 2006. Coupled Fe and S isotope evidence for Archean microbial Fe (III) and sulfate reduction. *Geology* 34, 153–156. <https://doi.org/10.1130/G22067.1>.
- Arndt, N.T., Nisbet, E.G., 2012. Processes on the young Earth and the habitats of early life. *Annu. Rev. Earth Planet. Sci.* 40, 521–549. <https://doi.org/10.1146/annurev-earth-042711-105316>.
- Arp, G., Reimer, A., Reitner, J., 2003. Microbialite formation in seawater of increased alkalinity, Satonda Crater Lake, Indonesia. *J. Sediment. Res.* 73, 105–127. <https://doi.org/10.1306/071002730105>.
- Awramik, S.M., 1976. Chapter 6.3 Gunflint Stromatolites: microfossil distribution in relation to stromatolite morphology, in: *Stromatolites. Dev. Sedimentol.* 20, 311–320. [https://doi.org/10.1016/S0070-4571\(08\)71141-5](https://doi.org/10.1016/S0070-4571(08)71141-5).
- Awramik, S.M., Buchheim, H.P., 2009. A giant, late Archean lake system: the Meentheena Member (Tumbiana Formation; Fortescue Group), Western Australia. *Precambrian Res.* 174, 215–240. <https://doi.org/10.1016/j.precamres.2009.07.005>.
- Awramik, S.M., Semikhatov, M.A., 1979. The relationship between morphology, microstructure, and microbiota in three vertically intergrading stromatolites from the Gunflint Iron Formation. *Can. J. Earth Sci.* 16, 484–495. <https://doi.org/10.1139/e79-044>.
- Awramik, S.M., Schopf, J.W., Walter, M.R., 1983. Filamentous fossil bacteria from the Archean of Western Australia. *Precambrian Res.* 20, 357–374. [https://doi.org/10.1016/S0166-2635\(08\)70251-2](https://doi.org/10.1016/S0166-2635(08)70251-2).
- Banerjee, N.R., Muehlenbachs, K., 2003. Tuff life: Bioalteration in volcanoclastic rocks from the Ontong Java Plateau. *Geochemistry, Geophys. Geosystems* 4. <https://doi.org/10.1029/2002GC000470>.
- Banerjee, N.R., Furnes, H., Muehlenbachs, K., Staudigel, H., de Wit, M., 2006. Preservation of ~3.4–3.5 Ga microbial biomarkers in pillow lavas and hyaloclastites from the Barberton Greenstone Belt, South Africa. *Earth Planet. Sci. Lett.* 241, 707–722. <https://doi.org/10.1016/j.epsl.2005.11.011>.
- Banerjee, N.R., Simonetti, A., Furnes, H., Muehlenbachs, K., Staudigel, H., Heaman, L., Van Kranendonk, M.J., 2007. Direct dating of Archean microbial ichnofossils. *Geology* 35, 487–490. <https://doi.org/10.1130/G23534A.1>.
- Barbieri, R., Cavalazzi, B., Stivaletta, N., López-García, P., 2014. Silicified biota in high-altitude, geothermally influenced ignimbrites at El Tatio Geyser Field, Andean Cordillera (Chile). *Geomicrobiol. J.* 31, 493–508. <https://doi.org/10.1080/01490451.2013.836691>.
- Barlow, E.V., van Kranendonk, M.J., 2018. Snapshot of an early Paleoproterozoic ecosystem: two diverse microfossil communities from the Turee Creek Group, Western Australia. *Geobiology* 16, 449–475. <https://doi.org/10.1111/gbi.12304>.
- Baumgartner, R.J., van Kranendonk, M.J., Wacey, D., Fiorentini, M.L., Saunders, M., Caruso, S., Pages, A., Homann, M., Guagliardo, P., 2019. Nano-porous pyrite and organic matter in 3.5-billion-year-old stromatolites record primordial life. *Geology* 47, 1039–1043. <https://doi.org/10.1130/G46365.1>.
- Baumgartner, R.J., Caruso, S., Fiorentini, M.L., van Kranendonk, M.J., Martin, L., Jeon, H., Pagès, A., Wacey, D., 2020a. Sulfidization of 3.48 billion-year-old stromatolites of the Dresser Formation, Pilbara Craton: Constraints from in-situ sulfur isotope analysis of pyrite. *Chem. Geol.* 538, 119488. <https://doi.org/10.1016/j.chemgeo.2020.119488>.
- Baumgartner, R.J., van Kranendonk, M.J., Fiorentini, M.L., Pagès, A., Wacey, D., Kong, C., Saunders, M., Ryan, C., 2020b. Formation of micro-spherulitic barite in association with organic matter within sulfidized stromatolites of the 3.48 billion-year-old Dresser Formation, Pilbara Craton. *Geobiology* 18, 415–425. <https://doi.org/10.1111/gbi.12392>.
- Baumgartner, R.J., van Kranendonk, M.J., Pagès, A., Fiorentini, M.L., Wacey, D., Ryan, C., 2020c. Accumulation of transition metals and metalloids in sulfidized stromatolites of the 3.48 billion-year-old Dresser Formation, Pilbara Craton. *Precambrian Res.* 337, 105534. <https://doi.org/10.1016/j.precamres.2019.105534>.
- Beal, E.J., House, C.H., Orphan, V.J., 2009. Manganese- and iron-dependent marine methane oxidation. *Science* 325, 184–187. <https://doi.org/10.1126/science.1169984>.
- Beaumont, V., Robert, F., 1999. Nitrogen isotope ratios of kerogens in Precambrian cherts: a record of the evolution of atmosphere chemistry? *Precambrian Res.* 96, 63–82. [https://doi.org/10.1016/S0301-9268\(99\)00005-4](https://doi.org/10.1016/S0301-9268(99)00005-4).
- Bell, E.A., Boehnke, P., Harrison, T.M., Mao, W.L., 2015. Potentially biogenic carbon preserved in a 4.1 billion-year-old zircon. *Proc. Natl. Acad. Sci. U. S. A.* 112, 14518–14521. <https://doi.org/10.1073/pnas.1517557112>.
- Benning, L.G., Phoenix, V.R., Mountain, B.W., 2005. Biosilicification: the role of cyanobacteria in silica sinter deposition. *Micro-Organisms Earth Syst. - Adv. Geomicrobiol. Publ. Soc. Gen. Microbiol.* 131–150. <https://doi.org/10.1017/CBO9780511754852.008>.
- Benzerara, K., Menguy, N., Lopez-Garcia, P., Yoon, T.-H., Kazmierczak, J., Tylliszczak, T., Guyot, F., Brown, G.E., 2006. Nanoscale detection of organic signatures in carbonate microbialites. *Proc. Natl. Acad. Sci. U. S. A.* 103, 9440–9445. <https://doi.org/10.1073/pnas.1517557112>.

- 1073/pnas.0603255103.
- Benzerara, K., Menguy, N., Banerjee, N.R., Tyliszczak, T., Brown, G.E., Guyot, F., 2007. Alteration of submarine basaltic glass from the Ontong Java Plateau: a STXM and TEM study. *Earth Planet. Sci. Lett.* 260, 187–200. <https://doi.org/10.1016/j.epsl.2007.05.029>.
- Berndt, M.E., Allen, D.E., Seyfried, W.E., 1996. Reduction of CO₂ during serpentinization of olivine at 300 °C and 500 bar. *Geology* 24, 351. [https://doi.org/10.1130/0091-7613\(1996\)024<0351:ROCDSO>2.3.CO;2](https://doi.org/10.1130/0091-7613(1996)024<0351:ROCDSO>2.3.CO;2).
- Bisdorn, E.B.A., Stoops, G., Delvigne, J., Curmi, P., Altemüller, H., 1982. Micromorphology of weathering biotite and its secondary products. *Pedologie* 32, 225–252.
- Bizić, M., Klintzsch, T., Ionescu, D., Hindiyeh, M.Y., Günthel, M., Muro-Pastor, A.M., Eckert, W., Ulrich, T., Keppler, F., Grossart, H.-P., 2020. Aquatic and terrestrial cyanobacteria produce methane. *Sci. Adv.* 6 <https://doi.org/10.1126/sciadv.aax5343>. eaax5343.
- Blaser, M.B., Dreisbach, L.K., Conrad, R., 2013. Carbon isotope fractionation of 11 acetogenic strains grown on H₂ and CO₂. *Appl. Environ. Microbiol.* 79, 1787–1794. <https://doi.org/10.1128/AEM.03203-12>.
- Bontognali, T.R.R., Vasconcelos, C., Warthmann, R.J., Dupraz, C., Bernasconi, S.M., McKenzie, J.A., 2008. Microbes produce nanobacteria-like structures, avoiding cell entombment. *Geology* 36, 663–666. <https://doi.org/10.1130/G24755A.1>.
- Bontognali, T.R.R., Sessions, A.L., Allwood, A.C., Fischer, W.W., Grotzinger, J.P., Summons, R.E., Eiler, J.M., 2012. Sulfur isotopes of organic matter preserved in 3.45-billion-year-old stromatolites reveal microbial metabolism. *Proc. Natl. Acad. Sci. U. S. A.* 109, 15146–15151. <https://doi.org/10.1073/pnas.1207491109>.
- Bosak, T., Souza-Egipsy, V., Newman, D.K., 2004. A laboratory model of abiotic peloid formation. *Geobiology* 2, 189–198. <https://doi.org/10.1111/j.1472-4677.2004.00031.x>.
- Bosak, T., Knoll, A.H., Petroff, A.P., 2013. The meaning of stromatolites. *Annu. Rev. Earth Planet. Sci.* 41, 21–44. <https://doi.org/10.1146/annurev-earth-042711-105327>.
- Böttcher, M.E., Thamdrup, B., Vennemann, T.W., 2001. Oxygen and sulfur isotope fractionation during anaerobic bacterial disproportionation of elemental sulfur. *Geochim. Cosmochim. Acta* 65, 1601–1609. [https://doi.org/10.1016/S0016-7037\(00\)00628-1](https://doi.org/10.1016/S0016-7037(00)00628-1).
- Botz, R., Pokojski, H.-D.D., Schmitt, M., Thomm, M., 1996. Carbon isotope fractionation during bacterial methanogenesis by CO₂ reduction. *Org. Geochem.* 25, 255–262. [https://doi.org/10.1016/S0146-6380\(96\)00129-5](https://doi.org/10.1016/S0146-6380(96)00129-5).
- Brasier, M.D., Green, O.R., Jephcoat, A.P., Klepe, A.K., Van Kranendonk, M.J., Lindsay, J.F., Steele, A., Grassineau, N.V., 2002. Questioning the evidence for Earth's oldest fossils. *Nature* 416, 76–81. <https://doi.org/10.1038/416076a>.
- Brasier, M.D., Green, O.R., Lindsay, J.F., McLoughlin, N., Steele, A., Stoakes, C., 2005. Critical testing of Earth's oldest putative fossil assemblage from the ~3.5 Ga Apex chert, Chinaman Creek, Western Australia. *Precambrian Res.* 140, 55–102. <https://doi.org/10.1016/j.precamres.2005.06.008>.
- Brasier, M.D., Antcliffe, J., Saunders, M., Wacey, D., 2015. Changing the picture of Earth's earliest fossils (3.5–1.9 Ga) with new approaches and new discoveries. *Proc. Natl. Acad. Sci. U. S. A.* 112, 4859–4864. <https://doi.org/10.1073/pnas.1405338111>.
- Braunstein, D., Lowe, D.R., 2001. Relationship between spring and Geyser activity and the deposition and morphology of high temperature (> 73°C) Siliceous Sinter, Yellowstone National Park, Wyoming, U.S.A. *J. Sediment. Res.* 71, 747–763. <https://doi.org/10.1306/d4268d88-2b26-11d7-8648000102c1865d>.
- Bridge, N.J., Banerjee, N.R., Mueller, W., Muehlenbachs, K., Chacko, T., 2010. A volcanic habitat for early life preserved in the Abitibi Greenstone belt, Canada. *Precambrian Res.* 179, 88–98. <https://doi.org/10.1016/j.precamres.2010.02.017>.
- Brocks, J.J., 2011. Millimeter-scale concentration gradients of hydrocarbons in Archean shales: Live-oil escape or fingerprint of contamination? *Geochim. Cosmochim. Acta* 75, 3196–3213. <https://doi.org/10.1016/j.gca.2011.03.014>.
- Brocks, J.J., Logan, G.A., Buick, R., Summons, R.E., 1999. Archean molecular fossils and the early rise of eukaryotes. *Science* 285, 1033–1036. <https://doi.org/10.1126/science.285.5430.1033>.
- Brocks, J.J., Love, G.D., Snape, C.E., Logan, G.A., Summons, R.E., Buick, R., 2003. Release of bound aromatic hydrocarbons from late Archean and Mesoproterozoic kerogens via hydrolysis. *Geochim. Cosmochim. Acta* 67, 1521–1530. [https://doi.org/10.1016/S0016-7037\(00\)01302-9](https://doi.org/10.1016/S0016-7037(00)01302-9).
- Buick, R., 1984. Carbonaceous filaments from North Pole, Western Australia: are they fossil bacteria in Archean stromatolites? *Precambrian Res.* 24, 157–172. [https://doi.org/10.1016/0301-9268\(84\)90056-1](https://doi.org/10.1016/0301-9268(84)90056-1).
- Buick, R., 1990. Microfossil recognition in Archean rocks: an appraisal of spheroids and filaments from a 3500 m.y. old chert-barite unit at North Pole, Western Australia. *Palaios* 5, 441. <https://doi.org/10.2307/3514837>.
- Buick, R., 1992. The antiquity of oxygenic photosynthesis: evidence from stromatolites in sulphate-deficient Archean lakes. *Science* 255, 74–77. <https://doi.org/10.1126/science.11536492>.
- Buick, R., 2008. When did oxygenic photosynthesis evolve? *Philos. Trans. R. Soc. B Biol. Sci.* 363, 2731–2743. <https://doi.org/10.1098/rstb.2008.0041>.
- Buick, R., 2010. Ancient acritarchs. *Nature* 463, 885–886. <https://doi.org/10.1038/463885a>.
- Buick, R., Dunlop, J.S.R., Groves, D.I., 1981. Stromatolite recognition in ancient rocks: an appraisal of irregularly laminated structures in an early Archean chert-barite unit from North Pole, Western Australia. *Alcheringa* 5, 161–181. <https://doi.org/10.1080/03115518108566999>.
- Burne, R.V., Moore, L.S., 1987. Microbialites: organosedimentary deposits of benthic microbial communities. *Palaios* 2, 241. <https://doi.org/10.2307/3514674>.
- Burne, R.V., Moore, L.S., Christy, A.G., Troitzsch, U., King, P.L., Carnerup, A.M., Joseph Hamilton, P., 2014. Stevensite in the modern thrombolites of Lake Clifton, Western Australia: a missing link in microbialite mineralization? *Geology* 42, 575–578. <https://doi.org/10.1130/G35484.1>.
- Busigny, V., Lebeau, O., Ader, M., Krapež, B., Bekker, A., 2013. Nitrogen cycle in the late Archean ferruginous ocean. *Chem. Geol.* 362, 115–130. <https://doi.org/10.1016/j.chemgeo.2013.06.023>.
- Busigny, V., Marin-Carbone, J., Muller, E., Cartigny, P., Rollion-Bard, C., Assayag, N., Philippot, P., 2017. Iron and sulfur isotope constraints on redox conditions associated with the 3.2 Ga barite deposits of the Mapepe Formation (Barberton Greenstone Belt, South Africa). *Geochim. Cosmochim. Acta* 210, 247–266. <https://doi.org/10.1016/j.gca.2017.05.002>.
- Butterfield, N.J., 2015. Proterozoic photosynthesis - a critical review. *Palaeontology* 58, 953–972. <https://doi.org/10.1111/pala.12211>.
- Byerly, G.R., Palmer, M.R., 1991. Tourmaline mineralization in the Barberton greenstone belt, South Africa: early Archean metasomatism by evaporite-derived boron. *Contrib. Mineral. Petrol.* 107, 387–402. <https://doi.org/10.1007/BF00325106>.
- Byerly, G.R., Lower, D.R., Walsh, M.M., 1986. Stromatolites from the 3,300-3,500-Myr Swaziland supergroup, Barberton Mountain land, South Africa. *Nature* 319, 489–491. <https://doi.org/10.1038/319489a0>.
- Cady, S.L., Farmer, J.D., 1996. Fossilization Processes in Siliceous Thermal Springs: Trends in Preservation along Thermal Gradients, in: *Evolution of Hydrothermal Ecosystems on Earth (and Mars?)*. John Wiley & Sons, Chichester, pp. 150–173. <https://doi.org/10.1002/9780470514986.ch9>.
- Cai, P., Huang, Q., Jiang, D., Rong, X., Liang, W., 2006. Microcalorimetric studies on the adsorption of DNA by soil colloidal particles. *Colloids Surfaces B Biointerfaces* 49, 49–54. <https://doi.org/10.1016/j.colsurfb.2006.02.011>.
- Campbell, K.A., Lynne, B.Y., Handley, K.M., Jordan, S., Farmer, J.D., Guido, D.M., Foucher, F., Turner, S., Perry, R.S., 2015. Tracing biosignature preservation of geothermally silicified microbial textures into the geological record. *Astrobiology* 15, 858–882. <https://doi.org/10.1089/ast.2015.1307>.
- Canfield, D.E., Ngombi-Pemba, L., Hammarlund, E.U., Bengtson, S., Chaussidon, M., Gauthier-Lafaye, F., Meunier, A., Riboulleau, A., Rollion-Bard, C., Rouxel, O., Asael, D., Pierson-Wickmann, A.C., El Albani, A., 2013. Oxygen dynamics in the aftermath of the Great Oxidation of Earth's atmosphere. *Proc. Natl. Acad. Sci. U. S. A.* 110, 16736–16741. <https://doi.org/10.1073/pnas.1315570110>.
- Canfield, D.E., Poulton, S.W., Knoll, A.H., Narbonne, G.M., Ross, G., Goldberg, T., Strauss, H., 2008. Ferruginous conditions dominated later neoproterozoic deep-water chemistry. *Science* 321, 949–952. <https://doi.org/10.1126/science.1154499>.
- Cangemi, M., Bellanca, A., Borin, S., Hopkinson, L., Mapelli, F., Neri, R., 2010. The genesis of actively growing siliceous stromatolites: evidence from Lake Specchio di Veneri, Pantelleria Island, Italy. *Chem. Geol.* 276, 318–330. <https://doi.org/10.1016/j.chemgeo.2010.06.017>.
- Castanier, S., Le Métayer-Lével, G., Perthuisot, J.P., 1999. Ca-carbonates precipitation and limestone genesis - the microbiogeologist point of view. *Sediment. Geol.* 126, 9–23. [https://doi.org/10.1016/S0037-0738\(99\)00028-7](https://doi.org/10.1016/S0037-0738(99)00028-7).
- Catling, D.C., 2006. Comment on "A Hydrogen-Rich Early Earth Atmosphere". *Science* 311 <https://doi.org/10.1126/science.1117827>. 38a–38a.
- Catling, D.C., Zahnle, K.J., 2020. The Archean atmosphere. *Sci. Adv.* 6 <https://doi.org/10.1126/sciadv.aax1420>. eaax1420.
- Chacko, T., Cole, D.R., Horita, J., 2001. Equilibrium oxygen, hydrogen and carbon isotope fractionation factors applicable to geologic systems. In: Valley, J.W., Cole, D.R. (Eds.), *Reviews in Mineralogy and Geochemistry*. Mineralogical Society of America, Washington, pp. 1–81. <https://doi.org/10.2138/gsmg.43.1.1>.
- Chi Fru, E., Rodríguez, N.P., Partin, C.A., Lalonde, S.V., Andersson, P., Weiss, D.J., El Albani, A., Rodushkin, I., Konhauser, K.O., 2016. Cu isotopes in marine black shales record the great oxidation event. *Proc. Natl. Acad. Sci. U. S. A.* 113, 4941–4946. <https://doi.org/10.1073/pnas.1523544113>.
- Chowens, T.M., Elkins, J.E., 1974. The origin of quartz geodes and cauliflower cherts through the silicification of anhydrite nodules. *J. Sediment. Res. Vol.* 44, 885–903. <https://doi.org/10.1306/212f6bd1-2b24-11d7-8648000102c1865d>.
- Claeys, P., Mount, J., 1991. Diagenetic origin of carbonate, sulfide and oxide inclusions in biotites of the Great Valley Group (cretaceous), Sacramento Valley, California. *J. Sediment. Res.* 61, 719–731. <https://doi.org/10.1306/D42677BC-2B26-11D7-8648000102c1865D>.
- Close, H.G., Bovee, R., Pearson, A., 2011. Inverse carbon isotope patterns of lipids and kerogen record heterogeneous primary biomass. *Geobiology* 9, 250–265. <https://doi.org/10.1111/j.1472-4669.2011.00273.x>.
- Cockell, C.S., Raven, J.A., 2007. Ozone and life on the Archean Earth. *Philos. Trans. R. Soc. A Math. Phys. Eng. Sci.* 365, 1889–1901. <https://doi.org/10.1098/rsta.2007.2049>.
- Cockell, C.S., van Calsteren, P., Mosselmans, J.F.W., Franchi, I.A., Gilmour, I., Kelly, L., Olsson-Francis, K., Johnson, D., 2010. Microbial endolithic colonization and the geochemical environment in young seafloor basalts. *Chem. Geol.* 279, 17–30. <https://doi.org/10.1016/j.chemgeo.2010.09.015>.
- Coffey, J.M., Flannery, D.T., Walter, M.R., George, S.C., 2013. Sedimentology, stratigraphy and geochemistry of a stromatolite biofacies in the 2.72Ga Tumbiana formation, Fortescue Group, Western Australia. *Precambrian Res.* 236, 282–296. <https://doi.org/10.1016/j.precamres.2013.07.021>.
- Conrad, R., Claus, P., Chidthaisong, A., Liu, Y., Fernandez Scavino, A., Liu, Y., Angel, R., Galand, P.E., Casper, P., Guerin, F., Enrich-Prast, A., 2014. Stable carbon isotope geochemistry of propionate and acetate in methanogenic soils and lake sediments. *Org. Geochem.* 73, 1–7. <https://doi.org/10.1016/j.orggeochem.2014.03.010>.
- Cosmidis, J., Templeton, A.S., 2016. Self-assembly of biomorphic carbon/sulfur microstructures in sulfidic environments. *Nat. Commun.* 7, 12812. <https://doi.org/10.1038/ncomms12812>.
- Cox, G.M., Lyons, T.W., Mitchell, R.N., Hasterok, D., Gard, M., 2018. Linking the rise of atmospheric oxygen to growth in the continental phosphorus inventory. *Earth Planet. Sci. Lett.* 489, 28–36. <https://doi.org/10.1016/j.epsl.2018.02.016>.

- Craddock, P.R., Dauphas, N., 2011. Iron and carbon isotope evidence for microbial iron respiration throughout the Archean. *Earth Planet. Sci. Lett.* 303, 121–132. <https://doi.org/10.1016/j.epsl.2010.12.045>.
- Crovisier, J.L., Advocat, T., Dussosoy, J.L., 2003. Nature and role of natural alteration gels formed on the surface of ancient volcanic glasses (Natural analogs of waste containment glasses). *J. Nucl. Mater.* 321, 91–109. [https://doi.org/10.1016/s0022-3115\(03\)00206-x](https://doi.org/10.1016/s0022-3115(03)00206-x).
- Crowe, S.A., Døssing, L.N., Beukes, N.J., Bau, M., Kruger, S.J., Frei, R., Canfield, D.E., 2013. Atmospheric oxygenation three billion years ago. *Nature* 501, 535–538. <https://doi.org/10.1038/nature12426>.
- Crowe, S.A., Paris, G., Katsev, S., Jones, C., Kim, S.-T., Zerkle, A.L., Nomosatryo, S., Fowle, D.A., Adkins, J.F., Sessions, A.L., Farquhar, J., Canfield, D.E., 2014. Sulfate was a trace constituent of Archean seawater. *Science* 346, 735–739. <https://doi.org/10.1126/science.1258966>.
- Cuerno, R., Escudero, C., García-Ruiz, J.M., Herrero, M.A., 2012. Pattern formation in stromatolites: Insights from mathematical modelling. *J. R. Soc. Interface* 9, 1051–1062. <https://doi.org/10.1098/rsif.2011.0516>.
- Czaja, A.D., Johnson, C.M., Beard, B.L., Eigenbrode, J.L., Freeman, K.H., Yamaguchi, K.E., 2010. Iron and carbon isotope evidence for ecosystem and environmental diversity in the ~ 2.7 to 2.5 Ga Hamersley Province, Western Australia. *Earth Planet. Sci. Lett.* 292, 170–180. <https://doi.org/10.1016/j.epsl.2010.01.032>.
- Czaja, A.D., Johnson, C.M., Beard, B.L., Roden, E.E., Li, W., Moorbath, S., 2013. Biological Fe oxidation controlled deposition of banded iron formation in the ca. 3770Ma Isua Supracrustal Belt (West Greenland). *Earth Planet. Sci. Lett.* 363, 192–203. <https://doi.org/10.1016/j.epsl.2012.12.025>.
- Czaja, A.D., Beukes, N.J., Osterhout, J.T., 2016. Sulfur-oxidizing bacteria prior to the Great Oxidation Event from the 2.52 Ga Gamohaan Formation of South Africa. *Geology* 44, 983–986. <https://doi.org/10.1130/G38150.1>.
- Davies, N.S., Liu, A.G., Gibling, M.R., Miller, R.F., 2016. Resolving MISS conceptions and misconceptions: a geological approach to sedimentary surface textures generated by microbial and abiotic processes. *Earth-Science Rev.* 154, 210–246. <https://doi.org/10.1016/j.earscirev.2016.01.005>.
- De Gregorio, B.T., Sharp, T.G., Rushdi, A.I., Simoneit, B.R.T., 2010. Bugs or Gunk? Nanoscale methods for assessing the biogenicity of ancient microfossils and organic matter. In: Golding, S.D., Glikson, M. (Eds.), *Earliest Life on Earth: Habitats, Environments and Methods of Detection*. Springer Netherlands, Dordrecht, pp. 239–289. <https://doi.org/10.1007/978-90-481-8794-2>.
- Delarue, F., Robert, F., Derenne, S., Tartèse, R., Jauvion, C., Bernard, S., Pont, S., Gonzalez-Cano, A., Duhamel, R., Sugitani, K., 2020. Out of rock: a new look at the morphological and geochemical preservation of microfossils from the 3.46 Gyr-old Strelley Pool Formation. *Precambrian Res.* 336, 105472. <https://doi.org/10.1016/j.precamres.2019.105472>.
- Dell'Anno, A., Danovaro, R., 2005. Ecology: Extracellular DNA plays a key role in deep-sea ecosystem functioning. *Science* 309, 2179. <https://doi.org/10.1126/science.1117475>.
- Derenne, S., Robert, F., 2010. Model of molecular structure of the insoluble organic matter isolated from Murchison meteorite. *Meteorit. Planet. Sci.* 45, 1461–1475. <https://doi.org/10.1111/j.1945-5100.2010.01122.x>.
- Derenne, S., Robert, F., Skrzypczak-Bonduelle, A., Gourier, D., Binet, L., Rouzard, J.N., 2008. Molecular evidence for life in the 3.5 billion year old Warrawoona chert. *Earth Planet. Sci. Lett.* 272, 476–480. <https://doi.org/10.1016/j.epsl.2008.05.014>.
- Des Marais, D.J., 2001. Isotopic evolution of the biogeochemical carbon cycle during the Precambrian. In: Valley, J.W., Cole, D.R. (Eds.), *Reviews in Mineralogy and Geochemistry*. Mineralogical Society of America, pp. 555–578. <https://doi.org/10.2138/gsrmg.43.1.555>.
- Djokic, T., van Kranendonk, M.J., Campbel, K.A., Walter, M.R., Ward, C.R., 2017. Earliest signs of life on land preserved in ca. 3.5 Ga hot spring deposits. *Nat. Commun.* 8, 1–8. <https://doi.org/10.1038/ncomms15263>.
- Dodd, M.S., Papineau, D., Grenne, T., Slack, J.F., Rittner, M., Pirajno, F., O'Neil, J., Little, C.T.S., 2017. Evidence for early life in Earth's oldest hydrothermal vent precipitates. *Nature* 543, 60–64. <https://doi.org/10.1038/nature21377>.
- Duda, J.-P., van Kranendonk, M.J., Thiel, V., Ionescu, D., Strauss, H., Schäfer, N., Reitner, J., 2016. A rare glimpse of Paleoproterozoic life: Geobiology of an exceptionally preserved microbial mat facies from the 3.4 Ga Strelley Pool Formation, Western Australia. *PLoS One* 11. <https://doi.org/10.1371/journal.pone.0147629>. e0147629.
- Duda, J.-P., Thiel, V., Bauersachs, T., Mißbach, H., Reinhardt, M., Schäfer, N., van Kranendonk, M.J., Reitner, J., 2018. Ideas and perspectives: hydrothermally driven redistribution and sequestration of early Archean biomass – the “hydrothermal pump hypothesis”. *Biogeosciences* 15, 1535–1548. <https://doi.org/10.5194/bg-15-1535-2018>.
- Dufaud, F., Martinez, I., Shilobreeva, S., 2009. Experimental study of Mg-rich silicates carbonation at 400 and 500 °C and 1 kbar. *Chem. Geol.* 265, 79–87. <https://doi.org/10.1016/j.chemgeo.2009.01.026>.
- Dunlop, J.S.R., Milne, V.A., Groves, D.I., Muir, M.D., 1978. A new microfossil assemblage from the Archean of Western Australia. *Nature* 274, 676–678. <https://doi.org/10.1038/274676a0>.
- Dupraz, C., Visscher, P.T., Baumgartner, L.K., Reid, R.P., 2004. Microbe-mineral interactions: early carbonate precipitation in a hypersaline lake (Eleuthera Island, Bahamas). *Sedimentology* 51, 745–765.
- Dupraz, C., Reid, R.P., Braissant, O., Decho, A.W., Norman, R.S., Visscher, P.T., 2009. Processes of carbonate precipitation in modern microbial mats. *Earth-Science Rev.* 96, 141–162. <https://doi.org/10.1016/j.earscirev.2008.10.005>.
- Dupraz, C., Fowler, A., Tobias, C., Visscher, P.T., 2013. Stromatolitic knobs in Storr's Lake (San Salvador, Bahamas): a model system for formation and alteration of laminae. *Geobiology* 11, 527–548. <https://doi.org/10.1111/gbi.12063>.
- Dutkiewicz, A., George, S.C., Mossman, D.J., Ridley, J., Volk, H., 2007. Oil and its biomarkers associated with the Palaeoproterozoic Oklo natural fission reactors. *Gabon. Chem. Geol.* 244, 130–154. <https://doi.org/10.1016/j.chemgeo.2007.06.010>.
- Eguchi, J., Seales, J., Dasgupta, R., 2020. Great Oxidation and Lomagundi events linked by deep cycling and enhanced degassing of carbon. *Nat. Geosci.* 13, 71–76. <https://doi.org/10.1038/s41561-019-0492-6>.
- Eickmann, B., Hofmann, A., Wille, M., Bui, T.H., Wing, B.A., Schoenberg, R., 2018. Isotopic evidence for oxygenated Neoproterozoic shallow oceans. *Nat. Geosci.* <https://doi.org/10.1038/s41561-017-0036-x>.
- Eigenbrode, J.L., Freeman, K.H., 2006. Late Archean rise of aerobic microbial ecosystems. *Proc. Natl. Acad. Sci. U. S. A.* 103, 15759–15764. <https://doi.org/10.1073/pnas.0607540103>.
- Eigenbrode, J.L., Freeman, K.H., Summons, R.E., 2008. Methylhopane biomarker hydrocarbons in Hamersley Province sediments provide evidence for Neoproterozoic aerobic biosynthesis. *Earth Planet. Sci. Lett.* 273, 323–331. <https://doi.org/10.1016/j.epsl.2008.06.037>.
- Engel, A.E.J., Nagy, B., Nagy, L.A., Engel, C.G., Kremp, G.O.W., Drew, C.M., 1968. Algal-like forms in Onverwacht Series, South Africa: Oldest recognized lifelike forms on Earth. *Science* 161, 1005–1008. <https://doi.org/10.1126/science.161.3845.1005>.
- Etique, M., Jorand, F.P.A., Ruby, C., 2016. Magnetite as a precursor for green rust through the hydrogenotrophic activity of the iron-reducing bacteria *Shewanella putrefaciens*. *Geobiology* 14, 237–254. <https://doi.org/10.1111/gbi.12170>.
- Fadel, A., 2018. *Micro et nanoanalyses des microfossiles du Protérozoïque et de tapis microbiens fossiles*. PhD thesis. Université de Lille, pp. 258.
- Fadel, A., Lepot, K., Busigny, V., Addad, A., Troade, D., 2017. Iron mineralization and taphonomy of microfossils of the 2.45–2.21 Ga Turee Creek Group, Western Australia. *Precambrian Res.* 298, 530–551. <https://doi.org/10.1016/j.precamres.2017.07.003>.
- Fadel, A., Lepot, K., Nuns, N., Regnier, S., Riboulleau, A., 2020. New preparation techniques for molecular and in-situ analysis of ancient organic micro- and nanostructures. *Geobiology* 18, 445–461. <https://doi.org/10.1111/gbi.12380>.
- Farquhar, J., Wing, B.A., 2003. Multiple sulfur isotopes and the evolution of the atmosphere. *Earth Planet. Sci. Lett.* 213, 1–13. [https://doi.org/10.1016/S0012-821X\(03\)00296-6](https://doi.org/10.1016/S0012-821X(03)00296-6).
- Farquhar, J., Cliff, J., Zerkle, A.L., Kamysny, A., Poulton, S.W., Claire, M., Adams, D., Harms, B., 2013. Pathways for Neoproterozoic pyrite formation constrained by mass-independent sulfur isotopes. *Proc. Natl. Acad. Sci. U. S. A.* 110, 17638–17643. <https://doi.org/10.1073/pnas.1218851110>.
- Fischer, W.W., Hemp, J., Johnson, J.E., 2016. Evolution of oxygenic photosynthesis. *Annu. Rev. Earth Planet. Sci.* 44, 647–683. <https://doi.org/10.1146/annurev-earth-060313-054810>.
- Fisk, M., McLoughlin, N., 2013. Atlas of alteration textures in volcanic glass from the ocean basins. *Geosphere* 9, 317–341. <https://doi.org/10.1130/GES00827.1>.
- Fisk, M.R., Giovannoni, S.J., Thorseth, I.H., 1998. Alteration of oceanic volcanic glass: Textural evidence of microbial activity. *Science* 281, 978–980. <https://doi.org/10.1126/science.281.5379.978>.
- Fisk, M.R., Storrie-Lombardi, M.C., Douglas, S., Popa, R., McDonald, G., Di Meo-Savoie, C., 2003. Evidence of biological activity in Hawaiian subsurface basalts. *Geochemistry, Geophys. Geosystems* 4. <https://doi.org/10.1029/2002GC000387>.
- Fisk, M.R., Popa, R., Mason, O.U., Storrie-Lombardi, M.C., Vicenzi, E.P., 2006. Iron-Magnesium Silicate Bioweathering on Earth (and Mars?). *Astrobiology* 6, 48–68. <https://doi.org/10.1089/ast.2006.6.48>.
- Fisk, M.R., Crovisier, J.-L., Honnorez, J., 2013. Experimental abiotic alteration of igneous and manufactured glasses. *Comptes Rendus Geosci.* 345, 176–184. <https://doi.org/10.1016/j.crte.2013.02.001>.
- Fisk, M.R., Popa, R., Wacey, D., 2019. Tunnel formation in basalt glass. *Astrobiology* 19, 132–144. <https://doi.org/10.1089/ast.2017.1791>.
- Flannery, D.T., Walter, M.R., 2012. Archean tufted microbial mats and the Great Oxidation Event: new insights into an ancient problem. *Aust. J. Earth Sci.* 59, 1–11. <https://doi.org/10.1080/08120099.2011.607849>.
- Flannery, D.T., Allwood, A.C., Van Kranendonk, M.J., 2016. Lacustrine facies dependence of highly 13C-depleted organic matter during the global age of methanotrophy. *Precambrian Res.* 285, 216–241. <https://doi.org/10.1016/j.precamres.2016.09.021>.
- Flannery, D.T., Allwood, A.C., Summons, R.E., Williford, K.H., Abbey, W., Matys, E.D., Ferralis, N., 2018. Spatially-resolved isotopic study of carbon trapped in ~3.43 Ga Strelley Pool Formation stromatolites. *Geochim. Cosmochim. Acta* 223, 21–35. <https://doi.org/10.1016/j.gca.2017.11.028>.
- Fliegel, D., Kosler, J., McLoughlin, N., Simonetti, A., de Wit, M.J., Wirth, R., Furnes, H., 2010. In-situ dating of the Earth's oldest trace fossil at 3.34 Ga. *Earth Planet. Sci. Lett.* 299, 290–298. <https://doi.org/10.1016/j.epsl.2010.09.008>.
- Fliegel, D., Wirth, R., Simonetti, A., Shrieber, A., Furnes, H., Muehlenbach, K., 2011. Tubular textures in pillow lavas from a Caledonian west Norwegian ophiolite: a combined TEM, LA-ICP-MS, and STXM study. *Geochem. Geophys. Geosyst.* 12, Q02010. <https://doi.org/10.1029/2010GC003255>.
- Fliegel, D., Knowles, E., Wirth, R., Templeton, A., Staudigel, H., Muehlenbachs, K., Furnes, H., 2012. Characterization of alteration textures in cretaceous oceanic crust (pillow lava) from the N-Atlantic (DSDP Hole 418A) by spatially-resolved spectroscopy. *Geochim. Cosmochim. Acta* 96, 80–93. <https://doi.org/10.1016/j.gca.2012.08.026>.
- Foriel, J., Philippot, P., Rey, P., Somogyi, A., Banks, D., Ménez, B., 2004. Biological control of Cl/Br and low sulfate concentration in a 3.5-Gyr-old seawater from North Pole, Western Australia. *Earth Planet. Sci. Lett.* 228, 451–463. <https://doi.org/10.1016/j.epsl.2004.09.034>.
- Foustoukos, D.I., 2012. Metastable equilibrium in the C-H-O system: Graphite deposition in crustal fluids. *Am. Mineral.* 97, 1373–1380. <https://doi.org/10.2138/am.2012.4086>.

- Fox, S.W., Yuyama, S., 2006. Abiotic production of primitive protein and formed microparticles. *Ann. N. Y. Acad. Sci.* 108, 487–494. <https://doi.org/10.1111/j.1749-6632.1963.tb13404.x>.
- Fray, N., Bardyn, A., Cottin, H., Altwegg, K., Baklouti, D., Brioso, C., Colangeli, L., Engrand, C., Fischer, H., Glasmachers, A., Grün, E., Haerendel, G., Henkel, H., Höfner, H., Hornung, K., Jessberger, E.K., Koch, A., Krüger, H., Langevin, Y., Lehto, H., Lehto, K., Le Roy, L., Merouane, S., Modica, P., Orthous-Daunay, F.R., Paquette, J., Raulin, F., Rynö, J., Schulz, R., Silén, J., Siljeström, S., Steiger, W., Stenzel, O., Stephan, T., Thirkell, L., Thomas, R., Torkar, K., Varmuza, K., Wanczek, K.P., Zaprudin, B., Kissel, J., Hilchenbach, M., 2016. High-molecular-weight organic matter in the particles of comet 67P/Churyumov-Gerasimenko. *Nature* 538, 72–74. <https://doi.org/10.1038/nature19320>.
- Frei, R., Gaucher, C., Poulton, S.W., Canfield, D.E., 2009. Fluctuations in Precambrian atmospheric oxygenation recorded by chromium isotopes. *Nature* 461, 250–253. <https://doi.org/10.1038/nature08266>.
- Frei, R., Crowe, S.A., Bau, M., Polat, A., Fowle, D.A., Dössing, L.N., 2016. Oxidative elemental cycling under the low O₂ Eoarchean atmosphere. *Sci. Rep.* 6, 21058. <https://doi.org/10.1038/srep21058>.
- French, K.L., Hallmann, C., Hope, J.M., Schoon, P.L., Zumbeke, J.A., Hoshino, Y., Peters, C.A., George, S.C., Love, G.D., Brocks, J.J., Buick, R., Summons, R.E., 2015. Reappraisal of hydrocarbon biomarkers in Archean rocks. *Proc. Natl. Acad. Sci. U. S. A.* 112, 5915–5920. <https://doi.org/10.1073/pnas.1419563112>.
- Freude, C., Blaser, M., 2016. Carbon isotope fractionation during catabolism and anaerobiosis in acetogenic bacteria growing on different substrates. *Appl. Environ. Microbiol.* 82, 2728–2737. <https://doi.org/10.1128/AEM.03502-15>.
- Furnes, H., Staudigel, H., Thorseth, I.H., Torsvik, T., Muehlenbachs, K., Tumyr, O., 2001. Bioalteration of basaltic glass in the oceanic crust. *Geochemistry, Geophys. Geosystems* 2(NR.). <https://doi.org/10.1029/2000GC000150>. 2000GC000150.
- Furnes, H., Banerjee, N.R., Muehlenbachs, K., Staudigel, H., De Wit, M., 2004. Early Life Recorded in Archean Pillow Lavas. *Science* 304, 578–581. <https://doi.org/10.1126/science.1095858>.
- Furnes, H., Banerjee, N.R., Staudigel, H., Muehlenbachs, K., McLoughlin, N., de Wit, M., van Kranendonk, M., 2007. Comparing petrographic signatures of bioalteration in recent to Mesoproterozoic pillow lavas: Tracing subsurface life in oceanic igneous rocks. *Precambrian Res.* 158, 156–176. <https://doi.org/10.1016/j.precamres.2007.04.012>.
- Gaillard, F., Scaillet, B., Arndt, N.T., 2011. Atmospheric oxygenation caused by a change in volcanic degassing pressure. *Nature* 478, 229–232. <https://doi.org/10.1038/nature10460>.
- Galimov, E.M., 2006. Isotope organic geochemistry. *Org. Geochem.* 37, 1200–1262. <https://doi.org/10.1016/j.orggeochem.2006.04.009>.
- Galvez, M.E., Beyssac, O., Martinez, I., Benzerara, K., Chaduteau, C., Malvoisin, B., Malavieille, J., 2013. Graphite formation by carbonate reduction during subduction. *Nat. Geosci.* 6, 473–477. <https://doi.org/10.1038/ngeo1827>.
- Gao, S., Huang, F., Wang, Y., Gao, W., 2016. A review of research progress in the genesis of colloform pyrite and its environmental indications. *Acta Geol. Sin.* 90, 1353–1369. <https://doi.org/10.1111/1755-6724.12774>.
- García-Ruiz, J.M., Hyde, S.T., Carnerup, A.M., Christy, A.G., Van Kranendonk, M.J., Welham, N.J., 2003. Self-Assembled Silica-Carbonate Structures and Detection of Ancient Microfossils. *Science* 302, 1194–1197. <https://doi.org/10.1126/science.1090163>.
- García-Ruiz, J.M., Nakouzi, E., Kotopoulou, E., Tamborrino, L., Steinbock, O., 2017. Biomimetic mineral self-organization from silica-rich spring waters. *Sci. Adv.* 3, 1–7. <https://doi.org/10.1126/sciadv.1602285>.
- Garvie, L.A.J., Buseck, P.R., 2004. Nanosized carbon-rich grains in carbonaceous chondrite meteorites. *Earth Planet. Sci. Lett.* 224, 431–439. <https://doi.org/10.1016/j.epsl.2004.05.024>.
- Garvin, J., Buick, R., Anbar, A.D., Arnold, G.L., Kaufman, A.J., 2009. Isotopic evidence for an aerobic Nitrogen cycle in the latest Archean. *Science* 323, 1045–1048. <https://doi.org/10.1126/science.1165675>.
- Gelwicks, J.T., Risatti, J.B., Hayes, J.M., 1989. Carbon isotope effects associated with autotrophic acetogenesis. *Org. Geochem.* 14, 441–446. [https://doi.org/10.1016/0146-6380\(89\)90009-0](https://doi.org/10.1016/0146-6380(89)90009-0).
- George, S.C., Volk, H., Dutkiewicz, A., Ridley, J., Buick, R., 2008. Preservation of hydrocarbons and biomarkers in oil trapped inside fluid inclusions for > 2 billion years. *Geochim. Cosmochim. Acta* 72, 844–870. <https://doi.org/10.1016/j.gca.2007.11.021>.
- Gerdes, G., 2007. Structures left by modern microbial mats in their host sediments. In: Schieber, J., Bose, P.K., Eriksson, P.G., Banerjee, S., Sarkar, S., Altermann, W., Catuneau, O. (Eds.), *Atlas of Microbial Mat Features Preserved within the Clastic Rock Record*. Elsevier, pp. 5–38.
- Girard-Lauriat, P.-L., Illgen, R., Ruiz, J.-C., Wertheimer, M.R., Unger, W.E.S., 2012. Surface functionalization of graphite and carbon nanotubes by vacuum-ultraviolet photochemical reactions. *Appl. Surf. Sci.* 258, 8448–8454. <https://doi.org/10.1016/j.apsusc.2012.03.012>.
- Glikson, M., Duck, L.J., Golding, S.D., Hofmann, A., Bolhar, R., Webb, R., Baiano, J.C.F., Sly, L.L., 2008. Microbial remains in some earliest Earth rocks: Comparison with a potential modern analogue. *Precambrian Res.* 164, 187–200. <https://doi.org/10.1016/j.precamres.2008.05.002>.
- Godfrey, L.V., Falkowski, P.G., 2009. The cycling and redox state of nitrogen in the Archean Ocean. *Nat. Geosci.* 2, 725–729. <https://doi.org/10.1038/ngeo633>.
- Govert, D., Conrad, R., 2008. Carbon isotope fractionation by sulfate-reducing bacteria using different pathways for the oxidation of acetate. *Environ. Sci. Technol.* 42, 7813–7817. <https://doi.org/10.1021/es800308z>.
- Govert, D., Conrad, R., 2009. Effect of substrate concentration on carbon isotope fractionation during acetoclastic methanogenesis by *Methanosarcina barkeri* and *M. acetivorans* and in rice field soil. *Appl. Environ. Microbiol.* 75, 2605–2612. <https://doi.org/10.1128/AEM.02680-08>.
- Grassineau, N.V., Nisbet, E.G., Bickle, M.J., Fowler, C.M.R., Lowry, D., Matthey, D.P., Abell, P., Martin, A., 2001. Antiquity of the biological Sulphur cycle: evidence from Sulphur and carbon isotopes in 2700 million-year-old rocks of the Belingwe Belt, Zimbabwe. *Proc. R. Soc. B Biol. Sci.* 268, 113–119. <https://doi.org/10.1098/rspb.2000.1338>.
- Grey, K., 1986. Problematic microstructures in the Proterozoic Discovery Chert, Bangemall Group, Western Australia. Ambient grains or microfossils? *West. Aust. Geol. Surv. Prof. Pap.* 1984, 22–31.
- Grey, K., Sugitani, K., 2009. Palynology of Archean microfossils (c. 3.0 Ga) from the Mount Grant area, Pilbara Craton, Western Australia: further evidence of biogenicity. *Precambrian Res.* 173, 60–69. <https://doi.org/10.1016/j.precamres.2009.02.003>.
- Grey, K., Willman, S., 2009. Taphonomy of Ediacaran Acritarchs from Australia: significance for taxonomy and biostratigraphy. *Palaios* 24, 239–256. <https://doi.org/10.2110/palo.2008.p08-020r>.
- Grosch, E.G., McLoughlin, N., 2014. Reassessing the biogenicity of Earth's oldest trace fossil with implications for biosignatures in the search for early life. *Proc. Natl. Acad. Sci. U. S. A.* 111, 8380–8385. <https://doi.org/10.1073/pnas.1402565111>.
- Grotzinger, J.P., Knoll, A.H., 1999. Stromatolites in Precambrian carbonates: evolutionary mileposts or environmental dipsticks? *Annu. Rev. Earth Planet. Sci.* 27, 313–358. <https://doi.org/10.1146/annurev.earth.27.1.313>.
- Grotzinger, J.P., Rothman, D.H., 1996. An abiotic model for stromatolite morphogenesis. *Nature* 383, 423–425. <https://doi.org/10.1038/383423a0>.
- Guan, Q.S., Cao, W.Z., Wang, M., Wu, G.J., Wang, F.F., Jiang, C., Tao, Y.R., Gao, Y., 2018. Nitrogen loss through anaerobic ammonium oxidation coupled with iron reduction in a mangrove wetland. *Eur. J. Soil Sci.* 69, 732–741. <https://doi.org/10.1111/ejss.12552>.
- Guidry, S.A., Chafetz, H.S., 2003. Anatomy of siliceous hot springs: examples from Yellowstone National Park, Wyoming, USA. *Sediment. Geol.* 157, 71–106. [https://doi.org/10.1016/S0037-0738\(02\)00195-1](https://doi.org/10.1016/S0037-0738(02)00195-1).
- Guilbaud, R., Butler, I.B., Ellam, R.M., 2011. Abiotic pyrite formation produces a large Fe isotope fractionation. *Science* 332, 1548–1551. <https://doi.org/10.1126/science.1202924>.
- Guo, Q., Strauss, H., Kaufman, A.J., Schröder, S., Gutzmer, J., Wing, B., Baker, M.A., Bekker, A., Jin, Q., Kim, S.T., Farquhar, J., 2009. Reconstructing Earth's surface oxidation across the Archean-Proterozoic transition. *Geology* 37, 399–402. <https://doi.org/10.1130/G25423A.1>.
- Guo, Z., Peng, X., Czaja, A.D., Chen, S., Ta, K., 2018. Cellular taphonomy of well-preserved Gaoyuzhuang microfossils: a window into the preservation of ancient cyanobacteria. *Precambrian Res.* 304, 88–98. <https://doi.org/10.1016/j.precamres.2017.11.007>.
- Habicht, K.S., Gade, M., Thamdrup, B., Berg, P., Canfield, D.E., 2002. Calibration of sulfate levels in the Archean Ocean. *Science* 298, 2372–2374. <https://doi.org/10.1126/science.1078265>.
- Halevy, I., Johnston, D.T., Schrag, D.P., 2010. Explaining the structure of the Archean mass-independent sulfur isotope record. *Science* 329, 204–207. <https://doi.org/10.1126/science.1190298>.
- Handley, K.M., Turner, S.J., Campbell, K.A., Mountain, B.W., 2008. Silicifying biofilm exopolymers on a hot-spring microstromatolite: templating nanometer-thick laminae. *Astrobiology* 8, 747–770. <https://doi.org/10.1089/ast.2007.0172>.
- Hannington, M.D., Scott, S.D., 1988. Mineralogy and geochemistry of a hydrothermal silica-sulfide-sulfate spire in the caldera of axial Seamount, Juan de Fuca Ridge. *Can. Mineral.* 26 (pt 3), 603–625.
- Hassenkam, T., Andersson, M.P., Dalby, K.N., Mackenzie, D.M.A., Rosing, M.T., 2017. Elements of Eoarchean life trapped in mineral inclusions. *Nature* 548, 78–81. <https://doi.org/10.1038/nature23261>.
- Hayes, J.M., 1994. Global methanotrophy of the Archean-Proterozoic transition. In: Bengtson, S. (Ed.), *Early Life on Earth*, Nobel Symposium No. 84. Columbia University Press, New York, pp. 220–235.
- Hayes, J.M., 2001. Fractionation of Carbon and Hydrogen isotopes in biosynthetic processes. In: Valley, J.W., Cole, D. (Eds.), *Reviews in Mineralogy and Geochemistry*. Mineralogical Society of America, pp. 225–277. <https://doi.org/10.2138/gsrmg.43.1.225>.
- Hayes, J.M., Kaplan, I.R., Wedeking, K.W., 1983. Precambrian organic geochemistry, preservation of the record. In: Schopf, J.W. (Ed.), *Earth's Earliest Biosphere: Its Origin and Evolution*. Princeton University Press, Princeton, New Jersey, pp. 93–134.
- Hazen, R.M., Papineau, D., Bleeker, W., Downs, R.T., Ferry, J.M., McCoy, T.J., Sverjensky, D.A., Yang, H., 2008. Mineral evolution. *Am. Mineral.* 93, 1693–1720. <https://doi.org/10.2138/am.2008.2955>.
- Heijnen, W., Appel, P.W.U., Frezzotti, M.-L., Horsewell, A., Touret, J.L.R., 2006. Metamorphic fluid flow in the northeastern part of the 3.8–3.7 Ga Isua Greenstone Belt (SW Greenland): a re-evaluation of fluid inclusion evidence for early Archean seafloor-hydrothermal systems. *Geochim. Cosmochim. Acta* 70, 3075–3095. <https://doi.org/10.1016/j.gca.2006.04.005>.
- Hemraj-Benny, T., Banerjee, S., Sambasivan, S., Balasubramanian, M., Fischer, D.A., Eres, G., Puzosky, A.A., Geohegan, D.B., Lowndes, D.H., Han, W., Misewich, J.A., Wong, S.S., 2006. Near-edge X-ray absorption fine structure spectroscopy as a tool for investigating nanomaterials. *Small* 2, 26–35. <https://doi.org/10.1002/sml.200500256>.
- Heubeck, C., 2009. An early ecosystem of Archean tidal microbial mats (Moodies Group, South Africa, ca. 3.2 Ga). *Geology* 37, 931–934. <https://doi.org/10.1130/G30101A.1>.
- Heubeck, C., 2019. The Moodies Group—a high-resolution archive of Archean surface processes and basin-forming mechanisms. In: Kröner, A., Hofmann, A. (Eds.), *The Archean Geology of the Kaapvaal Craton*. Springer Nature, Southern Africa, pp. 133–169. https://doi.org/10.1007/978-3-319-78652-0_6.

- Hickman-Lewis, K., Garwood, R.J., Brasier, M.D., Goral, T., Jiang, H., McLoughlin, N., Wacey, D., 2016. Carbonaceous microstructures from sedimentary laminated chert within the 3.46 Ga Apex Basalt, Chinaman Creek locality, Pilbara, Western Australia. *Precambrian Res.* 278, 161–178. <https://doi.org/10.1016/j.precamres.2016.03.013>.
- Hickman-Lewis, K., Cavalazzi, B., Foucher, F., Westall, F., 2018. Most ancient evidence for life in the Barberton greenstone belt: Microbial mats and biofabrics of the ~3.47 Ga Middle Marker horizon. *Precambrian Res.* 312, 45–67. <https://doi.org/10.1016/j.precamres.2018.04.007>.
- Hickman-Lewis, K., Westall, F., Cavalazzi, B., 2019. Traces of early Life from the Barberton Greenstone Belt, South Africa. In: *Earth's Oldest Rocks*. Elsevier, pp. 1029–1058. <https://doi.org/10.1016/B978-0-444-63901-1.00042-3>.
- Hinrichs, K.U., 2002. Microbial fixation of methane carbon at 2.7 Ga: Was an anaerobic mechanism possible? *Geochemistry, Geophys. Geosystems* 3, 1042. <https://doi.org/10.1029/2001GC000286>.
- Hoehler, T.M., Alperin, M.J., Albert, D.B., Martens, C.S., 1998. Thermodynamic control on hydrogen concentrations in anoxic sediments. *Geochim. Cosmochim. Acta* 62, 1745–1756. [https://doi.org/10.1016/S0016-7037\(98\)00106-9](https://doi.org/10.1016/S0016-7037(98)00106-9).
- Hoffmann, J.E., Zhang, C., Moyer, J.-F., Nagel, T.J., 2019. The formation of Tonalites–Trondjemite–Granodiorites in early continental crust. In: van Kranendonk, M.J., Bennett, V.C., Hoffmann, J.E. (Eds.), *Earth's Oldest Rocks*. Elsevier, pp. 133–168. <https://doi.org/10.1016/B978-0-444-63901-1.00007-1>.
- Hofmann, H.J., 1976. Precambrian microfolia, Belcher Islands, Canada: significance and systematics. *J. Paleontol.* 50, 1040–1073.
- Hofmann, H.J., 2000. Archean stromatolites as microbial archives. In: Riding, R.E., Awramik, S.M. (Eds.), *Microbial Sediments*. Springer, Berlin Heidelberg, Berlin, Heidelberg, pp. 315–327. https://doi.org/10.1007/978-3-662-04036-2_34.
- Hofmann, A., Bolhar, R., 2007. Carbonaceous cherts in the Barberton Greenstone Belt and their significance for the study of early life in the Archean record. *Astrobiology* 7, 355–388. <https://doi.org/10.1089/ast.2005.0288>.
- Hofmann, H.J., Grey, K., Hickman, A.H., Thorpe, R.I., 1999. Origin of 3.45 Ga coniform stromatolites in Warrawoona Group, Western Australia. *Geol. Soc. Am. Bull.* 111, 1256–1262. [https://doi.org/10.1130/0016-7606\(1999\)111<1256:OOGCSI>2.3.CO;2](https://doi.org/10.1130/0016-7606(1999)111<1256:OOGCSI>2.3.CO;2).
- Homann, M., 2019. Earliest life on Earth: evidence from the Barberton Greenstone Belt, South Africa. *Earth-Science Rev.* 196, 102888. <https://doi.org/10.1016/j.earscirev.2019.102888>.
- Homann, M., Heubeck, C., Airo, A., Tice, M.M., 2015. Morphological adaptations of 3.22 Ga-old tufted microbial mats to Archean coastal habitats (Moodies Group, Barberton Greenstone Belt, South Africa). *Precambrian Res.* 266, 47–64. <https://doi.org/10.1016/j.precamres.2015.04.018>.
- Homann, M., Heubeck, C., Bontognali, T.R.R., Bouvier, A.S., Baumgartner, L.P., Airo, A., 2016. Evidence for cavity-dwelling microbial life in 3.22 Ga tidal deposits. *Geology* 44, 51–54. <https://doi.org/10.1130/G37272.1>.
- Homann, M., Sansjofre, P., Van Zuilen, M., Heubeck, C., Gong, J., Killingsworth, B., Foster, I.S., Airo, A., van Kranendonk, M.J., Ader, M., Lalonde, S.V., 2018. Microbial life and biogeochemical cycling on land 3,220 million years ago. *Nat. Geosci.* 11, 665–671. <https://doi.org/10.1038/s41561-018-0190-9>.
- Horita, J., Polyakov, V.B., 2015. Carbon-bearing iron phases and the carbon isotope composition of the deep Earth. *Proc. Natl. Acad. Sci. U. S. A.* 112, 31–36. <https://doi.org/10.1073/pnas.1401782112>.
- House, C.H., 2015. Penciling in details of the Hadean. *Proc. Natl. Acad. Sci. U. S. A.* 112, 14410–14411. <https://doi.org/10.1073/pnas.1519765112>.
- House, C.H., Schopf, J.W., Stetter, K.O., 2003. Carbon isotopic fractionation by Archaeans and other thermophilic prokaryotes. *Org. Geochem.* 34, 345–356. [https://doi.org/10.1016/S0146-6380\(02\)00237-1](https://doi.org/10.1016/S0146-6380(02)00237-1).
- House, C.H., Oehler, D.Z., Sugitani, K., Mimura, K., 2013. Carbon isotopic analyses of ca. 3.0 Ga microstructures imply planktonic autotrophs inhabited Earth's early oceans. *Geology* 41, 651–654. <https://doi.org/10.1130/G34055.1>.
- Huang, S., Jaffé, P.R., 2018. Isolation and characterization of an ammonium-oxidizing iron reducer: *Acidimicrobiaceae* sp. A6. *PLoS One* 13. <https://doi.org/10.1371/journal.pone.0194007>. e0194007.
- Huston, D.L., Logan, G.A., 2004. Barite, BIFs and bugs: Evidence for the evolution of the Earth's early hydrosphere. *Earth Planet. Sci. Lett.* 220, 41–55. [https://doi.org/10.1016/S0012-821X\(04\)00034-2](https://doi.org/10.1016/S0012-821X(04)00034-2).
- Ivarsson, M., Lausmaa, J., Lindblom, S., Broman, C., Holm, N.G., 2008. Fossilized microorganisms from the Emperor Seamounts: Implications for the search for a sub-surface fossil record on Earth and Mars. *Astrobiology* 8, 1139–1157. <https://doi.org/10.1089/ast.2007.0226>.
- Izon, G., Zerkle, A.L., Zhelezinskaia, I., Farquhar, J., Newton, R.J., Poulton, S.W., Eigenbrode, J.L., Claire, M.W., 2015. Multiple oscillations in Neoproterozoic atmospheric chemistry. *Earth Planet. Sci. Lett.* 431, 264–273. <https://doi.org/10.1016/j.epsl.2015.09.018>.
- Izon, G., Zerkle, A.L., Williford, K.H., Farquhar, J., Poulton, S.W., Claire, M.W., 2017. Biological regulation of atmospheric chemistry en route to planetary oxygenation. *Proc. Natl. Acad. Sci. U. S. A.* 114, E2571–E2579. <https://doi.org/10.1073/pnas.1618798114>.
- Javaux, E.J., 2019. Challenges in evidencing the earliest traces of life. *Nature* 572, 451–460. <https://doi.org/10.1038/s41586-019-1436-4>.
- Javaux, E.J., Lepot, K., 2018. The Paleoproterozoic fossil record: Implications for the evolution of the biosphere during Earth's middle-age. *Earth-Science Rev.* 176, 68–86. <https://doi.org/10.1016/j.earscirev.2017.10.001>.
- Javaux, E.J., Knoll, A.H., Walter, M.R., 2004. TEM evidence for eukaryotic diversity in mid-Proterozoic oceans. *Geobiology* 2, 121–132. <https://doi.org/10.1111/j.1472-4677.2004.00027.x>.
- Javaux, E.J., Marshall, C.P., Bekker, A., 2010. Organic-walled microfossils in 3.2-billion-year-old shallow-marine siliciclastic deposits. *Nature* 463, 934–938. <https://doi.org/10.1038/nature08793>.
- Jettsetuen, E., Jamtveit, B., Podladchikov, Y.Y., deVilliers, S., Amundsen, H.E.F., Meakin, P., 2006. Growth and characterization of complex mineral surfaces. *Earth Planet. Sci. Lett.* 249, 108–118. <https://doi.org/10.1016/j.epsl.2006.06.045>.
- Johannessen, K.C., McLoughlin, N., Vullum, P.E., Thorseth, I.H., 2020. On the biogenicity of Fe-oxyhydroxide filaments in silicified low-temperature hydrothermal deposits: implications for the identification of Fe-oxidizing bacteria in the rock record. *Geobiology* 18, 31–53. <https://doi.org/10.1111/gbi.12363>.
- Johnson, C.M., Beard, B.L., Klein, C., Beukes, N.J., Roden, E.E., 2008. Iron isotopes constrain biologic and abiologic processes in banded iron formation genesis. *Geochim. Cosmochim. Acta* 72, 151–169. <https://doi.org/10.1016/j.gca.2007.10.013>.
- Johnston, D.T., 2011. Multiple sulfur isotopes and the evolution of Earth's surface sulfur cycle. *Earth-Science Rev.* 106, 161–183. <https://doi.org/10.1016/j.earscirev.2011.02.003>.
- Johnston, D.T., Wolfe-Simon, F., Pearson, A., Knoll, A.H., 2009. Anoxygenic photosynthesis modulated Proterozoic oxygen and sustained Earth's middle age. *Proc. Natl. Acad. Sci. U. S. A.* 106, 16925–16929. <https://doi.org/10.1073/pnas.0909248106>.
- Jones, B., Renaut, R.W., 2007. Microstructural changes accompanying the opal-a to opal-CT transition: New evidence from the siliceous sinters of Geysir, Haukadalur, Iceland. *Sedimentology* 54, 921–948. <https://doi.org/10.1111/j.1365-3091.2007.00866.x>.
- Kappler, A., Pasquero, C., Konhauser, K.O., Newman, D.K., 2005. Deposition of banded iron formations by anoxygenic phototrophic Fe(II)-oxidizing bacteria. *Geology* 33, 865–868. <https://doi.org/10.1130/G21658.1>.
- Kasting, J.F., 2019. Early Earth Atmosphere and Oceans. In: van Kranendonk, M.J., Bennett, V.C., Hoffmann, J.E. (Eds.), *Earth's Oldest Rocks* (Second Edition). Elsevier, pp. 49–61. <https://doi.org/10.1016/B978-0-444-63901-1.00003-4>.
- Kaufman, A.J., Xiao, S., 2003. High CO₂ levels in the Proterozoic atmosphere estimated from analyses of individual microfossils. *Nature* 425, 279–282. <https://doi.org/10.1038/nature01902>.
- Kaufman, A.J., Johnston, D.T., Farquhar, J., Masterson, A.L., Lyons, T.W., Bates, S., Anbar, A.D., Arnold, G.L., Garvin, J., Buick, R., 2007. Late archaean biospheric oxygenation and atmospheric evolution. *Science* 317, 1900–1903. <https://doi.org/10.1126/science.1138700>.
- Każmierczak, J., Kempe, S., 2003. Modern terrestrial analogues for the carbonate globules in Martian meteorite ALH84001. *Naturwissenschaften* 90, 167–172. <https://doi.org/10.1007/s00114-003-0411-x>.
- Każmierczak, J., Kremer, B., 2009. Thermally altered Silurian cyanobacterial mats: a key to Earth's oldest fossils. *Astrobiology* 9, 731–743. <https://doi.org/10.1089/ast.2008.0332>.
- Kendall, B., Creaser, R.A., Reinhard, C.T., Lyons, T.W., Anbar, A.D., 2015. Transient episodes of mild environmental oxygenation and oxidative continental weathering during the late Archean. *Sci. Adv.* 1, e1500777. <https://doi.org/10.1126/sciadv.1500777>.
- Kendall, B., Dahl, T.W., Anbar, A.D., 2017. The stable isotope geochemistry of Molybdenum. *Rev. Mineral. Geochemistry* 82, 683–732. <https://doi.org/10.2138/rmg.2017.82.16>.
- Kipp, M.A., Stieken, E.E., 2017. Biomass recycling and Earth's early phosphorus cycle. *Sci. Adv.* 3, 1–7. <https://doi.org/10.1126/sciadv.aao4795>.
- Kirkland, B.L., Lynch, F.L., Rahnis, M.A., Folk, R.L., Molineux, I.J., McLean, R.J.C., 1999. Alternative origins for nanobacteria-like objects in calcite. *Geology* 27, 347–350. [https://doi.org/10.1130/0091-7613\(1999\)027<0347:AOFNLO>2.3.CO](https://doi.org/10.1130/0091-7613(1999)027<0347:AOFNLO>2.3.CO).
- Kiyokawa, S., Ito, T., Ikehara, M., Kitajima, F., 2006. Middle Archean volcano-hydrothermal sequence: Bacterial microfossil-bearing 3.2 Ga Dixon Island Formation, coastal Pilbara terrane, Australia. *Bull. Geol. Soc. Am.* 118, 3–22. <https://doi.org/10.1130/B25748.1>.
- Kiyokawa, S., Koge, S., Ito, T., Ikehara, M., 2014. An ocean-floor carbonaceous sedimentary sequence in the 3.2-Ga Dixon Island Formation, coastal Pilbara terrane, Western Australia. *Precambrian Res.* 255, 124–143. <https://doi.org/10.1016/j.precamres.2014.09.014>.
- Klauff, P., Wilhelm, R., Klumpp, E., Poschen, L., Groeneweg, J., 2004. Enumeration of soil bacteria with the green fluorescent nucleic acid dye Sytox green in the presence of soil particles. *J. Microbiol. Methods* 59, 189–198. <https://doi.org/10.1016/j.mimet.2004.07.004>.
- Klein, C., Beukes, N.J., Schopf, J.W., 1987. Filamentous microfossils in the early proterozoic transvaal supergroup: their morphology, significance, and paleoenvironmental setting. *Precambrian Res.* 36, 81–94. [https://doi.org/10.1016/0301-9268\(87\)90018-0](https://doi.org/10.1016/0301-9268(87)90018-0).
- Kleit, Z., Wilczok, U., Schüth, F., Marlow, F., 2001. Hollow mesoporous silica fibers: tubules by coils of tubules. *Phys. Chem. Chem. Phys.* 3, 3486–3489. <https://doi.org/10.1039/b105083b>.
- Klueglein, N., Zeitvogel, F., Stierhof, Y.D., Floetenmeyer, M., Konhauser, K.O., Kappler, A., Obst, M., 2014. Potential role of nitrite for abiotic Fe(II) oxidation and cell encrustation during nitrate reduction by denitrifying bacteria. *Appl. Environ. Microbiol.* 80, 1051–1061. <https://doi.org/10.1128/AEM.03277-13>.
- Knittel, K., Boetius, A., 2009. Anaerobic oxidation of methane: progress with an unknown process. *Annu. Rev. Microbiol.* 63, 311–334. <https://doi.org/10.1146/annurev.micro.61.080706.093130>.
- Knoll, A.H., Barghoorn, E.S., 1974. Ambient pyrite in Precambrian chert: New evidence and a theory. *Proc. Natl. Acad. Sci. U. S. A.* 71, 2329–2331. <https://doi.org/10.1073/pnas.71.6.2329>.
- Knoll, A.H., Barghoorn, E.S., 1977. Archean microfossils showing cell division from the Swaziland System of South Africa. *Science* 198, 396–398. <https://doi.org/10.1126/science.198.4315.396>.
- Knoll, A.H., Strother, P.K., Rossi, S., 1988. Distribution and diagenesis of microfossils from the lower Proterozoic Duck Creek Dolomite, Western Australia. *Precambrian*

- Res. 38, 257–279. [https://doi.org/10.1016/0301-9268\(88\)90005-8](https://doi.org/10.1016/0301-9268(88)90005-8).
- Knoll, A.H., Wornle, S., Kah, L.C., 2013. Covariance of microfossil assemblages and microbialite textures across an Upper Mesoproterozoic carbonate platform. *Palaios* 28, 453–470. <https://doi.org/10.2110/palo.2013.p13-005r>.
- Knoll, A.H., Bergmann, K.D., Strauss, J.V., 2016. Life: the first two billion years. *Philos. Trans. R. Soc. B Biol. Sci.* 371, 20150493. <https://doi.org/10.1098/rstb.2015.0493>.
- Köhler, I., Heubeck, C., 2019. Microbial-mat-associated tephra of the Archean Moodies Group, Barberton Greenstone Belt (BGB), South Africa: Resemblance to potential biostructures and ecological implications. *South African J. Geol.* 122, 221–236. <https://doi.org/10.25131/sajg.122.0015>.
- Köhler, I., Konhauser, K.O., Papineau, D., Bekker, A., Kappler, A., 2013. Biological carbon precursor to diagenetic siderite with spherical structures in iron formations. *Nat. Commun.* 4, 1741. <https://doi.org/10.1038/ncomms2770>.
- Konhauser, K.O., Phoenix, V.R., Bottrell, S.H., Adams, D.G., Head, I.M., 2001. Microbial-silica interactions in Icelandic hot spring sinter: possible analogues for some Precambrian siliceous stromatolites. *Sedimentology* 48, 415–433. <https://doi.org/10.1046/j.1365-3091.2001.00372.x>.
- Konhauser, K.O., Jones, B., Phoenix, V.R., Ferris, G., Renaut, R.W., 2004. The microbial role in hot spring silicification. *AMBIO A J. Hum. Environ.* 33, 552–558. <https://doi.org/10.1579/0044-7447-33.8.552>.
- Konhauser, K.O., Amskold, L., Lalonde, S.V., Posth, N.R., Kappler, A., Anbar, A., 2007. Decoupling photochemical Fe(II) oxidation from shallow-water BIF deposition. *Earth Planet. Sci. Lett.* 258, 87–100. <https://doi.org/10.1016/j.epsl.2007.03.026>.
- Konhauser, K.O., Robbins, L.J., Pecoits, E., Peacock, C., Kappler, A., Lalonde, S.V., 2015. The Archean Nickel famine revisited. In: *Astrobiology*, pp. 804–815. <https://doi.org/10.1089/ast.2015.1301>.
- Konhauser, K.O., Planavsky, N.J., Hardisty, D.S., Robbins, L.J., Warchola, T.J., Haugaard, R., Lalonde, S.V., Partin, C.A., Oonk, P.B.H., Tsikos, H., Lyons, T.W., Bekker, A., Johnson, C.M., 2017. Iron formations: a global record of Neoproterozoic to Palaeoproterozoic environmental history. *Earth-Science Rev.* 172, 140–177. <https://doi.org/10.1016/j.earscirev.2017.06.012>.
- Konn, C., Charlou, J.L., Holm, N.G., Mousis, O., 2015. The production of methane, hydrogen, and organic compounds in ultramafic-hosted hydrothermal vents of the Mid-Atlantic Ridge. *Astrobiology* 15, 381–399. <https://doi.org/10.1089/ast.2014.1198>.
- Kopp, R.E., Kirschvink, J.L., Hilburn, I.A., Nash, C.Z., 2005. The Paleoproterozoic snowball Earth: a climate disaster triggered by the evolution of oxygenic photosynthesis. *Proc. Natl. Acad. Sci. U. S. A.* 102, 11131–11136. <https://doi.org/10.1073/pnas.0504878102>.
- Korenaga, J., 2013. Initiation and evolution of plate tectonics on Earth: theories and observations. *Annu. Rev. Earth Planet. Sci.* 41, 117–151. <https://doi.org/10.1146/annurev-earth-050212-124208>.
- Kremer, B., Kaźmierczak, J., 2017. Cellularly preserved microbial fossils from ~3.4 Ga deposits of South Africa: a testimony of early appearance of oxygenic life? *Precambrian Res.* 295, 117–129. <https://doi.org/10.1016/j.precamres.2017.04.023>.
- Krull, D., Davatzes, A., Goderis, S., Simonson, B.M., 2019. Archean Asteroid Impacts on Earth. In: *van Kranendonk, M.J., Bennett, V.C., Hoffmann, J.E. (Eds.), Earth's Oldest Rocks*. Elsevier, pp. 169–185. <https://doi.org/10.1016/b978-0-444-63901-1.00008-3>.
- Kump, L.R., Barley, M.E., 2007. Increased subaerial volcanism and the rise of atmospheric oxygen 2.5 billion years ago. *Nature* 448, 1033–1036. <https://doi.org/10.1038/nature06058>.
- Kump, L.R., Seyfried, W.E., 2005. Hydrothermal Fe fluxes during the Precambrian: effect of low oceanic sulfate concentrations and low hydrostatic pressure on the composition of black smokers. *Earth Planet. Sci. Lett.* 235, 654–662. <https://doi.org/10.1016/j.epsl.2005.04.040>.
- Kurzweil, F., Claire, M., Thomazo, C., Peters, M., Hannington, M., Strauss, H., 2013. Atmospheric sulfur rearrangement 2.7 billion years ago: evidence for oxygenic photosynthesis. *Earth Planet. Sci. Lett.* 366, 17–26. <https://doi.org/10.1016/j.epsl.2013.01.028>.
- Lalonde, S.V., Konhauser, K.O., 2015. Benthic perspective on Earth's oldest evidence for oxygenic photosynthesis. *Proc. Natl. Acad. Sci. U. S. A.* 112, 995–1000. <https://doi.org/10.1073/pnas.1415718112>.
- Large, R.R., Halpin, J.A., Danyushevsky, L.V., Maslennikov, V.V., Bull, S.W., Long, J.A., Gregory, D.D., Lounejeva, E., Lyons, T.W., Sack, P.J., McGoldrick, P.J., Calver, C.R., 2014. Trace element content of sedimentary pyrite as a new proxy for deep-time ocean-atmosphere evolution. *Earth Planet. Sci. Lett.* 389, 209–220. <https://doi.org/10.1016/j.epsl.2013.12.020>.
- Le Guillou, C., Bernard, S., Brearley, A.J., Remusat, L., 2014. Evolution of organic matter in Orgueil, Murchison and Renazzo during parent body aqueous alteration: In situ investigations. *Geochim. Cosmochim. Acta* 131, 368–392. <https://doi.org/10.1016/j.gca.2013.11.020>.
- Lekele Baghekema, S.G., Lepot, K., Riboulleau, A., Fadel, A., Trentesaux, A., El Albani, A., 2017. Nanoscale analysis of preservation of ca. 2.1 Ga old Francevillian microfossils, Gabon. *Precambrian Res.* 301, 1–18. <https://doi.org/10.1016/j.precamres.2017.08.024>.
- Lepland, A., van Zuilen, M.A., Philippot, P., 2011. Fluid-deposited graphite and its geochemical implications in early Archean gneiss from Akilia, Greenland. *Geobiology* 9, 2–9. <https://doi.org/10.1111/j.1472-4669.2010.00261.x>.
- Lepot, K., Benzerara, K., Brown, G.E., Philippot, P., 2008. Microbially influenced formation of 2,724-million-year-old stromatolites. *Nat. Geosci.* 1, 118–121. <https://doi.org/10.1038/ngeo107>.
- Lepot, K., Benzerara, K., Rividi, N., Cotte, M., Brown, G.E., Philippot, P., 2009a. Organic matter heterogeneities in 2.72 Ga stromatolites: Alteration versus preservation by sulfur incorporation. *Geochim. Cosmochim. Acta* 73, 6579–6599. <https://doi.org/10.1016/j.gca.2009.08.014>.
- Lepot, K., Philippot, P., Benzerara, K., Wang, G.Y., 2009b. Garnet-filled trails associated with carbonaceous matter mimicking microbial filaments in Archean basalt. *Geobiology* 7, 393–402. <https://doi.org/10.1111/j.1472-4669.2009.00208.x>.
- Lepot, K., Benzerara, K., Philippot, P., 2011. Biogenic versus metamorphic origins of diverse microtubes in 2.7 Gyr old volcanic ashes: Multi-scale investigations. *Earth Planet. Sci. Lett.* 312, 37–47. <https://doi.org/10.1016/j.epsl.2011.10.016>.
- Lepot, K., Williford, K.H., Ushikubo, T., Sugitani, K., Mimura, K., Spicuzza, M.J., Valley, J.W., 2013. Texture-specific isotopic compositions in 3.4 Gyr old organic matter support selective preservation in cell-like structures. *Geochim. Cosmochim. Acta* 112, 66–86. <https://doi.org/10.1016/j.gca.2013.03.004>.
- Lepot, K., Compère, P., Gérard, E., Namsaraev, Z., Verleyen, E., Tavernier, I., Hodgson, D.A., Vyverman, W., Gilbert, B., Wilmette, A., Javaux, E.J., 2014. Organic and mineral imprints in fossil photosynthetic mats of an East Antarctic lake. *Geobiology* 12, 424–450. <https://doi.org/10.1111/gbi.12096>.
- Lepot, K., Addad, A., Knoll, A.H., Wang, J., Trodec, D., Béché, A., Javaux, E.J., 2017. Iron minerals within specific microfossil morphologies of the 1.88 Ga Gunflint Formation. *Nat. Commun.* 8, 14890. <https://doi.org/10.1038/ncomms14890>.
- Lepot, K., Williford, K.H., Philippot, P., Thomazo, C., Ushikubo, T., Kitajima, K., Mostefauoi, S., Valley, J.W., 2019. Extreme 13C-depletions and organic sulfur content argue for S-fueled anaerobic methane oxidation in 2.72 Ga old stromatolites. *Geochim. Cosmochim. Acta* 244, 522–547. <https://doi.org/10.1016/j.gca.2018.10.014>.
- Léveillé, R.J., Longstaffe, F.J., Fyfe, W.S., 2007. An isotopic and geochemical study of carbonate-clay mineralization in basaltic caves: Abiotic versus microbial processes. *Geobiology* 5, 235–249. <https://doi.org/10.1111/j.1472-4669.2007.00109.x>.
- Li, J., Kusky, T.M., 2007. World's largest known Precambrian fossil black smoker chimneys and associated microbial vent communities, North China: Implications for early life. *Gondwana Res.* 12, 84–100. <https://doi.org/10.1016/j.gr.2006.10.024>.
- Li, W., Johnson, C.M., Beard, B.L., 2012. U-Th-Pb isotope data indicate Phanerozoic age for oxidation of the 3.4 Ga Apex Basalt. *Earth Planet. Sci. Lett.* 319–320, 197–206. <https://doi.org/10.1016/j.epsl.2011.12.035>.
- Li, W., Czaja, A.D., van Kranendonk, M.J., Beard, B.L., Roden, E.E., Johnson, C.M., 2013. An anoxic, Fe(II)-rich, U-poor ocean 3.46 billion years ago. *Geochim. Cosmochim. Acta* 120, 65–79. <https://doi.org/10.1016/j.gca.2013.06.033>.
- Li, M.-L., Liu, S.-A., Xue, C.-J., Li, D., 2019. Zinc, cadmium and sulfur isotope fractionation in a supergiant MVT deposit with bacteria. *Geochim. Cosmochim. Acta* 265, 1–18. <https://doi.org/10.1016/j.gca.2019.08.018>.
- Lindsay, J.F., Brasier, M.D., McLoughlin, N., Green, O.R., Fogel, M., Steele, A., Mertzman, S.A., 2005. The problem of deep carbon - an Archean paradox. *Precambrian Res.* 143, 1–22. <https://doi.org/10.1016/j.precamres.2005.09.003>.
- Liu, D., Dong Hailiang, H., Bishop, M.E., Wang, H., Agrawal, A., Tritschler, S., Eberl, D.D., Xie, S., 2011. Reduction of structural Fe(III) in nontronite by methanogen *Methanosarcina barkeri*. *Geochim. Cosmochim. Acta* 75, 1057–1071. <https://doi.org/10.1016/j.gca.2010.11.009>.
- Lollar, B.S., McCollom, T.M., 2006. Geochemistry: Biosignatures and abiotic constraints on early life. *Nature* 444, E18. <https://doi.org/10.1038/nature05499>.
- Londry, K.L., Des Marais, D.J., 2003. Stable carbon isotope fractionation by sulfate-reducing bacteria. *Appl. Environ. Microbiol.* 69, 2942–2949. <https://doi.org/10.1128/AEM.69.5.2942>.
- Londry, K.L., Dawson, K.G., Grover, H.D., Summons, R.E., Bradley, A.S., 2008. Stable carbon isotope fractionation between substrates and products of *Methanosarcina barkeri*. *Org. Geochem.* 39, 608–621. <https://doi.org/10.1016/j.orggeochem.2008.03.002>.
- Lovley, D.R., 1991. Dissimilatory Fe (III) and Mn (IV) reduction. *Microbiol. Rev.* 55, 259–287.
- Lowe, D.R., 1980. Stromatolites 3,400-Myr old from the Archean of Western Australia. *Nature* 284, 441–443. <https://doi.org/10.1038/284441a0>.
- Lowe, D.R., 1994. Abiological origin of described stromatolites older than 3.2 Ga. *Geology* 22, 387–390. [https://doi.org/10.1130/0091-7613\(1994\)022<0387:AODSO>2.3.CO](https://doi.org/10.1130/0091-7613(1994)022<0387:AODSO>2.3.CO).
- Lowe, D.R., Tice, M.M., 2007. Tectonic controls on atmospheric, climatic, and biological evolution 3.5–2.4 Ga. *Precambrian Res.* 158, 177–197. <https://doi.org/10.1016/j.precamres.2007.04.008>.
- Luo, G., Ono, S., Beukes, N.J., Wang, D.T., Xie, S., Summons, R.E., 2016. Rapid oxygenation of Earth's atmosphere 2.33 billion years ago. *Sci. Adv.* 2. <https://doi.org/10.1126/sciadv.1600134>. e1600134.
- Luo, M., SHI, G.R., Chen, Z.Q., Hu, S., Huang, J., Zhang, Q., Zhou, C., Fang, Y., 2018. Youngest ambient inclusion trails from Middle Triassic phosphatized coprolites, southwestern China: New insights into an old intriguing phenomenon. *Gondwana Res.* 55, 60–73. <https://doi.org/10.1016/j.gr.2017.11.011>.
- Lyons, T.W., Gill, B.C., 2010. Ancient sulfur cycling and oxygenation of the early biosphere. *Elements* 6, 93–99. <https://doi.org/10.2113/gselements.6.2.93>.
- Lyons, T.W., Reinhard, C.T., Planavsky, N.J., 2014. The rise of oxygen in Earth's early ocean and atmosphere. *Nature* 506, 307–315. <https://doi.org/10.1038/nature13068>.
- Madigan, M.T., Martinko, J.M., Bensen, K.S., Buckley, D.H., Stahl, D.A., 2009. *Brock Biology of Microorganisms*. Pearson, ed. Glenview.
- Maillard, J., Carrasco, N., Schmitz-Afonso, I., Gautier, T., Afonso, C., 2018. Comparison of soluble and insoluble organic matter in analogues of Titan's aerosols. *Earth Planet. Sci. Lett.* 495, 185–191. <https://doi.org/10.1016/j.epsl.2018.05.014>.
- Maliva, R.G., Knoll, A.H., Simonson, B.M., 2005. Secular change in the Precambrian silica cycle: Insights from chert petrology. *Bull. Geol. Soc. Am.* 117, 835–845. <https://doi.org/10.1130/B25555.1>.
- Mansor, M., Fantle, M.S., 2019. A novel framework for interpreting pyrite-based Fe isotope records of the past. *Geochim. Cosmochim. Acta* 253, 39–62. <https://doi.org/10.1016/j.gca.2019.03.017>.
- Marin-Carbonne, J., Remusat, L., Sforna, M.C., Thomazo, C., Cartigny, P., Philippot, P., 2018. Sulfur isotope's signal of nanopyrrites enclosed in 2.7 Ga stromatolitic organic remains reveal microbial sulfate reduction. *Geobiology* 16, 121–138. <https://doi.org/10.1111/gbi.12096>.

- 10.1111/gbi.12275.
- Marin-Carbonne, J., Busigny, V., Miot, J., Rollion-Bard, C., Muller, E., Drabon, N., Jacob, D., Pont, S., Robyr, M., Bontognali, T.R.R., François, C., Reynaud, S., Van Zuilen, M., Philippot, P., 2020. In Situ Fe and S isotope analyses in pyrite from the 3.2 Ga Mendon Formation (Barberton Greenstone Belt, South Africa): Evidence for early microbial iron reduction. *Geobiology* Gbi 12385. <https://doi.org/10.1111/gbi.12385>.
- Mariotti, G., Pruss, S.B., Perron, J.T., Bosak, T., 2014. Microbial shaping of sedimentary wrinkle structures. *Nat. Geosci.* 7, 736–740. <https://doi.org/10.1038/ngeo2229>.
- Marshall, C.P., Love, G.D., Snape, C.E., Hill, A.C., Allwood, A.C., Walter, M.R., van Kranendonk, M.J., Bowden, S.A., Sylva, S.P., Summons, R.E., 2007. Structural characterization of kerogen in 3.4 Ga Archaean cherts from the Pilbara Craton, Western Australia. *Precambrian Res.* 155, 1–23. <https://doi.org/10.1016/j.precamres.2006.12.014>.
- Marshall, A.O., Emry, J.R., Marshall, C.P., 2012. Multiple generations of Carbon in the Apex Chert and implications for preservation of microfossils. *Astrobiology* 12, 160–166. <https://doi.org/10.1089/ast.2011.0729>.
- Martindale, R.C., Strauss, J.V., Sperling, E.A., Johnson, J.E., van Kranendonk, M.J., Flannery, D., French, K., Lepot, K., Mazumder, R., Rice, M.S., Schrag, D.P., Summons, R., Walter, M., Abelson, J., Knoll, A.H., 2015. Sedimentology, chemostratigraphy, and stromatolites of lower Paleoproterozoic carbonates, Turee Creek Group, Western Australia. *Precambrian Res.* 266, 194–211. <https://doi.org/10.1016/j.precamres.2015.05.021>.
- Maslennikov, V.V., Maslennikova, S.P., Large, R.R., Danyushevsky, L.V., Herrington, R.J., Ayupova, N.R., Zaykov, V.V., Lein, A.Y., Tseluyko, A.S., Melekesteva, I.Y., Tessalina, S.G., 2017. Chimneys in Paleozoic massive sulfide mounds of the Urals VMS deposits: mineral and trace element comparison with modern black, grey, white and clear smokers. *Ore Geol. Rev.* 85, 64–106. <https://doi.org/10.1016/j.oregeorev.2016.09.012>.
- McCorm, T.M., 2013. Miller-Urey and beyond: what have we learned about prebiotic organic synthesis reactions in the past 60 years? *Annu. Rev. Earth Planet. Sci.* 41, 207–229. <https://doi.org/10.1146/annurev-earth-040610-133457>.
- McCorm, T.M., 2016. Abiotic methane formation during experimental serpentinization of olivine. *Proc. Natl. Acad. Sci. U. S. A.* 113, 13965–13970. <https://doi.org/10.1073/pnas.1611843113>.
- McCorm, T.M., Donaldson, C., 2019. Experimental constraints on abiotic formation of tubules and other proposed biological structures in subsurface volcanic glass. *Astrobiology* 19, 53–63. <https://doi.org/10.1089/ast.2017.1811>.
- McCorm, T.M., Seewald, J.S., 2006. Carbon isotope composition of organic compounds produced by abiotic synthesis under hydrothermal conditions. *Earth Planet. Sci. Lett.* 243, 74–84. <https://doi.org/10.1016/j.epsl.2006.01.027>.
- McCorm, T.M., Seewald, J.S., 2013. Serpentinites, hydrogen, and life. *Elements* 9, 129–134. <https://doi.org/10.2113/gselements.9.2.129>.
- McCorm, T.M., Ritter, G., Simoneit, B.R.T., 1999. Lipid synthesis under hydrothermal conditions by Fischer-Tropsch-type reactions. *Orig. Life Evol. Biosph.* 29, 153–166. <https://doi.org/10.1023/A:1006592502746>.
- McKeegan, K.D., Kudryavtsev, A.B., Schopf, J.W., 2007. Raman and ion microscopic imagery of graphitic inclusions in apatite from older than 3830 Ma Akilia supra-crustal rocks, West Greenland. *Geology* 35, 591–594. <https://doi.org/10.1130/G23465A.1>.
- McLoughlin, N., Wilson, L.A., Brasier, M.D., 2008. Growth of synthetic stromatolites and wrinkle structures in the absence of microbes – implications for the early fossil record. *Geobiology* 6, 95–105. <https://doi.org/10.1111/j.1472-4669.2007.00141.x>.
- McLoughlin, N., Fliegel, D.J., Furnes, H., Staudigel, H., Simonetti, A., Zhao, G.C., Robinson, P.T., 2010. Assessing the biogenicity and syngenicity of candidate bioalteration textures in pillow lavas of the ~2.52 Ga Wutai greenstone terrane of China. *Chin. Sci. Bull.* 55, 188–199. <https://doi.org/10.1007/s11434-009-0448-0>.
- McLoughlin, N., Wacey, D., Kruber, C., Kilburn, M.R., Thorseth, I.H., Pedersen, R.B., 2011. A combined TEM and NanoSIMS study of endolithic microfossils in altered seafloor basalt. *Chem. Geol.* 289, 154–162. <https://doi.org/10.1016/j.chemgeo.2011.07.022>.
- McLoughlin, N., Grosch, E.G., Kilburn, M.R., Wacey, D., 2012. Sulfur isotope evidence for a Paleoproterozoic seafloor biosphere, Barberton, South Africa. *Geology* 40, 1031–1034. <https://doi.org/10.1130/G33313.1>.
- McLoughlin, N., Wacey, D., Phungphungu, S., Saunders, M., Grosch, E.G., 2020. Deconstructing Earth's oldest ichnofossil record from the Pilbara Craton, West Australia: Implications for seeking life in the Archean seafloor. *Geobiology* gbi 12399. <https://doi.org/10.1111/gbi.12399>.
- McMahon, W.J., Davies, N.S., Went, D.J., 2017. Negligible microbial matground influence on pre-vegetation river functioning: evidence from the Ediacaran-Lower Cambrian Series Rouge, France. *Precambrian Res.* 292, 13–34. <https://doi.org/10.1016/j.precamres.2017.01.020>.
- McMahon, S., Bosak, T., Grotzinger, J.P., Milliken, R.E., Summons, R.E., Daye, M., Newman, S.A., Fraeman, A., Williford, K.H., Briggs, D.E.G., 2018. A field guide to finding fossils on Mars. *J. Geophys. Res. Planets* 123, 1012–1040. <https://doi.org/10.1029/2017JE005478>.
- Ménez, B., Pisapia, C., Andreani, M., Jammé, F., Vanbellinghen, Q.P., Brunelle, A., Richard, L., Dumas, P., Réfrégiers, M., 2018. Abiotic synthesis of amino acids in the recesses of the oceanic lithosphere. *Nature* 564, 59–63. <https://doi.org/10.1038/s41586-018-0684-z>.
- Meshoulam, A., Ellis, G.S., Said Ahmad, W., Deev, A., Sessions, A.L., Tang, Y., Adkins, J.F., Liu, J., Gilhooly, W.P., Aizenshtat, Z., Amrani, A., 2016. Study of thermochemical sulfate reduction mechanism using compound specific sulfur isotope analysis. *Geochim. Cosmochim. Acta* 188, 73–92. <https://doi.org/10.1016/j.gca.2016.05.026>.
- Mével, C., 2003. Serpentinization of abyssal peridotites at mid-ocean ridges. *Comptes Rendus Geosci.* 335, 825–852. <https://doi.org/10.1016/j.crte.2003.08.006>.
- Miao, L., Moczydlowska, M., Zhu, S., Zhu, M., 2019. New record of organic-walled, morphologically distinct microfossils from the late Paleoproterozoic Changcheng Group in the Yanshan Range, North China. *Precambrian Res.* 321, 172–198. <https://doi.org/10.1016/j.precamres.2018.11.019>.
- Milesi, V., Guyot, F., Brunet, F., Richard, L., Recham, N., Benedetti, M., Dairou, J., Prinzhofer, A., 2015. Formation of CO₂, H₂ and condensed carbon from siderite dissolution in the 200–300°C range and at 50MPa. *Geochim. Cosmochim. Acta* 154, 201–211. <https://doi.org/10.1016/j.gca.2015.01.015>.
- Milesi, V., McCollom, T.M., Guyot, F., 2016. Thermodynamic constraints on the formation of condensed carbon from serpentinization fluids. *Geochim. Cosmochim. Acta* 189, 391–403. <https://doi.org/10.1016/j.gca.2016.06.006>.
- Milucka, J., Ferdelman, T.G., Polerecky, L., Franzke, D., Wegener, G., Schmid, M., Lieberwirth, L., Wagner, M., Widdel, F., Kuyper, M.M.M., 2012. Zero-valent Sulphur is a key intermediate in marine methane oxidation. *Nature* 491, 541–546. <https://doi.org/10.1038/nature11656>.
- Miot, J., Benzerara, K., Morin, G., Kappler, A., Bernard, S., Obst, M., Férard, C., Skouri-Panet, F., Guigner, J.-M., Posth, N., Galvez, M., Brown, G.E., Guyot, F., 2009. Iron biomineralization by anaerobic neutrophilic iron-oxidizing bacteria. *Geochim. Cosmochim. Acta* 73, 696–711. <https://doi.org/10.1016/j.gca.2008.10.033>.
- Mißbach, H., Schmidt, B.C., Duda, J.-P., Lünsdorf, N.K., Goetz, W., Thiel, V., 2018. Assessing the diversity of lipids formed via Fischer-Tropsch-type reactions. *Org. Geochem.* 119, 110–121. <https://doi.org/10.1016/j.orggeochem.2018.02.012>.
- Mojzsis, S.J., Arrhenius, G., McKeegan, K.D., Harrison, T.M., Nutman, A.P., Friend, C.R.L., 1996. Evidence for life on Earth before 3,800 million years ago. *Nature* 384, 55–59. <https://doi.org/10.1038/384055a0>.
- Mongenet, T., Riboulleau, A., Garcette-Lepecq, A., Derenne, S., Pouet, Y., Baudin, F., Largeau, C., 2001. Occurrence of proteinaceous moieties in S- and O-rich late Tithonian kerogen (Kashpir oil Shales, Russia). *Org. Geochem.* 32, 199–203.
- Montinaro, A., Strauss, H., Mason, P.R.D., Roerdink, D., Münker, C., Schwarz-Schampera, U., Arndt, N.T., Farquhar, J., Beukes, N.J., Gutzmer, J., Peters, M., 2015. Paleoproterozoic sulfur cycling: Multiple sulfur isotope constraints from the Barberton Greenstone Belt, South Africa. *Precambrian Res.* 267, 311–322. <https://doi.org/10.1016/j.precamres.2015.06.008>.
- Monty, C.L.V., 1976. Chapter 5.1 The Origin and Development of Cryptalgal Fabrics, in: *Stromatolites. Dev. Sedimentol.* 20, 193–249. [https://doi.org/10.1016/S0070-4571\(08\)71137-3](https://doi.org/10.1016/S0070-4571(08)71137-3).
- Moore, E.K., Jelen, B.L., Giovannelli, D., Raanan, H., Falkowski, P.G., 2017. Metal availability and the expanding network of microbial metabolisms in the Archaean eon. *Nat. Geosci.* 10, 629–636. <https://doi.org/10.1038/ngeo3006>.
- Morag, N., Williford, K.H., Kitajima, K., Philippot, P., van Kranendonk, M.J., Lepot, K., Thomazo, C., Valley, J.W., 2016. Microstructure-specific carbon isotopic signatures of organic matter from ~3.5 Ga cherts of the Pilbara Craton support a biologic origin. *Precambrian Res.* 275, 429–449. <https://doi.org/10.1016/j.precamres.2016.01.014>.
- Muller, É., Philippot, P., Rollion-Bard, C., Cartigny, P., Assayag, N., Marin-Carbonne, J., Mohan, M.R., Sarma, D.S., 2017. Primary sulfur isotope signatures preserved in high-grade Archean barite deposits of the Sargur Group, Dharwar Craton, India. *Precambrian Res.* 295, 38–47. <https://doi.org/10.1016/j.precamres.2017.04.029>.
- Nabhan, S., Marin-Carbonne, J., Mason, P.R.D., Heubeck, C., 2020. In situ S-isotope compositions of sulfate and sulfide from the 3.2 Ga Moodies Group, South Africa: a record of oxidative sulfur cycling. *Geobiology* 18, 426–444. <https://doi.org/10.1111/gbi.12393>.
- Nie, N.X., Dauphas, N., Greenwood, R.C., 2017. Iron and oxygen isotope fractionation during iron UV photo-oxidation: Implications for early Earth and Mars. *Earth Planet. Sci. Lett.* 458, 179–191. <https://doi.org/10.1016/j.epsl.2016.10.035>.
- Noffke, N., 2009. The criteria for the biogenicity of microbially induced sedimentary structures (MISS) in Archean and younger, sandy deposits. *Earth-Science Rev.* 96, 173–180. <https://doi.org/10.1016/j.earscirev.2008.08.002>.
- Noffke, N., Eriksson, K.A., Hazen, R.M., Simpson, E.L., 2006. A new window into early Archean life: Microbial mats in Earth's oldest siliciclastic tidal deposits (3.2 Ga Moodies Group, South Africa). *Geology* 34, 253–256. <https://doi.org/10.1130/G22246.1>.
- Noffke, N., Beukes, N., Bower, D., Hazen, R.M., Swift, D.J.P., 2008. An actualistic perspective into Archean worlds - (cyano-)bacterially induced sedimentary structures in the siliciclastic Nhlazatse Section, 2.9 Ga Pongola Supergroup, South Africa. *Geobiology* 6, 5–20. <https://doi.org/10.1111/j.1472-4669.2007.00118.x>.
- Noffke, N., Christian, D., Wacey, D., Hazen, R.M., 2013. Microbially Induced Sedimentary Structures Recording an Ancient Ecosystem in the ca. 3.48 Billion-Year-Old Dresser Formation, Pilbara, Western Australia. *Astrobiology* 13, 1103–1124. <https://doi.org/10.1089/ast.2013.1030>.
- Nutman, A.P., Bennett, V.C., Friend, C.R.L., van Kranendonk, M.J., Chivas, A.R., 2016. Rapid emergence of life shown by discovery of 3,700-million-year-old microbial structures. *Nature* 537, 535–538. <https://doi.org/10.1038/nature19355>.
- Nutman, A.P., Bennett, V.C., Friend, C.R.L., van Kranendonk, M.J., Rothacker, L., Chivas, A.R., 2019. Cross-examining Earth's oldest stromatolites: seeing through the effects of heterogeneous deformation, metamorphism and metasomatism affecting Isua (Greenland) ~3700 Ma sedimentary rocks. *Precambrian Res.* 331, 105347. <https://doi.org/10.1016/j.precamres.2019.105347>.
- Oduro, H., Harms, B., Sintim, H.O., Kaufman, A.J., Cody, G., Farquhar, J., 2011. Evidence of magnetic isotope effects during thermochemical sulfate reduction. *Proc. Natl. Acad. Sci. U. S. A.* 108, 17635–17638. <https://doi.org/10.1073/pnas.1108112108>.
- Oehler, D.Z., Robert, F., Mostefaoui, S., Meibom, A., Selo, M., McKay, D.S., 2006. Chemical mapping of Proterozoic organic matter at submicron spatial resolution. *Astrobiology* 6, 838–850. <https://doi.org/10.1089/ast.2006.6.838>.
- Oehler, D.Z., Robert, F., Walter, M.R., Sugitani, K., Allwood, A.C., Meibom, A., Mostefaoui, S., Selo, M., Thomen, A., Gibson, E.K., 2009. NanoSIMS: Insights into

- biogenicity and syngenite of Archaean carbonaceous structures. *Precambrian Res.* 173, 70–78. <https://doi.org/10.1016/j.precamres.2009.01.001>.
- Oehler, D.Z., Robert, F., Walter, M.R., Sugitani, K., Meibom, A., Mostefaoui, S., Gibson, E.K., 2010. Diversity in the Archaean biosphere: new insights from NanoSIMS. *Astrobiology* 10, 413–424. <https://doi.org/10.1089/ast.2009.0426>.
- Oehler, D.Z., Walsh, M.M., Sugitani, K., Liu, M.-C., House, C.H., 2017. Large and robust lenticular microorganisms on the young Earth. *Precambrian Res.* 296, 112–119. <https://doi.org/10.1016/j.precamres.2017.04.031>.
- Olson, S.L., Kump, L.R., Kasting, J.F., 2013. Quantifying the areal extent and dissolved oxygen concentrations of Archaean oxygen oases. *Chem. Geol.* 362, 35–43. <https://doi.org/10.1016/j.chemgeo.2013.08.012>.
- Orange, F., Lalonde, S.V., Konhauser, K.O., 2013. Experimental simulation of evaporation-driven silica sinter formation and microbial silicification in hot spring systems. *Astrobiology* 13, 163–176. <https://doi.org/10.1089/ast.2012.0887>.
- Orphan, V.J., House, C.H., Hinrichs, K.U., McKeegan, K.D., DeLong, E.F., 2001. Methane-consuming archaea revealed by directly coupled isotopic and phylogenetic analysis. *Science* 293, 484–487. <https://doi.org/10.1126/science.1061338>.
- Orphan, V.J., House, C.H., Hinrichs, K.-U., McKeegan, K.D., DeLong, E.F., 2002. Multiple archaeal groups mediate methane oxidation in anoxic cold seep sediments. *Proc. Natl. Acad. Sci. U. S. A.* 99, 7663–7668. <https://doi.org/10.1073/pnas.072210299>.
- Ossa Ossa, F., Hofmann, A., Spangenberg, J.E., Poulton, S.W., Stüeken, E.E., Schoenberg, R., Eickmann, B., Wille, M., Butler, M., Bekker, A., 2019. Limited oxygen production in the Mesoproterozoic Ocean. *Proc. Natl. Acad. Sci. U. S. A.* 116, 6647–6652. <https://doi.org/10.1073/pnas.1818762116>.
- Ostrand, C.M., Nielsen, S.G., Owens, J.D., Kendall, B., Gordon, G.W., Romaniello, S.J., Anbar, A.D., 2019. Fully oxygenated water columns over continental shelves before the Great Oxidation Event. *Nat. Geosci.* 12, 186–191. <https://doi.org/10.1038/s41561-019-0309-7>.
- Overmann, J., 2006. The Family Chlorobiaceae. In: *The Prokaryotes*. Springer New York, New York, NY, pp. 359–378. https://doi.org/10.1007/0-387-30747-8_13.
- Pace, A., Bourillot, R., Bouton, A., Vennin, E., Galaup, S., Bundeleva, L., Patrier, P., Dupraz, C., Thomazo, C., Sansjofre, P., Yokoyama, Y., Franceschi, M., Anguy, Y., Pigot, L., Virgone, A., Visscher, P.T., 2016. Microbial and diagenetic steps leading to the mineralisation of Great Salt Lake microbialites. *Sci. Rep.* 6, 31495. <https://doi.org/10.1038/srep31495>.
- Papineau, D., De Gregorio, B.T., Stroud, R.M., Steele, A., Pecoits, E., Konhauser, K., Wang, J., Fogel, M.L., 2010a. Ancient graphite in the Eoarchean quartz-pyroxene rocks from Aklia in southern West Greenland II: Isotopic and chemical compositions and comparison with Paleoproterozoic banded iron formations. *Geochim. Cosmochim. Acta* 74, 5884–5905. <https://doi.org/10.1016/j.gca.2010.07.002>.
- Papineau, D., De Gregorio, B.T., Cody, G.D., Fries, M.D., Mojzsis, S.J., Steele, A., Stroud, R.M., Fogel, M.L., 2010b. Ancient graphite in the Eoarchean quartz-pyroxene rocks from Aklia in southern West Greenland I: Petrographic and spectroscopic characterization. *Geochim. Cosmochim. Acta* 74, 5862–5883. <https://doi.org/10.1016/j.gca.2010.05.025>.
- Papineau, D., De Gregorio, B.T., Cody, G.D., O'Neil, J., Steele, A., Stroud, R.M., Fogel, M.L., 2011. Young poorly crystalline graphite in the > 3.8-Gyr-old Nuvvuagittuq banded iron formation. *Nat. Geosci.* 4, 376–379. <https://doi.org/10.1038/ngeo1155>.
- Pasini, V., Brunelli, D., Dumas, P., Sandt, C., Frederick, J., Benzerara, K., Bernard, S., Ménez, B., 2013. Low temperature hydrothermal oil and associated biological precursors in serpentinites from mid-ocean ridge. *Lithos* 178, 84–95. <https://doi.org/10.1016/j.lithos.2013.06.014>.
- Pearson, A., 2010. Pathways of carbon assimilation and their impact on organic matter values $\delta^{13}C$. In: Timmis, K.N. (Ed.), *Handbook of Hydrocarbon and Lipid Microbiology*. Springer-Verlag, Berlin Heidelberg, pp. 143–156. <https://doi.org/10.1007/978-3-540-77587-4>.
- Pedersen, L.-E.R., McLoughlin, N., Vullum, P.E., Thorseth, I.H., 2015. Abiotic and candidate biotic micro-alteration textures in subseafloor basaltic glass: a high-resolution in-situ textural and geochemical investigation. *Chem. Geol.* 410, 124–137. <https://doi.org/10.1016/j.chemgeo.2015.06.005>.
- Pedley, M., Rogerson, M., Middleton, R., 2009. Freshwater calcite precipitates from in vitro mesocosm flume experiments: a case for biomediation of tufas. *Sedimentology* 56, 511–527. <https://doi.org/10.1111/j.1365-3091.2008.00983.x>.
- Penning, H., Conrad, R., 2006. Carbon isotope effects associated with mixed-acid fermentation of saccharides by *Clostridium paprysolvens*. *Geochim. Cosmochim. Acta* 70, 2283–2297. <https://doi.org/10.1016/j.gca.2006.01.017>.
- Penning, H., Claus, P., Casper, P., Conrad, R., 2006. Carbon isotope fractionation during acetoclastic methanogenesis by *Methanoseta concilia* in culture and a lake sediment. *Appl. Environ. Microbiol.* 72, 5648–5652. <https://doi.org/10.1128/AEM.00727-06>.
- Perri, E., Tucker, M.E., Spadafora, A., 2012. Carbonate organo-mineral micro- and ultrastructures in sub-fossil stromatolites: Marion lake, South Australia. *Geobiology* 10, 105–117. <https://doi.org/10.1111/j.1472-4669.2011.00304.x>.
- Petrash, D.A., Robbins, L.J., Shapiro, R.S., Mojzsis, S.J., Konhauser, K.O., 2016. Chemical and textural overprinting of ancient stromatolites: timing, processes, and implications for their use as paleoenvironmental proxies. *Precambrian Res.* 278, 145–160. <https://doi.org/10.1016/j.precamres.2016.03.010>.
- Pflug, H.D., 1967. Structured organic remains from the Fig Tree Series (Precambrian) of the Barberton mountain land (South Africa). *Rev. Palaeobot. Palynol.* 5, 9–29. [https://doi.org/10.1016/0034-6667\(67\)90205-9](https://doi.org/10.1016/0034-6667(67)90205-9).
- Philippot, P., van Zuilen, M., Lepot, K., Thomazo, C., Farquhar, J., van Kranendonk, M.J., 2007. Early Archaean microorganisms preferred reduced sulfur, not sulfate. *Science* 317, 1534–1537.
- Philippot, P., van Kranendonk, M.J., Van Zuilen, M., Lepot, K., Rividi, N., Teitler, Y., Thomazo, C., Blanc-Valleron, M.M., Rouchy, J.M., Grosch, E., de Wit, M., 2009. Early traces of life investigations in drilling Archaean hydrothermal and sedimentary rocks of the Pilbara Craton, Western Australia and Barberton Greenstone Belt, South Africa. *Comptes Rendus - Palevol* 8, 649–663. <https://doi.org/10.1016/j.crvp.2009.06.006>.
- Philippot, P., van Zuilen, M., Rollion-Bard, C., 2012. Variations in atmospheric Sulphur chemistry on early Earth linked to volcanic activity. *Nat. Geosci.* 5, 668–674. <https://doi.org/10.1038/ngeo1534>.
- Philippot, P., Ávila, J.N., Killingsworth, B.A., Tesselina, S., Baton, F., Caqueneau, T., Muller, E., Pecoits, E., Cartigny, P., Lalonde, S.V., Ireland, T.R., Thomazo, C., van Kranendonk, M.J., Busigny, V., 2018. Globally asynchronous Sulphur isotope signals require re-definition of the Great Oxidation Event. *Nat. Commun.* 9. <https://doi.org/10.1038/s41467-018-04621-x>.
- Pinti, D.L., Hashizume, K., Matsuda, J. Ichi, 2001. Nitrogen and argon signatures in 3.8 to 2.8 Ga metasediments: Clues on the chemical state of the Archaean Ocean and the deep biosphere. *Geochim. Cosmochim. Acta* 65, 2301–2315. [https://doi.org/10.1016/S0016-7037\(01\)00590-7](https://doi.org/10.1016/S0016-7037(01)00590-7).
- Pinti, D.L., Hashizume, K., Sugihara, A., Massault, M., Philippot, P., 2009. Isotopic fractionation of nitrogen and carbon in Paleoproterozoic cherts from Pilbara craton, Western Australia: Origin of ^{15}N -depleted nitrogen. *Geochim. Cosmochim. Acta* 73, 3819–3848. <https://doi.org/10.1016/j.gca.2009.03.014>.
- Planavsky, N.J., Asael, D., Hofmann, A., Reinhard, C.T., Lalonde, S.V., Knudsen, A., Wang, X., Ossa Ossa, F., Pecoits, E., Smith, A.J.B., Beukes, N.J., Bekker, A., Johnson, T.M., Konhauser, K.O., Lyons, T.W., Rouxel, O.J., 2014. Evidence for oxygenic photosynthesis half a billion years before the Great Oxidation Event. *Nat. Geosci.* 7, 283–286. <https://doi.org/10.1038/ngeo2122>.
- Planavsky, N.J., Robbins, L.J., Kamber, B.S., Schoenberg, R., 2020. Weathering, alteration and reconstructing Earth's oxygenation. *Interface Focus* 10, 20190140. <https://doi.org/10.1098/rsif.2019.0140>.
- Porada, H., Bouougri, E.H., 2007. Wrinkle structures—a critical review. *Earth-Science Rev.* 81, 199–215. <https://doi.org/10.1016/j.earscirev.2006.12.001>.
- Preiss, W.V., 1976. Chapter 2.1 Basic Field and Laboratory Methods for the Study of Stromatolites. pp. 5–13. [https://doi.org/10.1016/S0070-4571\(08\)71124-5](https://doi.org/10.1016/S0070-4571(08)71124-5).
- Preuß, A., Schauder, R., Fuchs, G., Stichter, W., 1989. Carbon isotope fractionation by autotrophic bacteria with three different CO_2 fixation pathways. *Zeitschrift für Naturforsch. C* 44. <https://doi.org/10.1515/znc-1989-5-610>.
- Rashby, S.E., Sessions, A.L., Summons, R.E., Newman, D.K., 2007. Biosynthesis of 2-methylbacteriohopane polyols by an anoxygenic phototroph. *Proc. Natl. Acad. Sci. U. S. A.* 104, 15099–15104. <https://doi.org/10.1073/pnas.0704912104>.
- Rasmussen, B., 2000. Filamentous microfossils in a 3,235-million-year-old volcanogenic massive sulphide deposit. *Nature* 405, 676–679. <https://doi.org/10.1038/35015063>.
- Rasmussen, B., Buick, R., 1999. Redox state of the Archaean atmosphere; evidence from detrital heavy minerals in ca. 3250–2750 Ma sandstones from the Pilbara Craton, Australia. *Geology* 27, 115–118.
- Rasmussen, B., Buick, R., 2000. Oily old ores: evidence for hydrothermal petroleum generation in an Archaean volcanogenic massive sulfide deposit. *Geology* 28, 731–734. [https://doi.org/10.1130/0091-7613\(2000\)28<731:OOEFH>2.0.CO;2](https://doi.org/10.1130/0091-7613(2000)28<731:OOEFH>2.0.CO;2).
- Rasmussen, B., Fletcher, I.R., Brocks, J.J., Kilburn, M.R., 2008. Reassessing the first appearance of eukaryotes and cyanobacteria. *Nature* 455, 1101–1104.
- Rasmussen, B., Blake, T.S., Fletcher, I.R., Kilburn, M.R., 2009. Evidence for microbial life in syndensitidite cavities from 2.75 Ga terrestrial environments. *Geology* 37, 423–426. <https://doi.org/10.1130/G25300A.1>.
- Rasmussen, B., Fletcher, I.R., Bekker, A., Muhling, J.R., Gregory, C.J., Thorne, A.M., 2012. Deposition of 1.88-billion-year-old iron formations as a consequence of rapid crustal growth. *Nature* 484, 498–501. <https://doi.org/10.1038/nature11021>.
- Reid, R.P., Visscher, P.T., Decho, A.W., Stolz, J.F., Bebout, B.M., Dupraz, C., Macintyre, I.G., Pael, H.W., Pinckney, J.L., Prufert-Bebout, L., Stepp, T.F., DesMarais, D.J., 2000. The role of microbes in accretion, lamination and early lithification of modern marine stromatolites. *Nature* 406, 989–992. <https://doi.org/10.1038/35023158>.
- Reid, R.P., James, N.P., Macintyre, I.G., Dupraz, C.P., Burne, R.V., 2003. Shark bay stromatolites: microfossils and reinterpretation of Origins. *Facies* 49, 299–324. <https://doi.org/10.1007/s10347-003-0036-8>.
- Reinhard, C.T., Planavsky, N.J., Gill, B.C., Ozaki, K., Robbins, L.J., Lyons, T.W., Fischer, W.W., Wang, C., Cole, D.B., Konhauser, K.O., 2017. Evolution of the global phosphorus cycle. *Nature* 541, 386–389. <https://doi.org/10.1038/nature20772>.
- Reinhardt, M., Goetz, W., Duda, J.-P., Heim, C., Reiter, J., Thiel, V., 2019. Organic signatures in Pleistocene cherts from Lake Magadi (Kenya) – implications for early Earth hydrothermal deposits. *Biogeosciences* 16, 2443–2465. <https://doi.org/10.5194/bg-16-2443-2019>.
- Revan, M.K., Genç, Y., Maslennikov, V.V., Maslennikova, S.P., Large, R.R., Danyushevsky, L.V., 2014. Mineralogy and trace-element geochemistry of sulfide minerals in hydrothermal chimneys from the Upper-cretaceous VMS deposits of the eastern Pontide orogenic belt (NE Turkey). *Ore Geol. Rev.* 63, 129–149. <https://doi.org/10.1016/j.oregeorev.2014.05.006>.
- Riding, R., Fralick, P., Liang, L., 2014. Identification of an Archaean marine oxygen oasis. *Precambrian Res.* 251, 232–237. <https://doi.org/10.1016/j.precamres.2014.06.017>.
- Roerdink, D.L., Mason, P.R.D., Whitehouse, M.J., Reimer, T., 2013. High-resolution quadruple sulfur isotope analyses of 3.2Ga pyrite from the Barberton Greenstone Belt in South Africa reveal distinct environmental controls on sulfide isotopic arrays. *Geochim. Cosmochim. Acta* 117, 203–215. <https://doi.org/10.1016/j.gca.2013.04.027>.
- Roerdink, D.L., Mason, P.R.D., Whitehouse, M.J., Brouwer, F.M., 2016. Reworking of atmospheric sulfur in a Paleoproterozoic hydrothermal system at Londozi, Barberton Greenstone Belt, Swaziland. *Precambrian Res.* 280, 195–204. <https://doi.org/10.1016/j.precamres.2016.05.007>.
- Roh, Y., Gao, H., Vali, H., Kennedy, D.W., Yang, Z.K., Gao, W., Dohnalkova, A.C., Stapleton, R.D., Moon, J.-W., Phelps, T.J., Fredrickson, J.K., Zhou, J., 2006. Metal reduction and iron biomineralization by a psychrotolerant Fe(III)-reducing bacterium, *Shewanella* sp. Strain PV-4. *Appl. Environ. Microbiol.* 72, 3236–3244. <https://doi.org/10.1128/AEM.72.5.3236-3244.2006>.

- Rosing, M.T., 1999. 13C-depleted Carbon Microparticles in > 3700-Ma Sea-Floor Sedimentary Rocks from West Greenland. *Science* 283, 674–676. <https://doi.org/10.1126/science.283.5402.674>.
- Ross, C.S., 1962. Microclitics in glass volcanic rocks. *Amer. Miner.* 47, 723–740.
- Rouillard, J., García-Ruiz, J.M., Gong, J., van Zuilen, M.A., 2018. A morphogram for silica-witherite biomorphs and its application to microfossil identification in the early earth rock record. *Geobiology* 16, 279–296. <https://doi.org/10.1111/gbi.12278>.
- Rushdi, A.I., Simoneit, B.R.T., 2004. Condensation reactions and formation of amides, esters, and nitriles under hydrothermal conditions. *Astrobiology* 4, 211–224. <https://doi.org/10.1089/153110704323175151>.
- Satkoski, A.M., Beukes, N.J., Li, W., Beard, B.L., Johnson, C.M., 2015. A redox-stratified ocean 3.2 billion years ago. *Earth Planet. Sci. Lett.* 430, 43–53. <https://doi.org/10.1016/j.epsl.2015.08.007>.
- Schidlowski, M., 2001. Carbon isotopes as biogeochemical recorders of life over 3.8 Ga of earth history: evolution of a concept. *Precambrian Res.* 106, 117–134. [https://doi.org/10.1016/S0301-9268\(00\)00128-5](https://doi.org/10.1016/S0301-9268(00)00128-5).
- Schopf, J.W., 1975. Precambrian paleobiology: problems and perspectives. *Annu. Rev. Earth Planet. Sci.* 3, 213–249.
- Schopf, J.W., 1992. Atlas of representative Proterozoic microfossils. In: Schopf, J.W., Klein, C. (Eds.), *The Proterozoic Biosphere: A Multidisciplinary Study*. Cambridge University Press, pp. 1055–1118. <https://doi.org/10.1017/CBO9780511601064.026>.
- Schopf, J.W., 1993. Microfossils of the early Archean Apex Chert: New evidence of the antiquity of life. *Science* 260, 640–646. <https://doi.org/10.1126/science.260.5108.640>.
- Schopf, J.W., 2006. Fossil evidence of Archaean life. *Philos. Trans. R. Soc. B Biol. Sci.* 361, 869–885. <https://doi.org/10.1098/rstb.2006.1834>.
- Schopf, J.W., Kudryavtsev, A.B., 2012. Biogenicity of Earth's earliest fossils: a resolution of the controversy. *Gondwana Res.* 22, 761–771. <https://doi.org/10.1016/j.gr.2012.07.003>.
- Schopf, J.W., Walter, M.R., 1983. Archean microfossils: new evidence of ancient microbes. In: Schopf, J.W. (Ed.), *Earth's Earliest Biosphere: Its Origin and Evolution*. Princeton University Press, pp. 214–239.
- Schopf, J.W., Kudryavtsev, A.B., Czaja, A.D., Tripathi, A.B., 2007. Evidence of Archaean life: Stromatolites and microfossils. *Precambrian Res.* 158, 141–155. <https://doi.org/10.1016/j.precamres.2007.04.009>.
- Schopf, J.W., Kudryavtsev, A.B., Sugitani, K., Walter, M.R., 2010. Precambrian microbe-like pseudofossils: a promising solution to the problem. *Precambrian Res.* 179, 191–205. <https://doi.org/10.1016/j.precamres.2010.03.003>.
- Schopf, J.W., Kudryavtsev, A.B., Walter, M.R., van Kranendonk, M.J., Williford, K.H., Kozdon, R., Valley, J.W., Gallardo, V.A., Espinoza, C., Flannery, D.T., 2015. Sulfur-cycling fossil bacteria from the 1.8-Ga Duck Creek Formation provide promising evidence of evolution's null hypothesis. *Proc. Natl. Acad. Sci. U. S. A.* 112, 2087–2092. <https://doi.org/10.1073/pnas.1419241112>.
- Schopf, J.W., Kudryavtsev, A.B., Osterhout, J.T., Williford, K.H., Kitajima, K., Valley, J.W., Sugitani, K., 2017. An anaerobic ~3400 Ma shallow-water microbial consortium: Presumptive evidence of Earth's Palaeoarchean anoxic atmosphere. *Precambrian Res.* 299, 309–318. <https://doi.org/10.1016/j.precamres.2017.07.021>.
- Schopf, J.W., Kitajima, K., Spicuzza, M.J., Kudryavtsev, A.B., Valley, J.W., 2018. SIMS analyses of the oldest known assemblage of microfossils document their taxon-correlated carbon isotope compositions. *Proc. Natl. Acad. Sci.* 115, 53–58. <https://doi.org/10.1073/pnas.1718063115>.
- Schröder, S., Beukes, N.J., Sumner, D.Y., 2009. Microbialite-sediment interactions on the slope of the Campbellrand carbonate platform (Neoproterozoic, South Africa). *Precambrian Res.* 169, 68–79. <https://doi.org/10.1016/j.precamres.2008.10.014>.
- Scirè, S., Ciliberto, E., Crisafulli, C., Scribano, V., Bellatreccia, F., Ventura, G., Della, 2011. Asphaltene-bearing mantle xenoliths from Hyblean diatremes, Sicily. *Lithos* 125, 956–968. <https://doi.org/10.1016/j.lithos.2011.05.011>.
- Semikhatov, M.A., Gebelein, C.D., Cloud, P., Awramik, S.M., Benmore, W.C., 1979. Stromatolite morphogenesis—progress and problems. *Can. J. Earth Sci.* 16, 992–1015. <https://doi.org/10.1139/e79-088>.
- Sephton, M.A., 2002. Organic compounds in carbonaceous meteorites. *Nat. Prod. Rep.* 19, 292–311. <https://doi.org/10.1039/b103775g>.
- Sergeev, V.N., Knoll, A.H., Grotzinger, J.P., 1995. Paleobiology of the Mesoproterozoic Billyyakh Group, Anabar Uplift, Northern Siberia. *Mem. Paleontol. Soc.* 39, 1–37.
- Sforna, M.C., van Zuilen, M.A., Philippot, P., 2014. Structural characterization by Raman hyperspectral mapping of organic carbon in the 3.46 billion-year-old Apex chert, Western Australia. *Geochim. Cosmochim. Acta* 124, 18–33. <https://doi.org/10.1016/j.gca.2013.09.031>.
- Sforna, M.C., Brunelli, D., Pisapia, C., Pasini, V., Malferrari, D., Ménez, B., 2018. Abiotic formation of condensed carbonaceous matter in the hydrating oceanic crust. *Nat. Commun.* 9, 5049. <https://doi.org/10.1038/s41467-018-07385-6>.
- Sharma, M., 2006. Palaeobiology of Mesoproterozoic Salkhan Limestone, Semri Group, Rohtas, Bihar, India: Systematics and significance. *J. Earth Syst. Sci.* 115, 67–98. <https://doi.org/10.1007/BF02703027>.
- Sharma, M., Sergeev, V.N., 2004. Genesis of carbonate precipitate patterns and associated microfossils in Mesoproterozoic formations of India and Russia - a comparative study. *Precambrian Res.* 134, 317–347. <https://doi.org/10.1016/j.precamres.2004.07.001>.
- Shen, Y., Buick, R., 2004. The antiquity of microbial sulfate reduction. *Earth-Science Rev.* 64, 243–272. [https://doi.org/10.1016/S0012-8252\(03\)00054-0](https://doi.org/10.1016/S0012-8252(03)00054-0).
- Shen, Y., Farquhar, J., Masterson, A., Kaufman, A.J., Buick, R., 2009. Evaluating the role of microbial sulfate reduction in the early Archean using quadruple isotope systematics. *Earth Planet. Sci. Lett.* 279, 383–391.
- Sherwood Lollar, B., Westgate, T., Ward, J., Slater, G., Lacrampe-Couloume, G., 2002. Abiogenic formation of alkanes in the Earth's crust as a minor source for global hydrocarbon reservoirs. *Nature* 416, 522–524. <https://doi.org/10.1038/416522a>.
- Sim, M.S., Liang, B., Petroff, A.P., Evans, A., Klepac-Ceraj, V., Flannery, D.T., Walter, M.R., Bosak, T., 2012. Oxygen-Dependent morphogenesis of modern clumped photosynthetic mats and implications for the archaic stromatolite record. *Geosciences* 2, 235–259. <https://doi.org/10.3390/geosciences2040235>.
- Sinningh-Damsté, J.S., Kok, M.D., Köster, J., Schouten, S., 1998. Sulfurized carbohydrates: an important sedimentary sink for organic carbon? *Earth Planet. Sci. Lett.* 164, 7–13. [https://doi.org/10.1016/S0012-821X\(98\)00234-9](https://doi.org/10.1016/S0012-821X(98)00234-9).
- Slotznick, S.P., Fischer, W.W., 2016. Examining Archean methanotrophy. *Earth Planet. Sci. Lett.* 441, 52–59. <https://doi.org/10.1016/j.epsl.2016.02.013>.
- Smit, M.A., Mezger, K., 2017. Earth's early O₂ cycle suppressed by primitive continents. *Nat. Geosci.* 10, 788–792. <https://doi.org/10.1038/ngeo3030>.
- Solomon, S.C., Aharonson, O., Aurnou, J.M., Banerdt, W.B., Carr, M.H., Dombard, A.J., Frey, H.V., Golombek, M.P., Hauck, S.A., Head, J.W., Jakosky, B.H., Johnson, C.L., McGovern, P.J., Neumann, G.A., Phillips, R.J., Smith, D.E., Zuber, M.T., 2005. New perspectives on ancient Mars. *Science* 307, 1214–1220. <https://doi.org/10.1126/science.1101812>.
- Spadafora, A., Perri, E., Mckenzie, J.A., Vasconcelos, C., 2010. Microbial biomineralization processes forming modern Ca:Mg carbonate stromatolites. *Sedimentology* 57, 27–40. <https://doi.org/10.1111/j.1365-3091.2009.01083.x>.
- Sperling, E.A., Rooney, A.D., Sergeev, V.N., Vorob'eva, N.G., Sergeeva, N.D., Selby, D., Johnston, D.T., Knoll, A.H., 2014. Redox heterogeneity of subsurface waters in the Mesoproterozoic Ocean. *Geobiology* 12, 373–386. <https://doi.org/10.1111/gbi.12091>.
- Sprachta, S., Camoin, G., Golubic, S., Le Campion, T., 2001. Microbialites in a modern lagoonal environment: Nature and distribution, Tikehau atoll (French Polynesia). *Palaeogeogr. Palaeoclimatol. Palaeoecol.* 175, 103–124. [https://doi.org/10.1016/S0031-0182\(01\)00388-1](https://doi.org/10.1016/S0031-0182(01)00388-1).
- Staudigel, H., Chastain, R.A., Yayanos, A., Bourcier, W., 1995. Biologically mediated dissolution of glass. *Chem. Geol.* 126, 147–154. [https://doi.org/10.1016/0009-2541\(95\)00115-X](https://doi.org/10.1016/0009-2541(95)00115-X).
- Staudigel, H., Yayanos, A., Chastain, R., Davies, G., Verdurmen, E.A.T., Schiffman, P., Bourcier, R., De Baar, H., 1998. Biologically mediated dissolution of volcanic glass in seawater. *Earth Planet. Sci. Lett.* 164, 233–244. [https://doi.org/10.1016/S0012-821X\(98\)00207-6](https://doi.org/10.1016/S0012-821X(98)00207-6).
- Steele, A., McCubbin, F.M., Fries, M., Kater, L., Boctor, N.Z., Fogel, M.L., Conrad, P.G., Glamoclija, M., Spencer, M., Morrow, A.L., Hammond, M.R., Zare, R.N., Vicenzi, E.P., Siljestrom, S., Bowden, R., Herd, C.D.K., Mysen, B.O., Shirey, S.B., Amundsen, H.E.F., Treiman, A.H., Bullock, E.S., Jull, A.J.T., 2012. A reduced organic carbon component in martian basalts. *Science* 337, 212–215. <https://doi.org/10.1126/science.1220715>.
- Stefurak, E.J.T., Lowe, D.R., Zentner, D., Fischer, W.W., 2014. Primary silica granules—a new mode of Palaeoarchean sedimentation. *Geology* 42, 283–286. <https://doi.org/10.1130/G35187.1>.
- Strother, P.K., Tobin, K., 1987. Observations on the genus *Huroniospora* Barghoorn: Implications for paleoecology of the Gunflint microbiota. *Precambrian Res.* 36, 323–333. [https://doi.org/10.1016/0301-9268\(87\)90029-5](https://doi.org/10.1016/0301-9268(87)90029-5).
- Stüeken, E.E., Buick, R., 2018. Environmental control on microbial diversification and methane production in the Mesoarchean. *Precambrian Res.* 304, 64–72. <https://doi.org/10.1016/j.precamres.2017.11.003>.
- Stüeken, E.E., Buick, R., Guy, B.M., Koehler, M.C., 2015a. Isotopic evidence for biological nitrogen fixation by molybdenum-nitrogenase from 3.2 Gyr. *Nature* 520, 666–669. <https://doi.org/10.1038/nature14180>.
- Stüeken, E.E., Buick, R., Anbar, A.D., 2015b. Selenium isotopes support free O₂ in the latest Archean. *Geology* 43, 259–262. <https://doi.org/10.1130/G36218.1>.
- Stüeken, E.E., Kipp, M.A., Koehler, M.C., Buick, R., 2016. The evolution of Earth's biogeochemical nitrogen cycle. *Earth-Science Rev.* 160, 220–239. <https://doi.org/10.1016/j.earscirev.2016.07.007>.
- Stüeken, E.E., Buick, R., Anderson, R.E., Baross, J.A., Planavsky, N.J., Lyons, T.W., 2017. Environmental niches and metabolic diversity in Neoproterozoic lakes. *Geobiology* 15, 767–783. <https://doi.org/10.1111/gbi.12251>.
- Subramanian, V., Cheng, K., Lancelot, C., Heyte, S., Paul, S., Moldovan, S., Ersen, O., Marinova, M., Ordonsky, V.V., Khodakov, A.Y., 2016. Nanoreactors: an Efficient Tool to Control the Chain-Length distribution in Fischer-Tropsch Synthesis. *ACS Catal.* 6, 1785–1792. <https://doi.org/10.1021/acscatal.5b01596>.
- Sugitani, K., 2019. Early Archean (Pre-3.0 Ga) Cellularly Preserved Microfossils and Microfossil-like Structures from the Pilbara Craton, Western Australia—A Review. In: van Kranendonk, M.J., Bennett, V.C., Hoffmann, J.E. (Eds.), *Earth's Oldest Rocks*. Elsevier, pp. 1007–1028. <https://doi.org/10.1016/B978-0-444-63901-1.00041-1>.
- Sugitani, K., Grey, K., Allwood, A., Nagaoka, T., Mimura, K., Minami, M., Marshall, C.P., van Kranendonk, M.J., Walter, M.R., 2007. Diverse microstructures from Archean chert from the Mount Goldsworthy-Mount Grant area, Pilbara Craton, Western Australia: Microfossils, dubiofossils, or pseudofossils? *Precambrian Res.* 158, 228–262. <https://doi.org/10.1016/j.precamres.2007.03.006>.
- Sugitani, K., Grey, K., Nagaoka, T., Mimura, K., 2009. Three-dimensional morphological and textural complexity of Archean putative microfossils from the Northeastern Pilbara craton: Indications of biogenicity of large (> 15µm) spheroidal and spindle-like structures. *Astrobiology* 9, 603–615. <https://doi.org/10.1089/ast.2008.0268>.
- Sugitani, K., Lepot, K., Nagaoka, T., Mimura, K., van Kranendonk, M.J., Oehler, D.Z., Walter, M.R., 2010. Biogenicity of Morphologically Diverse Carbonaceous Microstructures from the ca. 3400 Ma Strelley Pool Formation, in the Pilbara Craton, Western Australia. *Astrobiology* 10, 899–920. <https://doi.org/10.1089/ast.2010.0513>.
- Sugitani, K., Mimura, K., Nagaoka, T., Lepot, K., Takeuchi, M., 2013. Microfossil assemblage from the 3400 Ma Strelley Pool Formation in the Pilbara Craton, Western Australia: Results form a new locality. *Precambrian Res.* 226, 59–74. <https://doi.org/10.1016/j.precamres.2012.11.005>.
- Sugitani, K., Mimura, K., Takeuchi, M., Lepot, K., Ito, S., Javaux, E.J., 2015a. Early

- evolution of large micro-organisms with cytological complexity revealed by micro-analyses of 3.4 Ga organic-walled microfossils. *Geobiology* 13, 507–521. <https://doi.org/10.1111/gbi.12148>.
- Sugitani, K., Mimura, K., Takeuchi, M., Yamaguchi, T., Suzuki, K., Senda, R., Asahara, Y., Wallis, S., van Kranendonk, M.J., 2015b. A Paleoproterozoic coastal hydrothermal field inhabited by diverse microbial communities: the Strelley Pool Formation, Pilbara Craton, Western Australia. *Geobiology* 13, 522–545. <https://doi.org/10.1111/gbi.12150>.
- Summons, R.E., Jahnke, L.L., Roksandic, Z., 1994. Carbon isotopic fractionation in lipids from methanotrophic bacteria: Relevance for interpretation of the geochemical record of biomarkers. *Geochim. Cosmochim. Acta* 58, 2853–2863. [https://doi.org/10.1016/0016-7037\(94\)90119-8](https://doi.org/10.1016/0016-7037(94)90119-8).
- Sumner, D.Y., 1997. Late Archean calcite-microbe interactions; two morphologically distinct microbial communities that affected calcite nucleation differently. *Palaiois*. <https://doi.org/10.2307/3515333>.
- Sumner, D.Y., 2000. Microbial vs Environmental Influences on the Morphology of late Archean Fenestrate Microbialites. In: *Sediments, Microbial* (Ed.), Springer, Berlin Heidelberg, Berlin, Heidelberg, pp. 307–314. https://doi.org/10.1007/978-3-662-04036-2_33.
- Tang, Q., Pang, K., Xiao, S., Yuan, X., Ou, Z., Wan, B., 2013. Organic-walled microfossils from the early Neoproterozoic Liulaobei Formation in the Huainan region of North China and their biostratigraphic significance. *Precambrian Res.* 236, 157–181. <https://doi.org/10.1016/j.precamres.2013.07.019>.
- Tashiro, T., Ishida, A., Hori, M., Igisu, M., Koike, M., Méjean, P., Takahata, N., Sano, Y., Komiya, T., 2017. Early trace of life from 3.95 Ga sedimentary rocks in Labrador, Canada. *Nature* 549, 516–518. <https://doi.org/10.1038/nature24019>.
- Templeton, A.S., Chu, K.H., Alvarez-Cohen, L., Conrad, M.E., 2006. Variable carbon isotope fractionation expressed by aerobic CH₄-oxidizing bacteria. *Geochim. Cosmochim. Acta* 70, 1739–1752. <https://doi.org/10.1016/j.gca.2005.12.002>.
- Templeton, A.S., Knowles, E.J., Eldridge, D.L., Arey, B.W., Dohnalkova, A.C., Webb, S.M., Bailey, B.E., Tebo, B.M., Staudigel, H., 2009. A seafloor microbial biome hosted within incipient ferromanganese crusts. *Nat. Geosci.* 2, 872–876. <https://doi.org/10.1038/ngeo696>.
- Thomazo, C., Pinti, D.L., Busigny, V., Ader, M., Hashizume, K., Philippot, P., 2009a. Biological activity and the Earth's surface evolution: Insights from carbon, sulfur, nitrogen and iron stable isotopes in the rock record. *Comptes Rendus Palevol* 8, 665–678. <https://doi.org/10.1016/j.crpv.2009.02.003>.
- Thomazo, C., Ader, M., Farquhar, J., Philippot, P., 2009b. Methanotrophs regulated atmospheric sulfur isotope anomalies during the Mesoproterozoic (Tumbiana Formation, Western Australia). *Earth Planet. Sci. Lett.* 279, 65–75. <https://doi.org/10.1016/j.epsl.2008.12.036>.
- Thomazo, C., Ader, M., Philippot, P., 2011. Extreme 15N-enrichments in 2.72-Gyr-old sediments: evidence for a turning point in the nitrogen cycle. *Geobiology* 9, 107–120. <https://doi.org/10.1111/j.1472-4669.2011.00271.x>.
- Thomazo, C., Nisbet, E.G., Grassineau, N.V., Peters, M., Strauss, H., 2013. Multiple sulfur and carbon isotope composition of sediments from the Belingwe Greenstone Belt (Zimbabwe): a biogenic methane regulation on mass independent fractionation of sulfur during the Neoproterozoic? *Geochim. Cosmochim. Acta* 121, 120–138. <https://doi.org/10.1016/j.gca.2013.06.036>.
- Thomazo, C., Couradeau, E., Garcia-Pichel, F., 2018. Possible nitrogen fertilization of the early Earth Ocean by microbial continental ecosystems. *Nat. Commun.* 9, 2530. <https://doi.org/10.1038/s41467-018-04995-y>.
- Thorseth, I.H., Furnes, H., Tumyr, O., 1995a. Textural and chemical effects of bacterial activity on basaltic glass: an experimental approach. *Chem. Geol.* 119, 139–160. [https://doi.org/10.1016/0009-2541\(94\)00098-S](https://doi.org/10.1016/0009-2541(94)00098-S).
- Thorseth, I.H., Torsvik, T., Furnes, H., Muehlenbachs, K., 1995b. Microbes play an important role in the alteration of oceanic crust. *Chem. Geol.* 126, 137–146. [https://doi.org/10.1016/0009-2541\(95\)00114-8](https://doi.org/10.1016/0009-2541(95)00114-8).
- Thorseth, I.H., Torsvik, T., Torsvik, V., Daae, F.L., Pedersen, R.B., 2001. Diversity of life in ocean floor basalt. *Earth Planet. Sci. Lett.* 194, 31–37. [https://doi.org/10.1016/S0012-821X\(01\)00537-4](https://doi.org/10.1016/S0012-821X(01)00537-4).
- Thorseth, I.H., Pedersen, R.B., Christie, D.M., 2003. Microbial alteration of 0-30-Ma seafloor and sub-seafloor basaltic glasses from the Australian Antarctic Discordance. *Earth Planet. Sci. Lett.* 215, 237–247. [https://doi.org/10.1016/S0012-821X\(03\)00427-8](https://doi.org/10.1016/S0012-821X(03)00427-8).
- Tian, F., 2005. A Hydrogen-rich early Earth atmosphere. *Science* 308, 1014–1017. <https://doi.org/10.1126/science.1106983>.
- Tice, M.M., 2009. Environmental controls on photosynthetic microbial mat distribution and morphogenesis on a 3.42 Ga clastic-starved platform. *Astrobiology* 9, 989–1000. <https://doi.org/10.1089/ast.2008.0330>.
- Tice, M.M., Lowe, D.R., 2004. Photosynthetic microbial mats in the 3,416-Myr-old Ocean. *Nature* 431, 549–552. <https://doi.org/10.1038/nature02888>.
- Tice, M.M., Lowe, D.R., 2006. The origin of carbonaceous matter in pre-3.0 Ga greenstone terrains: a review and new evidence from the 3.42 Ga Buck Reef Chert. *Earth-Science Rev.* 76, 259–300. <https://doi.org/10.1016/j.earscirev.2006.03.003>.
- Tice, M.M., Bostick, B.C., Lowe, D.R., 2004. Thermal history of the 3.5-3.2 Ga Onverwacht and Fig Tree Groups, Barberton Greenstone Belt, South Africa, inferred by Raman microspectroscopy of carbonaceous material. *Geology* 32, 37–40. <https://doi.org/10.1130/G19915.1>.
- Torsvik, T., Furnes, H., Muehlenbachs, K., Thorseth, I.H., Tumyr, O., 1998. Evidence for microbial activity at the glass-alteration interface in oceanic basalts. *Earth Planet. Sci. Lett.* 162, 165–176. [https://doi.org/10.1016/S0012-821X\(98\)00164-2](https://doi.org/10.1016/S0012-821X(98)00164-2).
- Trainer, M.G., Pavlov, A.A., DeWitt, H.L., Jimenez, J.L., McKay, C.P., Toon, O.B., Tolbert, M.A., 2006. Organic haze on Titan and the early Earth. *Proc. Natl. Acad. Sci. U. S. A.* 103, 18035–18042. <https://doi.org/10.1073/pnas.0608561103>.
- Truede, T., Orphan, V., Knittel, K., Gieseke, A., House, C.H., Boetius, A., 2007. Consumption of methane and CO₂ by methanotrophic microbial mats from gas seeps of the anoxic Black Sea. *Appl. Environ. Microbiol.* 73, 2271–2283. <https://doi.org/10.1128/AEM.02685-06>.
- Tyler, S.A., Barghoom, E.S., 1963. Ambient pyrite grains in Precambrian cherts. *Am. J. Sci.* 261, 424–432. <https://doi.org/10.2475/ajs.261.5.424>.
- Ueno, Y., Isozaki, Y., Yurimoto, H., Maruyama, S., 2001a. Carbon Isotopic Signatures of Individual Archean Microfossils(?) from Western Australia. *Int. Geol. Rev.* 43, 196–212. <https://doi.org/10.1080/00206810109465008>.
- Ueno, Y., Maruyama, S., Isozaki, Y., Yurimoto, H., 2001b. Early Archean (ca. 3.5 Ga) microfossils and 13C-depleted carbonaceous matter in the North Pole area, Western Australia: Field occurrence and geochemistry. In: Nakashima, S., Maruyama, S., Brack, A., Windley, B.F. (Eds.), *Geochemistry and the Origin of Life. Universal Academy Press, Tokyo*, pp. 203–236.
- Ueno, Y., Yurimoto, H., Yoshioka, H., Komiya, T., Maruyama, S., 2002. Ion microprobe analysis of graphite from ca. 3.8 Ga metasediments, Isua supracrustal belt, West Greenland: Relationship between metamorphism and carbon isotopic composition. *Geochim. Cosmochim. Acta* 66, 1257–1268. [https://doi.org/10.1016/S0016-7037\(01\)00840-7](https://doi.org/10.1016/S0016-7037(01)00840-7).
- Ueno, Y., Yoshioka, H., Maruyama, S., Isozaki, Y., 2004. Carbon isotopes and petrography of kerogens in ~3.5-Ga hydrothermal silica dikes in the North Pole area, Western Australia. *Geochim. Cosmochim. Acta* 68, 573–589. [https://doi.org/10.1016/S0016-7037\(00\)00462-9](https://doi.org/10.1016/S0016-7037(00)00462-9).
- Ueno, Y., Yamada, K., Yoshida, N., Maruyama, S., Isozaki, Y., 2006a. Evidence from fluid inclusions for microbial methanogenesis in the early Archean era. *Nature* 440, 516–519. <https://doi.org/10.1038/nature04584>.
- Ueno, Y., Yamada, K., Yoshida, N., Maruyama, S., Isozaki, Y., 2006b. Biosignatures and abiotic constraints on early life (Reply). *Nature* 444, E18–E19. <https://doi.org/10.1038/nature05500>.
- Ueno, Y., Isozaki, Y., McNamara, K.J., 2006c. Coccolith-like Microstructures in a 3.0 Ga Chert from Western Australia. *Int. Geol. Rev.* 48, 78–88. <https://doi.org/10.2747/0020-6814.48.1.78>.
- Ueno, Y., Ono, S., Rumble, D., Maruyama, S., 2008. Quadruple sulfur isotope analysis of ca. 3.5 Ga Dresser Formation: New evidence for microbial sulfate reduction in the early Archean. *Geochim. Cosmochim. Acta* 72, 5675–5691. <https://doi.org/10.1016/j.gca.2008.08.026>.
- Valentine, D.L., Chidhaisong, A., Rice, A., Reeber, W.S., Tyler, S.C., 2004. Carbon and hydrogen isotope fractionation by moderately thermophilic methanogens. *Geochim. Cosmochim. Acta* 68, 1571–1590. <https://doi.org/10.1016/j.gca.2003.10.012>.
- Valley, J.W., 2001. *Reviews in mineralogy and geochemistry vol 43: stable isotope thermometry at high temperatures*. In: Valley, J.W., Cole, D.R. (Eds.), *Stable Isotope Geochemistry*, pp. 365–414.
- van Hunen, J., Moya, J.-F., 2012. Archean Subduction: Fact or Fiction? *Annu. Rev. Earth Planet. Sci.* 40, 195–219. <https://doi.org/10.1146/annurev-earth-042711-105255>.
- van Kranendonk, M.J., 2006. Volcanic degassing, hydrothermal circulation and the flourishing of early life on Earth: a review of the evidence from c. 3490-3240 Ma rocks of the Pilbara Supergroup, Pilbara Craton, Western Australia. *Earth-Science Rev.* 74, 197–240. <https://doi.org/10.1016/j.earscirev.2005.09.005>.
- van Kranendonk, M.J., 2007. Chapter 7.2 a Review of the evidence for Putative Paleoproterozoic Life in the Pilbara Craton, Western Australia. In: van Kranendonk, M.J., Scaillet, R.H., Bennett, V.C. (Eds.), *Earth's Oldest Rocks*. Elsevier, pp. 855–877. [https://doi.org/10.1016/S0166-2635\(07\)15072-6](https://doi.org/10.1016/S0166-2635(07)15072-6).
- van Kranendonk, M.J., Philippot, P., Lepot, K., 2006. The Pilbara drilling project: c. 2.72 Ga Tumbiana Formation and c. 3.49 Ga Dresser Formation, Pilbara Craton, Western Australia, Western Australia Geological Survey, Record 2006/14, 25p. *Western Australia Geological Survey (Record 2006/14, 25p)*.
- van Kranendonk, M.J., Philippot, P., Lepot, K., Bodorkos, S., Pirajno, F., 2008. Geological setting of Earth's oldest fossils in the ca. 3.5 Ga Dresser Formation, Pilbara Craton, Western Australia. *Precambrian Res.* 167, 93–124. <https://doi.org/10.1016/j.precamres.2008.07.003>.
- van Zuilen, M.A., 2018. Proposed early signs of life not set in stone. *Nature* 563, 190–191. <https://doi.org/10.1038/d41586-018-06994-x>.
- van Zuilen, M.A., Van Kranendonk, M.J., 2019. The significance of Carbonaceous Matter to Understanding Life Processes on early Earth. In: Bennett, V.C., Hoffmann, J.E. (Eds.), *Earth's Oldest Rocks*. Elsevier, pp. 945–963. <https://doi.org/10.1016/B978-0-444-63901-1.00038-1>.
- van Zuilen, M.A., Lepland, A., Arrhenius, G., 2002. Reassessing the evidence for the earliest traces of life. *Nature* 420, 202.
- van Zuilen, M.A., Lepland, A., Teranes, J., Finarelli, J., Wahlen, M., Arrhenius, G., 2003. Graphite and carbonates in the 3.8 Ga old Isua Supracrustal Belt, southern West Greenland. *Precambrian Res.* 126, 331–348. [https://doi.org/10.1016/S0301-9268\(03\)00103-7](https://doi.org/10.1016/S0301-9268(03)00103-7).
- van Zuilen, M.A., Mathew, K., Wopenka, B., Lepland, A., Marti, K., Arrhenius, G., 2005. Nitrogen and argon isotopic signatures in graphite from the 3.8-Ga-old Isua Supracrustal Belt, Southern West Greenland. *Geochim. Cosmochim. Acta* 69, 1241–1252. <https://doi.org/10.1016/j.gca.2004.08.033>.
- van Zuilen, M.A., Chaussidon, M., Röllion-bard, C., Marty, B., 2007. Carbonaceous cherts of the Barberton Greenstone Belt, South Africa: Isotopic, chemical and structural characteristics of individual microstructures. *Geochim. Cosmochim. Acta* 71, 655–669. <https://doi.org/10.1016/j.gca.2006.09.029>.
- van Zuilen, M.A., Philippot, P., Whitehouse, M.J., Lepland, A., 2014. Sulfur isotope mass-independent fractionation in impact deposits of the 3.2 billion-year-old Mapepe Formation, Barberton Greenstone Belt, South Africa. *Geochim. Cosmochim. Acta* 142, 429–441. <https://doi.org/10.1016/j.gca.2014.07.018>.
- Vasconcelos, C., Warthmann, R., McKenzie, J.A., Visscher, P.T., Bittermann, A.G., van Lith, Y., 2006. Lifting microbial mats in Lagoa Vermelha, Brazil: Modern Precambrian relics? *Sediment. Geol.* 185, 175–183. [38](https://doi.org/10.1016/j.</p>
</div>
<div data-bbox=)

- sedgelo.2005.12.022.
- Ventura, G.T., Kenig, F., Reddy, C.M., Schieber, J., Frysinger, G.S., Nelson, R.K., Dinle, E., Gaines, R.B., Schaeffer, P., 2007. Molecular evidence of late Archean archaea and the presence of a subsurface hydrothermal biosphere. *Proc. Natl. Acad. Sci. U. S. A.* 104, 14260–14265. <https://doi.org/10.1073/pnas.0610903104>.
- Visscher, P.T., Reid, P.R., Bebout, B.M., 2000. Microscale observations of sulfate reduction: Correlation of microbial activity with lithified micritic laminae in modern marine stromatolites. *Geology* 28, 919–922. [https://doi.org/10.1130/0091-7613\(2000\)028<0919:MOOSRC>2.3.CO;2](https://doi.org/10.1130/0091-7613(2000)028<0919:MOOSRC>2.3.CO;2).
- Vogel, W., 1971. *Structure and Crystallization of Glasses*. Pergamon Press, Oxford. <https://doi.org/10.1016/C2013-0-05249-8>.
- Wacey, D., Kilburn, M.R., Stoakes, C., Aggleton, H., Brasier, M.D., 2008a. Ambient Inclusion Trails: Their Recognition, Age Range and Applicability to early Life on Earth. In: Dilek, Y., Furnes, H., Muehlenbachs, K. (Eds.), *Links between Geological Processes, Microbial Activities & Evolution of Life*. Springer Netherlands, pp. 113–134. <https://doi.org/10.1007/978-1-4020-8306-8>.
- Wacey, D., Kilburn, M.R., McLoughlin, N., Parnell, J., Stoakes, C.A., Grovenor, C.R.M.M., Brasier, M.D., 2008b. Use of NanoSIMS in the search for early life on Earth: ambient inclusion trails in a c. 3400 Ma sandstone. *J. Geol. Soc. Lond.* 165, 43–53. <https://doi.org/10.1144/0016-76492007-032>.
- Wacey, D., Kilburn, M.R., Saunders, M., Cliff, J., Brasier, M.D., 2011. Microfossils of Sulphur-metabolizing cells in 3.4-billion-year-old rocks of Western Australia. *Nat. Geosci.* 4, 698–702. <https://doi.org/10.1038/ngeo1238>.
- Wacey, D., Menon, S., Green, L., Gerstmann, D., Kong, C., McLoughlin, N., Saunders, M., Brasier, M., 2012. Taphonomy of very ancient microfossils from the ~ 3400 Ma Strelley Pool Formation and ~ 1900 Ma Gunflint Formation: New insights using a focused ion beam. *Precambrian Res.* 220–221, 234–250. <https://doi.org/10.1016/j.precamres.2012.08.005>.
- Wacey, D., Saunders, M., Cliff, J., Kilburn, M.R., Kong, C., Barley, M.E., Brasier, M.D., 2014a. Geochemistry and nano-structure of a putative ~3240 million-year-old black smoker biota, Sulphur Springs Group, Western Australia. *Precambrian Res.* 249, 1–12. <https://doi.org/10.1016/j.precamres.2014.04.016>.
- Wacey, D., Saunders, M., Roberts, M., Menon, S., Green, L., Kong, C., Culwick, T., Strother, P., Brasier, M.D., 2014b. Enhanced cellular preservation by clay minerals in 1 billion-year-old lakes. *Sci. Rep.* 4. <https://doi.org/10.1038/srep05841>.
- Wacey, D., McLoughlin, N., Saunders, M., Kong, C., 2014c. The nano-scale anatomy of a complex carbon-lined microtube in volcanic glass from the ~92Ma Troodos Ophiolite. *Cyprus. Chem. Geol.* 363, 1–12. <https://doi.org/10.1016/j.chemgeo.2013.10.028>.
- Wacey, D., Noffke, N., Cliff, J., Barley, M.E., Farquhar, J., 2015. Micro-scale quadruple sulfur isotope analysis of pyrite from the ~3480Ma Dresser Formation: New insights into sulfur cycling on the early Earth. *Precambrian Res.* 258, 24–35. <https://doi.org/10.1016/j.precamres.2014.12.012>.
- Wacey, D., Saunders, M., Kong, C., Kilburn, M.R., 2016a. A new occurrence of ambient inclusion trails from the ~1900-million-year-old Gunflint Formation, Ontario: nano-characterization and testing of potential formation mechanisms. *Geobiology* 14, 440–456. <https://doi.org/10.1111/gbi.12186>.
- Wacey, D., Saunders, M., Kong, C., Brasier, A.T., Brasier, M.D., 2016b. 3.46 Ga Apex chert ‘microfossils’ reinterpreted as mineral artefacts produced during phyllosilicate exfoliation. *Gondwana Res.* 36, 296–313. <https://doi.org/10.1016/j.jgr.2015.07.010>.
- Wacey, D., Fisk, M., Saunders, M., Eiloart, K., Kong, C., 2017. Critical testing of potential cellular structures within microtubes in 145 Ma volcanic glass from the Argo Abyssal Plain. *Chem. Geol.* 466, 575–587. <https://doi.org/10.1016/j.chemgeo.2017.07.006>.
- Wacey, D., Saunders, M., Kong, C., 2018a. Remarkably preserved tephra from the 3430 Ma Strelley Pool Formation, Western Australia: Implications for the interpretation of Precambrian microfossils. *Earth Planet. Sci. Lett.* 487, 33–43. <https://doi.org/10.1016/j.epsl.2018.01.021>.
- Wacey, D., Noffke, N., Saunders, M., Guagliardo, P., Pyle, D.M., 2018b. Volcanogenic Pseudo-Fossils from the ~3.48 Ga Dresser Formation, Pilbara, Western Australia. *Astrobiology* 18, 539–555. <https://doi.org/10.1089/ast.2017.1734>.
- Wacey, D., Urosevic, L., Saunders, M., George, A.D., 2018c. Mineralisation of filamentous cyanobacteria in Lake Thetis stromatolites, Western Australia. *Geobiology* 16, 203–215. <https://doi.org/10.1111/gbi.12272>.
- Wacey, D., Eiloart, K., Saunders, M., 2019. Comparative multi-scale analysis of filamentous microfossils from the c. 850 Ma Bitter Springs Group and filaments from the c. 3460 Ma Apex chert. *J. Geol. Soc. Lond.* 176, 1247–1260. <https://doi.org/10.1144/jgs2019-053>.
- Waldbauer, J.R., Sherman, L.S., Sumner, D.Y., Summons, R.E., 2009. Late Archean molecular fossils from the Transvaal Supergroup record the antiquity of microbial diversity and aerobicity. *Precambrian Res.* 169, 28–47. <https://doi.org/10.1016/j.precamres.2008.10.011>.
- Walsh, M.W., 1992. Microfossils and possible microfossils from the early Archean Onverwacht Group, Barberton mountain land, South Africa. *Precambrian Res.* 54, 271–293. [https://doi.org/10.1016/0301-9268\(92\)90074-X](https://doi.org/10.1016/0301-9268(92)90074-X).
- Walter, M.R., 1976a. Introduction. In: Walter, M.R. (Ed.), *Stromatolites*. Elsevier, Amsterdam, pp. 1–3. [https://doi.org/10.1016/S0070-4571\(08\)71123-3](https://doi.org/10.1016/S0070-4571(08)71123-3).
- Walter, M.R., 1976b. Geysirites of Yellowstone National Park: An Example of Abiogenic ‘Stromatolites’. In: Walter, M.R. (Ed.), *Stromatolites*. Elsevier, Amsterdam, pp. 87–112. [https://doi.org/10.1016/S0070-4571\(08\)71131-2](https://doi.org/10.1016/S0070-4571(08)71131-2).
- Walter, M.R., Bauld, J., Brock, T.D., 1976. Microbiology and Morphogenesis of Columnar Stromatolites (Conophyton, Vacerrilla) from Hot Springs in Yellowstone National Park, in: *Stromatolites*. Elsevier, Amsterdam, pp. 273–310. [https://doi.org/10.1016/S0070-4571\(08\)71140-3](https://doi.org/10.1016/S0070-4571(08)71140-3).
- Walton, A.W., 2008. Microtubules in basalt glass from Hawaii Scientific Drilling Project #2 phase 1 core and Hilina slope, Hawaii: evidence of the occurrence and behavior of endolithic microorganisms. *Geobiology* 6, 351–364. <https://doi.org/10.1111/j.1472-4669.2008.00149.x>.
- Walton, A.W., Schiffman, P., 2003. Alteration of hyaloclastites in the HSDP 2 phase 1 drill core 1. Description and paragenesis. *Geochemistry, Geophys. Geosystems* 4. <https://doi.org/10.1029/2002GC000368>.
- Watanabe, Y., Farquhar, J., Ohmoto, H., 2009. Anomalous fractionations of sulfur isotopes during thermochemical sulfate reduction. *Science* 324, 370–373. <https://doi.org/10.1126/science.1169289>.
- Waterbury, J.B., Stanier, R.Y., 1978. Patterns of growth and development in Pleurocapsalean Cyanobacteria. *Microbiol. Rev.* 42, 2–44.
- Wei, W., Klaebe, R., Ling, H.-F., Huang, F., Frei, R., 2020. Biogeochemical cycle of chromium isotopes at the modern Earth’s surface and its applications as a paleo-environment proxy. *Chem. Geol.* 541, 119570. <https://doi.org/10.1016/j.chemgeo.2020.119570>.
- Welander, P.V., Summons, R.E., 2012. Discovery, taxonomic distribution, and phenotypic characterization of a gene required for 3-methylhopanoid production. *Proc. Natl. Acad. Sci. U. S. A.* 109, 12905–12910. <https://doi.org/10.1073/pnas.1208255109>.
- Westall, F., Folk, R.L., 2003. Exogenous carbonaceous microstructures in early Archean cherts and BIFs from the Isua Greenstone Belt: Implications for the search for life in ancient rocks. *Precambrian Res.* 126, 313–330. [https://doi.org/10.1016/S0301-9268\(03\)00102-5](https://doi.org/10.1016/S0301-9268(03)00102-5).
- Westall, F., de Ronde, C.E., Southam, G., Grassineau, N., Colas, M., Cockell, C., Lammer, H., 2006. Implications of a 3.472–3.333 Gyr-old subaerial microbial mat from the Barberton greenstone belt, South Africa for the UV environmental conditions on the early Earth. *Philos. Trans. R. Soc. B Biol. Sci.* 361, 1857–1876. <https://doi.org/10.1098/rstb.2006.1896>.
- Westall, F., Cavalazzi, B., Lemelle, L., Marrocchi, Y., Rouzaud, J.N., Simionovici, A., Salomé, M., Mostefaoui, S., Andreatza, C., Foucher, F., Toporski, J., Jaus, A., Thiel, V., Southam, G., MacLean, L., Wirick, S., Hofmann, A., Meibom, A., Robert, F., Défarge, C., 2011. Implications of in situ calcification for photosynthesis in a ~3.3Ga-old microbial biofilm from the Barberton greenstone belt, South Africa. *Earth Planet. Sci. Lett.* 310, 468–479. <https://doi.org/10.1016/j.epsl.2011.08.029>.
- Westall, F., Campbell, K.A., Bréhéret, J.G., Foucher, F., Gautret, P., Hubert, A., Sorieul, S., Grassineau, N., Guido, D.M., 2015. Archean (3.33 Ga) microbe-sediment systems were diverse and flourished in a hydrothermal context. *Geology* 43, 615–618. <https://doi.org/10.1130/G36646.1>.
- White, L.M., Gibson, E.K., Thomas-Keprta, K.L., Clemett, S.J., McKay, D.S., 2014. Putative indigenous carbon-bearing alteration features in Martian meteorite Yamato 000593. *Astrobiology* 14, 170–181. <https://doi.org/10.1089/ast.2011.0733>.
- Williford, K.H., Ushikubo, T., Schopf, J.W., Lepot, K., Kitajima, K., Valley, J.W., 2013. Preservation and detection of microstructural and taxonomic correlations in the carbon isotopic compositions of individual Precambrian microfossils. *Geochim. Cosmochim. Acta* 104, 165–182. <https://doi.org/10.1016/j.gca.2012.11.005>.
- Williford, K.H., Ushikubo, T., Lepot, K., Kitajima, K., Hallmann, C., Spicuzza, M.J., Kozdon, R., Eigenbrode, J.L., Summons, R.E., Valley, J.W., 2016. Carbon and sulfur isotopic signatures of ancient life and environment at the microbial scale: Neoproterozoic shales and carbonates. *Geobiology* 14, 105–128. <https://doi.org/10.1111/gbi.12163>.
- Wilmeth, D.T., Corsetti, F.A., Beukes, N.J., Awramik, S.M., Petryshyn, V., Spear, J.R., Celestian, A.J., 2019. Neoproterozoic (2.7 Ga) lacustrine stromatolite deposits in the Hartbeesfontein Basin, Ventersdorp Supergroup, South Africa: implications for oxygen oases. *Precambrian Res.* 320, 291–302. <https://doi.org/10.1016/j.precamres.2018.11.009>.
- Yoshiya, K., Nishizawa, M., Sawaki, Y., Ueno, Y., Komiya, T., Yamada, K., Yoshida, N., Hirata, T., Wada, H., Maruyama, S., 2012. In situ iron isotope analyses of pyrite and organic carbon isotope ratios in the Fortescue Group: Metabolic variations of a late Archean ecosystem. *Precambrian Res.* 212–213, 169–193. <https://doi.org/10.1016/j.precamres.2012.05.003>.
- Yoshiya, K., Sawaki, Y., Shibuya, T., Yamamoto, S., Komiya, T., Hirata, T., Maruyama, S., 2015. In-situ iron isotope analyses of pyrites from 3.5 to 3.2Ga sedimentary rocks of the Barberton Greenstone Belt, Kaapvaal Craton. *Chem. Geol.* 403, 58–73. <https://doi.org/10.1016/j.chemgeo.2015.03.007>.
- Zawaski, M.J., Kelly, N.M., Orlandini, O.F., Nichols, C.I.O., Allwood, A.C., Mojzsis, S.J., 2020. Reappraisal of purported ca. 3.7 Ga stromatolites from the Isua Supracrustal Belt (West Greenland) from detailed chemical and structural analysis. *Earth Planet. Sci. Lett.* 545, 116409. <https://doi.org/10.1016/j.epsl.2020.116409>.
- Zegeye, A., Ona-Nguema, G., Carteret, C., Huguet, L., Abdelmoula, M., Jorand, F., 2005. Formation of Hydroxysulphate Green Rust 2 as a Single Iron(II-III) Mineral in Microbial Culture. *Geomicrobiol. J.* 22, 389–399. <https://doi.org/10.1080/0149045002048960>.
- Zerkle, A.L., Claire, M.W., Domagal-Goldman, S.D., Farquhar, J., Poulton, S.W., 2012. A bistable organic-rich atmosphere on the Neoproterozoic Earth. *Nat. Geosci.* 5, 359–363. <https://doi.org/10.1038/ngeo1425>.
- Zeuch, D.H., Green, H.W., 1977. Naturally decorated dislocations in olivine from peridotite xenoliths. *Contrib. Mineral. Petrol.* 62, 141–151. <https://doi.org/10.1007/BF00372873>.
- Zeyen, N., Benzerara, K., Li, J., Groleau, A., Balan, E., Robert, J., Estève, I., Tavera, R., Moreira, D., 2015. Formation of Low-T Hydrated Silicates in Modern Microbialites from Mexico and Implications for Microbial Fossilization. 3. pp. 1–23. <https://doi.org/10.3389/feart.2015.00064>.